Electron transfer through the outer membrane of *Geobacter sulfurreducens*

A DISSERTATION

SUBMITTED TO THE FACULTY OF THE

UNIVERSITY OF MINNESOTA

BY

Fernanda Jiménez Otero

IN PARTIAL FULFILLMENT OF THE REQUIREMENTS

FOR THE DEGREE OF

DOCTOR IN PHILOSOPHY

Dr. Daniel R. Bond

May, 2018

Acknowledgements

This dissertation and the degree I have gained with it, would not have been possible without the help and support from an invaluable group of people.

The training I received from Chi Ho Chan and Caleb Levar continues to be essential in the way I approach scientific endeavors. The quality of genetic studies and rigor in microbiology techniques they taught me is a standard I hope to meet throughout my career.

Daniel Bond has been much more than I ever expected from an advisor. I have not only gained scientific knowledge from him, but I will take with me the example of what a great mentor represents. His enthusiasm for science is only rivaled by his commitment to past and present members of his laboratory. I am extremely honored to be able to count myself in that group, and I will do my best to represent him proudly in future endeavors.

Throughout these five years, Jeff Gralnick has given me numerous opportunities to explore all aspects of a scientific career. Not only is Chapter 2 a result of his vision, but I feel less intimidated by a career in science as a result of his mentoring and support.

The faculty members in my committee- Carrie Wilmot, Brandy Toner, and Larry Wackett, have made sure I am well prepared for

every step through graduate school. I really appreciate the time they have invested in me.

Although I have enjoyed these past five years tremendously, it has not been a simple task. My mother, Adriana Otero, has had to constantly remind me that obtaining a PhD is not supposed to be easy. Growing up with your work ethic and enthusiasm for knowledge as an example has been instrumental in finding my own passion for science.

Finally, but most importantly, my family- Yumhali and Zoe- are the engine that keeps me going. Your support, emotional as well as logistical, is what made this work even possible. Thank you.

Fernanda Jimenez Otero was supported by the Mexican Council for Science and Technology (CONACYT) from September 2014 – May 2018.

Abstract

Microbial metabolism represents a rich source of catalytic tools available for biotechnological applications. Microbial metal reduction is no exception, as it represents a mechanism for transferring electrons stored within nonreactive organic compounds to inorganic redox-active compounds. Despite the usefulness of organisms capable of metal reduction, not enough is known about their electron transfer pathway to be able to engineer them for real-world applications. Specifically, how electrons cross cell membranes to be available on the extracellular surface where they can react with metals or electrodes remains one of the least well-studied aspects of extracellular electron transfer. In this thesis, a compilation of studies into extracellular electron transfer pathways of the model organism *Geobacter sulfurreducens,* and the characteristics of current-producing biofilms produced by this species uncovers fundamental steps and bottlenecks in this metabolic strategy. Through isotopic label incorporation, the first spatially resolved direct measurement of anabolic activity in *G. sulfurreducens* biofilms was obtained, concluding that metabolic activity is constrained to the layers within the first few microns from the electrode surface. Combinatorial deletion of putative outer membrane electron conduit gene clusters followed by analysis of the ability of this mutant collection to reduce different extracellular substrates showed that several electron

conduit gene clusters are necessary in tandem during metal reduction, while only a previously unstudied gene cluster *extABCD* was necessary for wild type levels of electrode reduction. Within this mutant collection, the strain lacking all studied gene clusters except *extABCD* (*extABCD*$^{+}$), reached higher current densities with faster doubling times than wild type. The *extABCD*$^{+}$ strain was found to form biofilms containing 30% more cells than wild type at the electrode:biofilm interface, where isotopic label incorporation showed 38% higher anabolic activity per cell in *extABCD*$^{+}$ biofilms compared to wild type. Thus, by focusing on the fundamental physiology of extracellular electron transfer, evidence for substrate-specific electron transfer pathways were found, and a strain with a streamlined pathway for increased electrode reduction could be constructed. The findings in this work suggest a route to engineering organisms with metal- or electrode-specific reduction pathways, and enhancing electron transfer rates in these systems.

Table of Contents

List of Tables

List of Figures

Chapter 4

Chapter 5

Chapter 1. Biological solutions to respiring extracellular substrates.

Fernanda Jiménez Otero

1.1 **Introduction**

All organisms derive energy from their environment in order to grow, but microorganisms are able to use a wide variety of substrates for this purpose ultimately guiding the flux of carbon, sulfur, nitrogen, metals and gases in our biosphere (1). Identifying the physiology that allows cells to use each one of those substrates is not only a basic research goal, but it also enables us to predict the composition of microbial communities present in the environment and to engineer systems where we can take advantage of diverse metabolic strategies for biotechnological purposes.

The respiration of metal substrates has lagged behind all other respiration strategies in terms of respiration pathway identification. For example, organisms that use aerobic respiration strategies, and those using nitrate or sulfate as substrates can be easily detected in microbial communities through the use of conserved marker proteins. This same task is much more complicated when trying to identify microorganisms that derive energy from metal reduction, due to the wide diversity of metal oxide substrates, and the need for these organisms to respire these compounds on the outside of the cell. **The purpose of this thesis is to identify fundamental steps in extracellular electron transfer pathways used by metal-reducing bacteria both as a physiological question and with the goal of finding**

bottlenecks which can be targeted for substrate-specific biotechnological systems. A collection of studies are presented describing new electron transfer pathways to extracellular substrates, and show how each pathway influences the growth properties of metal reducing microorganisms.

Two main characteristics make metal respiration different from soluble-substrate respiration strategies. Iron and manganese oxides, which are the most abundant and commonly used metal oxides, exist as large and insoluble particles in most soil and sediment environments (2). Being able to deliver electrons to an extracellular substrate becomes the first hurdle of metal oxide respiration. Additionally, both iron and manganese oxides exist in many different forms and their characteristics constantly change (3). A strategy is therefore necessary to be able to use metal oxides as substrates, regardless of shifts in their surface or redox characteristics.

The complexity of iron oxides focusing on the properties that may influence microbial growth is reviewed in section 1.2, while known strategies for the reduction of extracellular substrates is reviewed in section 1.4. This thesis will largely focus on the extracellular electron transfer pathways used by *Geobacter sulfurreducens* to respire poised electrodes, therefore, section 1.3 reviews techniques used to study these materials as respiration substrates and the applications of such technology.

Chapter 2 focuses on the growth of *G. sulfurreducens* using a poised electrode as terminal electron acceptor. It has been a long standing mystery why current producing biofilms reach a limit in current production independent of carbon source availability. This chapter describes the findings of an anabolic activity study of each layer of cells within a *G. sulfurreducens* biofilm. For the first time, measurements are able to show that cells closest to the electrode have the highest anabolic activity, and that pattern does not change with redox potential or age of the biofilm.

Chapter 3 is a study of the electron transfer pathways across the outer membrane of *G. sulfurreducens*. This organism is highly specialized in the reduction of extracellular terminal electron acceptors, and encodes several putative outer membrane electron transfer pathways. A genetic approach was used to determine which pathways are necessary or sufficient during respiration of different substrates. Results show that a cohort of pathways are necessary for wild type levels of metal reduction, while only one pathway is important for electrode reduction. While it is not yet known if these outer membrane complexes interact directly with extracellular electron acceptors, it is useful to keep in mind the variability in substrate characteristics that *G. sulfurreducens* encounters in the environment (see section 1.2) to understand why several

pathways would be necessary in tandem to use metal oxides as terminal electron acceptors.

Chapter 4 delves deeper into the finding that the *extABCD*$^{+}$ strain, containing only one outer membrane redox complex, grown using a poised electrode as terminal electron acceptor produces 40% more current and has a doubling time 30% faster than wild type. This study includes many different techniques, including- electrochemical analyses, proteomics, nanoSIMS, and microscopy- to try to understand the increase in current production of the *extABCD*$^{+}$ strain. Our results show that the anabolic activity of cells closest to the electrode is 40% higher in an *extABCD*$^{+}$ strain compared to wild type. In that same area, cells are 30% more densely packed as well, creating an additive effect on final current production.

Finally, Chapter 5 covers some of the questions that arise from the studies presented here.

1.2 **Iron oxide- the most abundant oxidant in the biosphere.**

All respiring cells must reduce a terminal electron acceptor in order to harvest energy form an electron donor and continue to grow. In the biosphere, there is a wide variety of compounds that are available for cells as reductants or oxidants in this process. Among bioavailable oxidants, the most abundant

is iron oxide (1). Despite their abundance, due to the insoluble nature of iron oxides in the environment, these metals are not the most widely used respiration substrate. In this section, the inherent characteristics of iron oxide particles that influence their quality as a respiration substrate and that may impact the enzymatic pathways used to reduce them will be reviewed.

Iron oxides are a large and diverse group of metal oxides that share a common composition of an iron atom coordinated by up to 6 oxygen atoms, hydroxide groups, or a combination of both (4). This composition gives way to either tetrahedral or octahedral units with oxygen atoms or hydroxide groups as corners, and which assemble into large crystal structures by sharing oxygen atoms along the faces, edges, or corners of each polyhedron (2). The distance between iron atoms within a crystal is mandated by the type of polyhedron sharing between them, *i.e.*, the number of oxygens shared between two iron atoms. The diverse ways in which coordinated iron atom polyhedra can be spatially arranged gives way to a variety of metal oxide microscopic and macroscopic properties. Iron oxide structures vary from stable to nano-crystalline, redox potentials span more than 500 mV, surface areas can be small or large and change with ageing, and magnetic properties and surface charge are also diverse.

Different iron oxides predominate in sediments throughout the biosphere depending on soil composition, temperature and

acidity. Some common forms of iron oxides known to be used by microbes as terminal electron acceptors are goethite, hematite, magnetite, and ferrihydrite (5).

Goethite. Goethite is the most abundant iron oxide in soils and rocks. It is a stable metal oxide, considered to be highly homogeneous and non-reactive. The structural formula of goethite is α-FeOOH. Each Fe(III) atom in goethite is coordinated by three oxygens and three hydroxides, making goethite a metal oxyhydroxide (6). Goethite is composed of octahedral edge-sharing double chains sharing corners with adjacent chains such that there is space between Fe ion chains, creating an illusion of 'tunnels' in schematic representations (6). In reality, hydroxyl groups fill those spaces but at a macroscopic level the space between octahedra double chains does create grooves on the surface of the mineral (2).

The surface area of goethite ranges from 8-200 m^2g^{-1}, placing it on the lower end of the surface area spectrum of ferric oxides (6). The relatively low redox potential of goethite (-170 mV vs. SHE, in aqueous solution, pH 7 (2, 7)) along with its stability and low surface area result in slow and low-yield microbial reduction (8, 9). While it is true that goethite is highly homogeneous, vacancies and impurities do appear in this ferric oxide. The structural charge created by vacancies is compensated by extra H atoms, creating extra OH groups. Isomorphic

substitution in environmental goethite is mainly due to Al(III) substitution (2). Al(III) has the same coordination number as Fe(III) and is very abundant in soils, making it a plausible candidate for isomorphic substitution, even if it is slightly smaller in size. Goethite can be found with up to 1/3 of Fe ions substituted by Al(III) (2). This substitution results in a decrease in crystal size and a decrease in the magnetic field of goethite. Other cations can also substitute Fe(III) in goethite, such as Mn(III), Zn(II), and Co(III). The dissolution rate and color of goethite are also affected by isomorphic substitution.

Hematite. Hematite is another stable ferric oxide widely distributed across the world, especially in warm climates, giving soils a red tone (2). The structural formula of hematite is α-Fe_2O_3. Each Fe(III) cation in hematite is coordinated by six oxygens, making it a ferric oxide. Its molecular structure consists of octahedra arranged in face-sharing pairs of Fe ions, and each pair shares edges with three other pairs (10). Face sharing is considered less stable than edge and corner sharing because it forces the cations to be closer. However, hematite is a stable ferric oxide, counteracting the face-sharing arrangement with a slight distortion in the octahedron shape by allowing Fe ions to be closer to the oxygens that are not part of the face-sharing side (4).

The surface area of hematite in soil samples can range from 10-42 cm^2g^{-1}, even lower than goethite, and it can also be porous depending on how it was formed (10). As in the case of goethite, the low reduction potential (-177 vs. SHE), low surface area, and high stability of hematite make this the most recalcitrant iron oxide to microbial reduction (9). Al(III) substitution is also prevalent with the same results as Al(III)-substituted goethite. Other cations can replace Fe ions in hematite (11), mainly Mn(II), which can replace up to 0.05% of the Fe ions (2).

Magnetite is a ferric-ferrous oxide, with a structural formula of $Fe^{3+}(Fe^{2+}Fe^{3+})O_4$. This iron oxide form is both a signature of biogenic Fe(III) reduction (5, 9), and a substrate for this process (12). Trivalent iron in magnetite can be found both in octahedral and tetrahedral coordination with oxygen, and divalent iron is always octahedral. Magnetite is assembled with layers of octahedra and mixed octaherda-tetrahedra in an inverse spinel structure (13).

Magnetite is prone to more isomorphic substitution than other metal oxides because there are more cations that can take the place of both Fe(II) and Fe(III) octahedra, and Fe(III) tetrahedra (2). The rate of substitution can be so high that hematite turns into a ferrite or other metal oxides. Magnetite crystals substituted with Al(III) tend to be smaller as Al

increases (14). Natural magnetite surface area can range from 4-100 m^2g^{-1} and it is non-porous[21].

Ferrihydrite. The structure of ferrihydrite has been a source of debate in the field. The nano-particle size of ferrihydrite crystals is too small for X-ray diffraction and it is also likely to be made up of several particle types (15). Recently a unit cell structure has been proposed for ferrihydrite (16), with a mixture of octahedral and tetrahedral Fe ions in some peculiar arrangements, such as edges shared by three octahedra and a tetrahedron sharing three faces with octaherda. The proposed structural formula for ferrihydrite is *ca* $Fe_{10}O_{14}(OH)_2$ (16).

The surface area of ferrihydrite in natural samples ranges from 200-400 m^2g^{-1} (2), making it a high surface area iron oxide. Ferrihydrite nanocrystals form aggregates of ~0.1 μm in diameter (15). These aggregates are microporous when freshly precipitated and pores become more numerous and larger as the metal oxide ages. The redox potential of ferrihydrite ranges between -100 mV to +100 mV vs. SHE (3, 17). Microorganisms reduce ferrihydrite easily due to its high surface area and favorable redox potential. An interesting interaction between ferrihydrite and organic carbon in soils is that organic carbon concentration is inversely proportional to surface area of ferrihydrite (18).

All of these characteristics affect the way a cell can interact with iron oxides. For example, surface area dictates the bioavailability of an iron oxide for microbial metal reduction. As an iron particle is reduced, its surface area decreases, and the redox potential of that particle increases (3), possibly changing the proteins necessary to reduce it (8). Surface charge and magnetic properties also influence the initial interaction between an iron oxide particle and other surfaces (2), including cells. It is not surprising that the pathway for extracellular electron transfer has been elusive for decades, since the characteristics of the terminal electron acceptor are highly variable. A summary of common iron oxides can be found on Table 1.1.

Table 1.1 Iron oxides found in subsurface environments (2–4, 6, 15, 19)

Metal oxide	Structural formula	Most commonly found	Redox potential (mV)	Additional notes
Goethite	α-FeOOH	Most common Fe(III)-oxide in all regions	-167	Highly stable
Ferrihydrite	Nano-crystalline with variable structure	Most abundant metastable Fe(III) oxide	24	Ages to goethite, depending on pH
Hematite	α-Fe_2O_3	Common throughout the world except temperate and cool regions	-177	Highly stable
Magnetite	Fe_3O_4	Most common biogenic Fe(III) oxide	-135	Ferrous-ferric oxide

Schwertmannite	$Fe(OH)_{3/4}(SO_4)_{1/8}$	Fe(III)- and sulfate-rich acidic environments	14	Unstable at higher pH
Lepidocrocite	γ-FeOOH	Most common layered Fe oxide	-67	

1.3 **Poised electrodes as terminal electron acceptors.**

While the importance of microbial metal reduction for geo-cycling of metals in sediments and subsurface environments cannot be overstated, another key aspect of metal-reducing bacteria is their ability to reduce poised electrodes. Electrochemical systems where bacteria use anodes as terminal electron acceptors are uniquely adept for biotechnological application because they produce current from microbial metabolism, bacterial growth in these systems is in the form of current-producing biofilms, and they are stable for months. Microbial electrochemical technology has been shown to be useful for water desalination (20, 21), electro-fermentation of profitable products (22, 23), oxidation of organic matter in waste water (24), and bio-production of electricity (25, 26).

Harvesting energy from living organisms is an idea that has been explored for centuries. The first electrochemical system using bacteria, however, was published in 1911 (27), where yeast and bacteria were first observed to produce current during the oxidation of organic matter. Since then, microbial electrochemistry has flourished with more than 30,000 citations

of publications in this field during 2016 alone (28). For the most part, research has focused on the engineering of more efficient reactors (29), anode characteristics (30, 31), and other abiotic components of electrochemical cells (32).

The biotic component within microbial electrochemical reactors consist of current-producing biofilms. These microbial macrostructures share many characteristics with better-studied pathogenic biofilms but they are also unique in that all cells within these biofilms are using a poised electrode as both terminal electron acceptor and attachment surface (25, 33). Because of the fruitful possibilities of the application of such systems, the limitations of the metabolic activity of current-producing biofilms have been studied using different approaches, often reaching conflicting conclusions.

Locating the layers of active/inactive cells within current-producing biofilms has been attempted by several groups. DNA stains with differing membrane permeability are used to differentiate between cells with intact membranes and those with damaged membranes (34). This technique has led to conclusions that cells with intact membranes are found in the layer of cells closest to the electrode (35, 36), furthest from the electrode (37, 38), or throughout the whole biofilm (39–41). One of the main problems with such a technique is that membrane potential influences the membrane permeability of DNA stains (42), making

it hard to differentiate between highly active cells and those with damaged membranes. The extracellular matrix in biofilms is also known to contain extracellular DNA (43), possibly interfering with the read-out of such competitive DNA staining techniques.

Another approach to inferring the location of active cells in current-producing biofilms has been measuring the concentration of nutrients, the acidity and redox potential throughout the different layers. The main findings of such studies are that pH (44, 45) and acetate (46) concentration decrease from the surface of the biofilm towards the bottom layers of cells closest to the electrode, and that the redox potential of the biofilm becomes less favorable with distance from the electrode (44, 47, 48). With these data, both pH and acetate gradients would suggest that active layers within biofilms are located at the surface of the biofilm where there is the most access to buffer and nutrients. On the other hand, redox potential measurements indicate that the layers furthest from the electrode experience a less favorable redox potential to transfer metabolic electrons towards. More direct assays to locate metabolically active cells will be needed in order to settle these conflicting hypothesis.

Genetic studies have been very useful to determine which electron transfer pathways are needed during electrode reduction

in *G. sulfurreducens*. The clearest example is *omcZ* which encodes for a secreted *c*-cytochrome and is upregulated during electrode reduction (49). Deletion of *omcZ* also results in a decrease in current production (49, 50), and OmcZ is localized at the anode:biofilm interface (51). Other electron transfer pathways to the electrode have been harder to delineate. The pili of *G. sulfurreducens* have an unusual enrichment in aromatic residues (52), which influences their conductivity (53, 54). The exact role of pili during electrode reduction is not clear, however, since this cellular appendage is also essential for initial attachment to surfaces (55, 56).

1.4 **Enzymatic pathways for electron transfer across membranes.**

Bilipid layers are efficient cell barriers due to their insulating nature, but organisms respiring extracellular terminal electron acceptors need pathways to transfer electrons across cellular membranes in order to deposit them on insoluble metal oxides. For organisms with a Gram-negative physiology, several pathways have been described for the four different steps of extracellular electron transfer: electron transfer across the inner membrane, the periplasm, the outer membrane, and the extracellular matrix. The energetics and physiology of each of these steps is different, but enzymatic components are essential for each. In this section, a review of these pathways will be

presented, with a focus on electron transfer across the outer membrane.

Shewanella oneidensis and *Geobacter sulfurreducens* are the most widely studied model organisms for extracellular electron transfer. *S. oneidensis* is a facultative anaerobe from the γ-proteobacteria, while *G. sulfurreducens* is a 'strict' anaerobe from the δ-proteobacteria. Each of these organisms present advantages and disadvantages as model systems. The most significant may be the flexible metabolic strategies of *S. oneidensis*, yet lower extracellular electron transfer rates, vs. the fewer metabolic strategies of *G. sulfurreducens*, which make it harder to grow in the laboratory, yet a higher specialization that produces the highest extracellular electron transfer rates reported. The field has benefited from parallel progress in the comparative study of these two extracellular electron transfer strategies.

Electron transfer across the inner membrane represents the energy harvesting step for cells. As in other respiratory strategies, this step allows cells to generate a proton motive force and produce energy for growth. In *S. oneidensis* a NapC/NirT homolog, the tetraheme cytochrome CymA, is responsible for transferring electrons from the menaquinone pool to the periplasm during the respiration of most extracellular electron acceptors tested to date (57–61). In *G. sulfurreducens*, two redox

potential-dependent pathways are known: the heptaheme *c*-cytochrome ImcH (62), and the cytochrome CbcL with nine *c*-type hemes and two *b*-type hemes (63).

Once electrons have crossed the inner membrane, they must be transported across the periplasm. Both *G. sulfurreducens* and *S. oneidensis* express high levels of periplasmic electron transfer proteins. *G. sulfurreducens* encodes at least five periplasmic multi-heme cytochromes of which PpcA is the most abundant (64). This triheme *c*-cytochrome has four more homologs in the *G. sulfurreducens* genome and, while their individual role is still unclear, mutants lacking these cytochromes are defective in electron transfer to extracellular acceptors (65). *S. oneidensis* has two periplasmic cytochromes which are documented to interact with outer membrane cytochromes and assist electron transfer across the periplasm (66): FccA (67) and CctA (68), both of which are highly abundant.

A pathway for electron transfer across the outer membrane was first described in *S. oneidensis* where the model of "electron conduits" was first proposed. This model consists of two cytochromes from either leaf of the outer membrane anchored to the membrane by an integral outer membrane protein (69, 70). This anchor serves to align heme groups of both cytochromes close enough to allow electrons to flow through the whole complex (71), from one side of the outer membrane to the other. The three

components of the *S. oneidensis* electron conduit, MtrCAB, are essential for Fe(III) (68), flavin (72), Co(III) (73), and electrode (72) reduction, and they form a tight complex able to transfer electrons across membranes of proteoliposomes (70). These three proteins are also able to confer extracellular electron transfer abilities to heterologous hosts (74), albeit at much lower levels. Together, these data provide enough evidence to classify the MtrCAB family of electron conduit complexes as the key electron transfer pathways across the outer membrane of *S. oneidensis*.

In *G. sulfurreducens*, one example of an electron conduit has been identified. A complex made up of the integral outer membrane protein OmbB, periplasmic cytochrome OmaB, and lipoprotein cytochrome OmcB is necessary for wild type levels of Fe(III)-reduction (75, 76). These three proteins assemble into a membrane-bound complex and in purified form can transfer electrons across proteoliposome membranes (77). This OmcB-based electron conduit has not yet been shown to be functional in a heterologous host, but it is widely cited as the pathway for electron transfer across the outer membrane of *G. sulfurreducens* (78).

There are some important differences between the *S. oneidensis* and *G. sulfurreducens* pathways described above. While there are many homologs of MtrCAB encoded in the *S. oneidensis*

genome (68, 79), only the MtrCAB complex has been found to be necessary for Fe(III), flavin, Co(III), and electrode reduction. In contrast, within *G. sulfurreducens* there exists a duplication of *ombB-omaB-omcB* directly downstream (*ombC-omaC-omcC*), but unlike *S. oneidensis*, both of these gene clusters are reported to be necessary for wild-type levels of Fe(III)-reduction (77) yet neither of them have been shown to be involved in electrode reduction. Another important difference lies in the expansion of the MtrAB family, such as homologs complexed with an extracellular DMSO reductase that allow *S. oneidensis* to respire DMSO extracellularly (80). In *G. sulfurreducens* there are no additional homologs of the OmcB-OmcC conduits known, while other unrelated putative electron conduits appear to be encoded in the genome of *G. sulfurreducens* (81).

These convergent outer membrane electron transfer pathways share a characteristic where the intracellular components of these complexes are better conserved than the extracellular redox-active lipoprotein component. For example, not only are MtrAB homologs paired with extracellular components which have different enzymatic functions in *S. oneidensis* (such as DMSO reductases), but MtrA and MtrB are better conserved at the sequence level within the Shewanella genus than MtrC (70). Similarly, in *G. sulfurreducens ombBC* and *omaBC* are 100% identical to the nucleotide level, while *omcBC* only share 70% identity. It is easy to hypothesize that the extracellular

exposure of OmcBC and MtrC places more pressure on these components to adapt to environmental changes and differences in metal oxide minerals, but with an incomplete picture of electron conduit variability and functionality this remains a hypothesis.

Beyond the outer membrane, in both *S. oneidensis* and *G. sulfurreducens*, there are pathways for electron transfer across the extracellular space. *S. oneidensis* uses self-secreted flavins as electron shuttles to reach terminal electron acceptors (82, 83), whether these are needed only for substrates not in direct contact with cells or for all extracellular substrates is yet unclear (84, 85). *G. sulfurreducens* has a more complex extracellular electron transfer profile. The extracellular matrix of *G. sulfurreducens* contains cellular appendages, exopolysaccharides, and secreted *c*-cytochromes. Both cellular appendages and exopolysaccharides are important for cell adhesion to surfaces (56, 86), which Geobacter species are specialized for. *G. sulfurreducens* pili are also known to have conductive properties under some conditions (54), with aromatic residue chains being proposed as the electron transfer mechanism (53).

While it is difficult to separate phenotypes due to defects in attachment from those due to conductivity during a process requiring surface attachment, and account for variations in mineral or electrode and protein surface charge (56), pili are shown to be involved in establishing long-range electron transfer

pathway. Adding to this complexity is the fact that *G. sulfurreducens* also secretes multiheme *c*-cytochromes into this extracellular space (49, 87), where they bind to pili, minerals, or polysaccharides, and are necessary for wild type levels of Fe(III)-oxide reduction (88) or electrode reduction (49–51, 89).

After nearly four decades of research on extracellular electron transfer pathways, it is reasonable to expect there should be a few fundamental or highly conserved genes that could be used as markers for identifying metal reduction in genomes. Unfortunately, the basic functions of most sequenced multi-heme *c*-cytochromes in these systems are unknown. Cytochromes, especially those secreted outside the cell, are not widely conserved the way sulfate, nitrate or oxygen reduction pathways are conserved. With the increase in available sequencing data, each new genome adds novel multiheme *c*-cytochromes to databases. Attempts at clustering available *c*-cytochromes with the few well understood proteins fails to predict their roles. What is needed is solid physiological data liking sequence to function.

Chapter 2. Stratification of metabolic activity in current producing biofilms.

Grayson Chadwick*, Fernanda Jiménez Otero*, Jeffrey A. Gralnick, Daniel R. Bond, and Victoria J. Orphan.

(Modified from Chadwick *et al.*, in prep, 2018)

*Both authors contributed equally to this work

2.1 **Summary**

Geobacter sulfurreducens uses extracellular electron transport to grow using metal oxides or solid electrodes as its terminal electron acceptor for the oxidation of acetate. This model organism has been the subject of extensive study in microbial electrochemical systems due to its ubiquitous nature in natural enrichments, its rapid development of thick electroactive biofilms, and genetic tractability. While much is known about the physiology and performance of *G. sulfurreducens* biofilms on electrodes, key questions remain about how microscale gradients of redox potential and substrate concentrations within the biofilms affect the growth of cells at different levels, and how the combination of these factors influence the overall system performance. Here, we directly measure the anabolic activity of *G. sulfurreducens* biofilms at single cell resolution using stable isotope probing and secondary ion mass spectrometry. Our results demonstrate that *G. sulfurreducens* cells are most active when in contact with the anode surface and that this activity drops off more quickly than is often assumed in the literature. These results have important implications for our understanding of extracellular electron transfer and the growth penalties associated with respiring insoluble electron acceptors at great distances.

2.2 **Materials and Methods**

***Geobacter* growth.** All experiments were performed with our laboratory strain of *Geobacter sulfurreducens* PCA as freshly streaked single colonies from freezer stocks. Anaerobic NB medium (0.38 g/L KCl, 0.2 g/L NH_4Cl, 0.069 g/L $NaH_2PO_4H_2O$, 0.04 g/L $CaCl_22H_2O$, 0.2 g/L $MgSO_47H_2O$, 1% v/v trace mineral mix, pH 6.8, buffered with 2 g/L $NaHCO_3$ and flushed with 20:80 N_2:CO_2 gas mix) with 20 mM acetate as electron donor, 40 mM fumarate as electron acceptor was used to grow liquid cultures from colony picks. 3 cm^2 graphite flags were polished using 1500 grade sand paper (Gator) followed by 0.05 micron alumina slurry (Buehler) to serve as working electrodes. Sterile three-electrode conical reactors containing 15 mL of NB with 40 mM acetate as electron donor and 50 mM NaCl to equilibrate salt concentration were flushed with a mix of N_2-CO_2 gas (80:20, v/v) until the O_2 concentration reached less than 2 ppm. Liquid cultures were prepared by inoculating 1 ml liquid cultures from single colonies inside an anaerobic chamber. Once these cultures reached late exponential to stationary phase, they were used to inoculate 10 ml cultures with 10% v/v. Each reactor was then inoculated with 25% v/v from this liquid culture as it approached acceptor limitation, at an OD_{600} between 0.48 and 0.52. Working electrodes were set at either -0.1 V or +0.24 V vs SHE and average current density recorded every 12 seconds. All experiments were carried out at 30 °C.

Stable isotope probing. Once the desired biofilm growth stage had been reached, media was carefully exchanged for 15 mL of anaerobic NB containing 20 mM 6% ^{13}C-enriched acetate, 0.2 g/L 6% ^{15}N-enriched NH_4Cl, and 2% ^{2}H-enriched water. For negative control samples, regular NB electrode growth media was used instead of stable isotope enriched media. Biofilms were then incubated for 6 hours with working electrodes poised at the same potential as during growth, or changed to -100 mV (Figure 5).

Fixation and embedding. After stable isotope incubation, graphite electrodes were harvested from each reactor, rinsed with NB media to remove planktonic cells, fixed at room temperature for 1 hr (2% glutaraldehyde, 50 mM HEPES, pH 6.8), and stored at 4 °C in fixing solution. Negative controls were rinsed and incubated for 6 hours in stable isotope enriched media before storing back in fixing solution. Samples (still attached to graphite flag) were rinsed twice (50 mM HEPES, pH 7) before negative staining in 1% OsO_4, 50 mM HEPES, ph 7 for 2h. After rinsing again, samples were incubated for 1 hr in 1% uranyl-acetate and rinsed. Samples were then dehydrated with sequential 10 minute incubations in 25%, 50%, 75%, and 100% ETOH. A 50/50 v/v LR White resin (Sigma-Aldrich, uncatalyzed) and ETOH solution was used to incubate samples at room temperature overnight. Samples were then placed in 2 mL microcentrifuge tubes containing enough LR White solution (catalyzed with benzoyl peroxide) to

cover ~0.5 cm above the graphite flag (~1.5 mL) and incubated at 60 °C overnight.

2.3 **Introduction**

Microbial communities in nature exist predominantly as biofilms, dense cell aggregates coating multicellular organisms and mineral surfaces (90, 91). Together, they control cycling of metals, sulfur, nitrogen, and carbon in aquatic environments, sediments, soils, and subsurface environments (92–95). With high cell densities, biofilms often become structured due to limited diffusion of soluble nutrients, buffering agents, and respiratory substrates (90, 96–100). Stratification of biofilms into phenotypically (101) and metabolically (102) separate layers is well documented, creating microhabitats that alter a biofilm's ability to respire organic matter (94), access substrates for biodegradation (103), or be inhibited by antibiotics (91).

Less well understood are biofilms comprised of cells that must transfer respiratory electrons to extracellular minerals or insoluble acceptors. Of particular interest are metal-reducing bacteria grown on electrode surfaces acting as electron acceptors, which are the basis for electrochemical systems using microbial metabolic activity to convert organic substrates into electricity (104). Many of these electrode-reducing bacteria form conductive biofilms, allowing cells to share contact with an

electrode to cell layers 5 to 10 microns away. This beneficial conductivity creates a paradox for the community; cell layers closest to the electrode have best access to the electron acceptor, but those farther from the electrode have best access to soluble electron donors and buffering agents diffusing in from the top of the biofilm (105).

G. sulfurreducens is a model organism used for the study of extracellular electron transfer and biofilm conductivity (25, 33, 106–109), and can be routinely grown using solid anodes, insoluble metal oxides, or co-cultured using other organisms (110) as their terminal electron acceptor. Under optimal conditions with acetate as sole electron donor and a suitably poised electrode as the electron acceptor, *G. sulfurreducens* can form biofilms over 20 cell layers thick to produce current densities on the order of 1 $mA \cdot cm^{-2}$ (51, 111–113). Mutant analysis shows that respiration of cells not in direct contact with the electrode is supported by production of a complex conductive matrix composed of multiheme *c*-cytochromes (51, 112), polysaccharides (86), and pili (114). While the electrode biofilm model has demonstrated the general phenomenon of long-range electron transfer, a fundamental question remains about the formation of microscale gradients that limit metabolic activity of cells at different positions within the biofilm.

A universal observation during *Geobacter* experiments on poised electrodes is that in the early stages of colonization, each new layer of cells results in a proportional increase in total respiration, measured as electrical current. However, as biofilm thickness exceeds about 10 µm, additional biomass fails to increase total current, suggesting only a portion of cells in thick biofilms are active and stratification has occurred. The most common direct method used to investigate possible stratification of populations in these biofilms is cell viability stains in conjunction with confocal microscopy. Methods based on dyes distinguishing between intact and compromised membranes at high spatial resolution have yielded conflicting results, ranging from live cells at the interface with growth media and dead cells at the anode surface (37, 38), dead cells more distant from the electrode (35, 36), or all live cells throughout (39–41). An additional limitation of this approach is the lack of ability to distinguish between "viable" and "actively growing" states, and the recent observation that dyes meant to indicate "dead" cells accumulate inside actively respiring cells in response to high membrane potential (42).

Assessment of gene expression data has provided another measurement of cellular activity in *G. sulfurreducens* biofilms, either through physical separation of inner (0-20 µm) and outer (20-40 µm) biofilm layers and subsequent whole genome microarray analysis (115), or by the development of fluorescent reporters

driven by the promoters of interest (116). These transcriptional studies detected a very modest (115) or complete lack (116) of differentiation between such layers in *G. sulfurreducens* biofilms.

Approaches that measure conditions within *G. sulfurreducens* current producing biofilms include measurements of redox, pH, metabolites, or *c*-cytochrome oxidation states in a spatially resolved manner. While not direct assessments of cellular activity *per se*, these factors should exert control over, or be a product of, *G. sulfurreducens* metabolic activity. *C*-cytochromes are important electron carriers in the extracellular electron transfer process in these biofilms and have the benefit of characteristic UV/Vis and Raman spectroscopic signatures when in the oxidized and reduced states. This enabled analysis of total *c*-cytochrome oxidation state within current producing biofilms using either visual light (117, 118) or confocal Raman microscopy (48, 119, 120). Spectral studies have demonstrated that *G. sulfurreducens* catabolic activity results in the reduction of cytochromes, and suggested lower metabolic activity in layers more distant from electrodes based on the ratio of reduced to oxidized cytochromes increasing with distance from the anode surface. Redox measurements with microelectrodes have mirrored those of Raman-based cytochrome oxidation state, demonstrating a decrease of potential with distance from the anode surface (121).

Models based on diffusion within biofilms suggest that pH or nutrient conditions may be inhibitory close to the electrode surface. Measurement of pH gradients, either with pH sensitive dyes (122) or microelectrodes (121) have shown that pH can decrease nearly linearly from the outer surface of the biofilm to the anode surface, potentially reaching inhibitory levels at the innermost layers. Direct measurement of acetate concentrations within a very thick (>100 µm) *G. sulfurreducens* biofilm inside a chamber custom built to fit within an NMR instrument (123) demonstrated a gradual decrease in acetate concentration from the bulk solution to the base of the biofilm.

The above studies create a conflicting picture of physicochemical parameters within *G. sulfurreducens* biofilms, and how they affect cell growth at different depths. If pH and acetate concentrations decrease with depth, metabolic activity near the anode surface should be inhibited near the electrode. Conversely, if redox potential and *c*-cytochrome oxidation state are highest at the anode surface, the energetics of *G. sulfurreducens* growth should be most favorable at the anode surface. If the electrical conductivity of the biofilm is sufficiently high, a zone of growth within the center of the biofilm could form representing the intersection of buffering and nutrient influx with access to the electrode.

Sophisticated models of *G. sulfurreducens* biofilms in microbial electrochemical systems have predicted many of these conflicting stratification scenarios, including an increase in active biomass near the anode surface (124), and a pH-dependent limitation of overall biofilm current (125). Additionally, the recent identification of multiple redox potential-specific extracellular electron transfer pathways in *G. sulfurreducens* (8, 62, 63) raises the possibility that the various microhabitats within the biofilm support different populations of cells utilizing different metabolic machinery based on the prevailing energetics in their immediate surroundings.

To improve our understanding of stratification within electrode-reducing biofilms, we directly imaged the spatial anabolic activity patterns of *G. sulfurreducens* cells in biofilms at sub-cellular resolution by coupling stable isotope probing with nanometer scale secondary ion mass spectrometry (nanoSIMS). Biofilms were grown on graphite electrodes under conditions that have previously been extensively characterized and are optimized for reproducible biofilm growth (126, 127). At various points in biofilm development unlabeled growth media was substituted for stable isotope enriched growth media containing ^{15}N-enriched ammonium, ^{13}C-enriched acetate and ^{2}H-enriched water. ^{15}N, ^{13}C and ^{2}H incorporation was visualized at <100 nm spatial resolution, allowing for unambiguous assignment of *G. sulfurreducens* activity patterns at the single-cell level within biofilms at various

stages of development. In all cases data revealed the highest anabolic activity at the electrode surface, with a near-linear decline in activity with distance from the electrode. This distance-dependent decline was also evident in biofilms only a few cells thick, suggesting that diffusion of nutrients or buffers was not the primary cause.

2.4 **Results**

2.4.1 **Metabolic activity gradient decreases from electron acceptor towards edge of biofilm.**

In order to analyze metabolic activity within current producing biofilms, *G. sulfurreducens* biofilms were grown with graphite electrodes poised at +240 mV vs SHE as sole terminal electron acceptor. Once the exponential phase of current production had ceased, and current had reached a plateau (see arrow on Fig. 2.1A), normal growth media was replaced by growth media containing ^{15}N-enriched ammonium, ^{13}C-enriched acetate and ^{2}H-enriched water. As previously shown these media exchanges had little effect on the overall current density (126), and the effect of isotopically labeled media paralleled that of a regular media control (Fig. 2.1A). After an incubation period corresponding to the known doubling time of *G. sulfurreducens* during exponential growth (6.2 +/- 0.7 h, n=7), biofilms were fixed, stained and embedded in resin for electron microscopy

(Fig. 2.1B) and nanoSIMS analysis (Fig. 2.2-2.3). Electron microscopy showed biofilms 15-20 µm in depth with cells in the inner layers oriented perpendicularly to the electrode surface (Figure 1B, 83 hours of growth). Beyond ~10 µm the cells in the upper layers of the biofilm lost this orientation and appeared less tightly packed. These ultrastructural features are similar to those previously demonstrated for *G. sulfurreducens* grown on electrodes (51, 112).

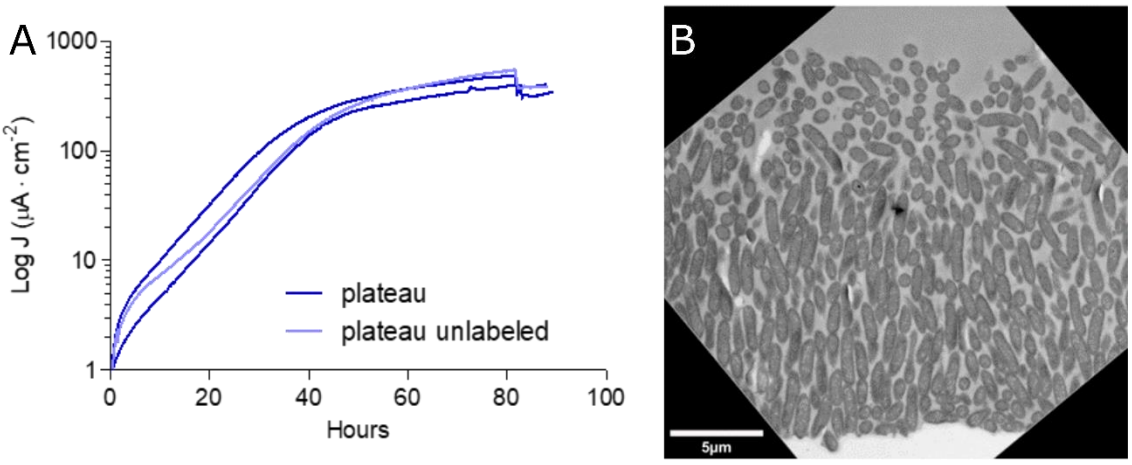

Figure 2.1 Current production and structure of *G. sulfurreducens* biofilm after current density plateau. Current density generation (**A**) and transmission electron microscopy images (**B**) of *G. sulfurreducens* biofilms. Cells were inoculated at time zero on anodes poised at +240 mV and after 83 hours of growth (see arrow), normal growth medium was exchanged with stable isotope labeled medium.

Thin sections of resin-embedded biofilms were deposited on silicon wafers and analyzed for stable isotope incorporation by collecting the $^{1}H^{-}$, $^{2}H^{-}$, $^{12}C^{-}$, $^{13}C^{-}$, $^{14}N^{12}C^{-}$ and $^{15}N^{12}C^{-}$ ions. The $^{14}N^{12}C^{-}$

ion image is best for visualizing the *G. sulfurreducens* biomass because there is no nitrogen in the embedding resin (Figure 2.2). The heavy nitrogen ion $^{15}N^{12}C^-$ alone, as well as the ^{15}N fractional abundance images show the same increase in incorporation of ^{15}N at the bottom surface of the biofilm where the cells interface with the anode (Figure 2.2B and C). This maximum at the anode interface decreases with distance from the anode surface to a minimum approximately 10 microns from the anode. After this minimum a second small peak in cellular anabolic activity is observed in the uppermost layers of the biofilm, although the distribution of activity is more heterogeneous than in the inner layers.

To quantify these observations all pixels were binned according to their distance from the anode surface at half micron increments. The ^{15}N fractional abundance for all nanoSIMS acquisitions of triplicate biofilms grown at +240 mV are shown in Figure 2.2D. The features of these isotope enrichment curves are reproducible, including an early peak in activity between 1-2 microns from the anode surface, a steady decrease to a minimum value, and a rise to secondary small symmetric peak between this minimum and the outer surface of the biofilm.

Because the fractional abundance of ^{15}N added to growth media was 0.06, a previously unlabeled cell doubling in 6 hours would be expected to reach a ^{15}N fractional abundance value of

approximately 0.03 in our experiments. Peak values of fractional abundance were observed to be between 0.015 and 0.025 at the anode surface, allowing us to infer that cells closest to the electrode may have nearly doubled in the six hours of the stable isotope probing experiment, even though they remain at the base of the biofilm farthest from the growth medium.

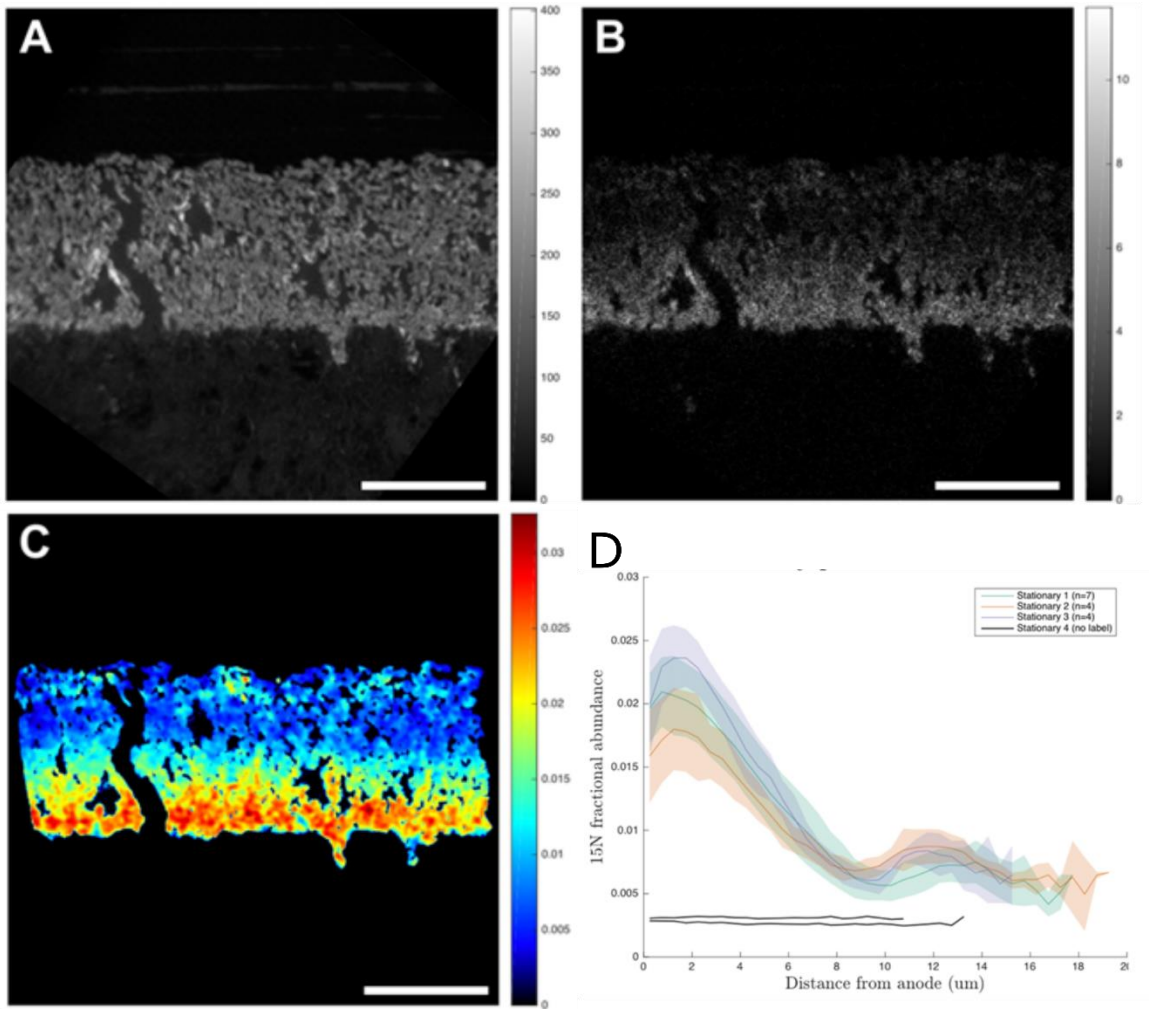

Figure 2.2 ^{15}N incorporation reveals anabolic activity pattern within *G. sulfurreducens* biofilms. Representative nanoSIMS analysis of *G. sulfurreducens* biofilms. **A**) $^{14}N^{12}C^-$ ion image demonstrating biofilm morphology and spatial resolution. Graphite anode is located below the biofilm. Heavy nitrogen isotope image $^{15}N^{12}C^-$ (**B**) and ^{15}N fractional

abundance image (**C**) reveal an enrichment at the anode surface. (**D**) Anabolic activity patterns in replicate *G. sulfurreducens* biofilms, n=3. Colored lines represent the average ^{15}N fractional abundance for analyses of different locations within a single biofilm. Transparent envelopes surrounding lines represent standard deviation of fractional abundance at each distance. Black lines represent controls that were chemically fixed before incubating with isotopically labeled media, indicating live cells are required for isotope incorporation.

The fractional abundances of ^{15}N, ^{13}C and ^{2}H depicted in Figure 2.3A-C show the clear enrichment at the biofilm-anode interface. The pattern of ^{15}N, ^{13}C, and ^{2}H incorporation with distance from the anode surface all behaved in a similar manner (Figure 2.3D-F) as was expected for these analogous anabolic activity markers, although the data from ^{15}N yielded the highest signal-to-noise ratio since there was no nitrogen in the resin diluting the signal from the stable isotope probing experiment (128).

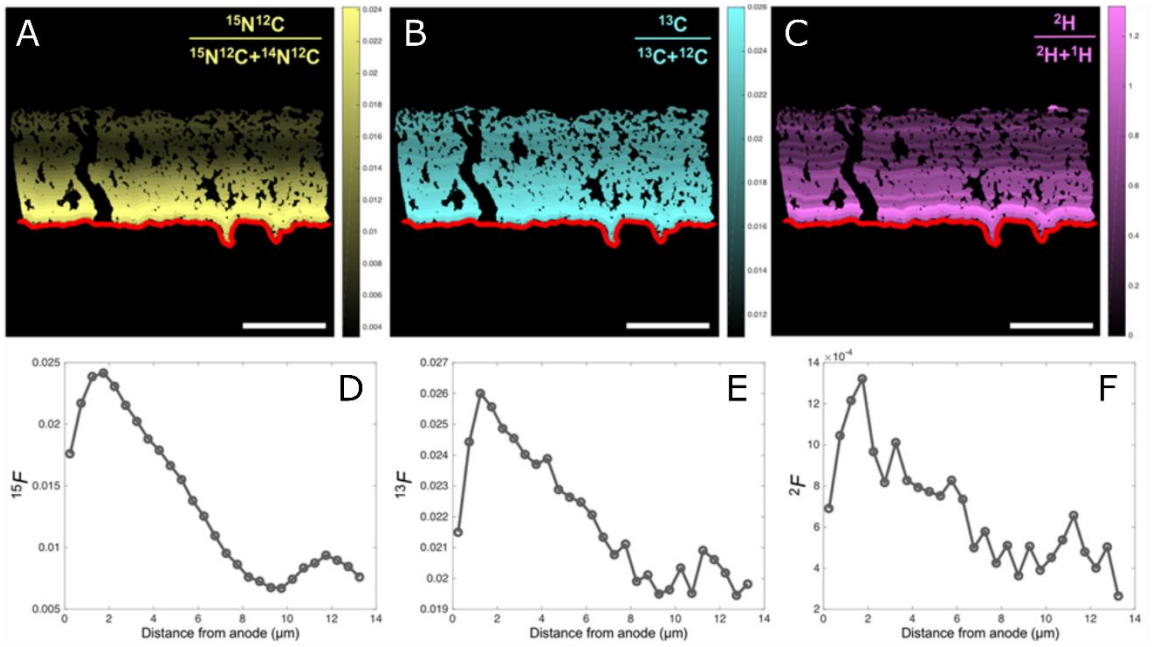

Figure 2.3 ^{13}C and ^{2}H incorporation follow ^{15}N pattern with higher background noise. Fractional abundance of ^{15}N (**A**), ^{13}C (**B**) and ^{2}H (**C**) binned every half micron from the anode surface (red line). **D**–**F**) half-micron binned fractional abundance as a function of distance from electrode for ^{15}N, ^{13}C, and ^{2}H, respectively from representative samples.

2.4.2 **Exponentially growing biofilms already develop anabolic activity gradient.**

Early in growth experiments, when current and biomass is increasing exponentially and biofilms are only ~5 µm thick, all cells are hypothesized to be doubling at a similar and maximal rate. Samples from this growth phase were analyzed to determine the maximum anabolic activity of growing cells, and test if such biofilms were free of metabolic stratification.

Duplicate biofilms harvested during exponential phase (Fig. 2.4A) had regions of biofilm width between 2-5 µm (Fig. 2.4B and C, 35 hours of growth), but all exhibited a similar trend of isotope incorporation (Fig. 2.4D). Importantly, the peak enrichment value reflecting anabolic rate was indistinguishable from thicker biofilms, and occurred at the same location in the biofilm as older biofilms. This indicates that the metabolic activity of cells in the upper layers of thick biofilms did not inhibit the growth of their brethren at the anode surface, either by consuming acetate before it diffused to the inner layers or by acidification. Even in these thin biofilms, a decline in metabolic activity was detected with increasing distance, following the same trend as seen in thicker biofilms.

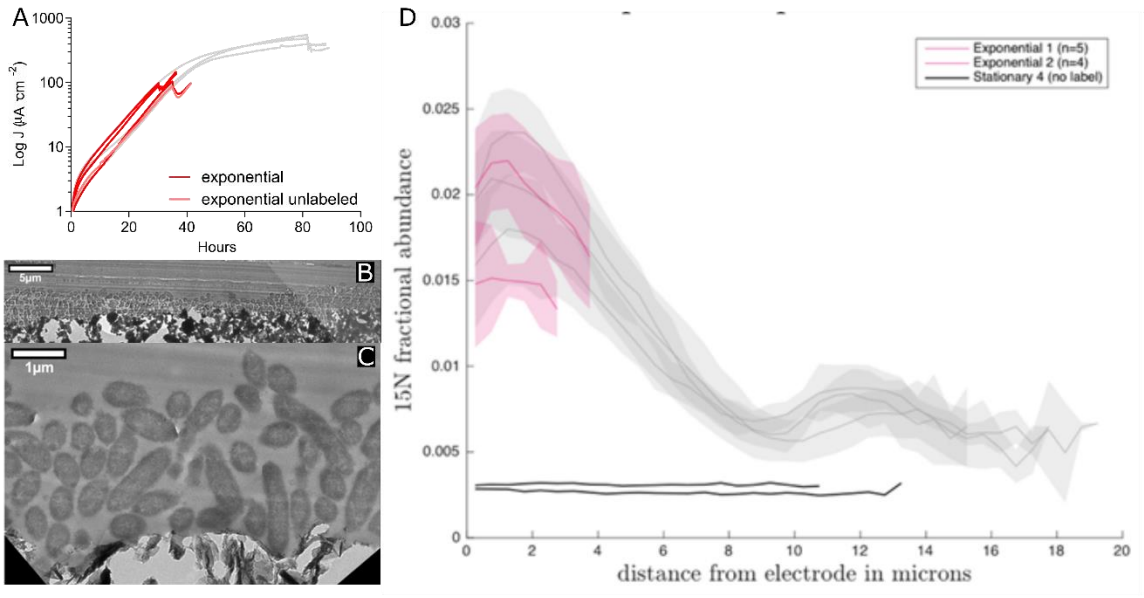

Figure 2.4 Anabolic activity pattern is already present during exponential phase. Current density generation (**A**) and transmission electron microscopy images (**B-C**) of representative *G. sulfurreducens* biofilms harvested during exponential phase. Graphite electrode poised at +240 mV vs. SHE served as sole terminal electron acceptor and normal growth media was exchanged with stable isotope labeled media after 35 hours of growth (arrow on A). (**D**) Anabolic activity patterns in duplicate *G. sulfurreducens* biofilms. Red lines represent the average ^{15}N fractional abundance for analyses of different locations within a single biofilm. Transparent envelopes surrounding lines represent standard deviation of fractional abundance at each distance. Black lines represent controls that were chemically fixed before incubating with isotopically labeled media. For comparison, data from **A** and **D** is overlayed on data in gray from **Fig. 2.1A** and **Fig. 2.2D**, respectively.

2.4.3 **Reduction potential has modest effect on anabolic activity gradient**

Lowering the redox potential of the anode can slow electron transfer by *G. sulfurreducens*, but could also lower demands on the conductive network or slow consumption of nutrients relative to diffusion into the film. To test whether the stratification patterns were affected by the potential of the anode, we analyzed

the isotope incorporation pattern of *G. sulfurreducens* biofilms grown at -100 mV vs. SHE (129). Four separate biofilms were grown at this lower potential, subjected to labeled media at various points during stationary phase (Fig. 2.5A), and analyzed as before with isotope incorporation data binned every half micron from the surface of the anode (Fig. 2.5B and C). The major similarity between these biofilms and those grown at +240 mV is the dominant trend of decreasing metabolic activity with increasing distance from the anode surface, with the decline in activity occurring more rapidly when redox potential was lower. At -100 mV, both the initial subtle increase in current over the first 1-2 microns, and the second peak of activity beyond 10 µm are absent, yielding a much simpler activity pattern which decreases monotonically with distance from the anode.

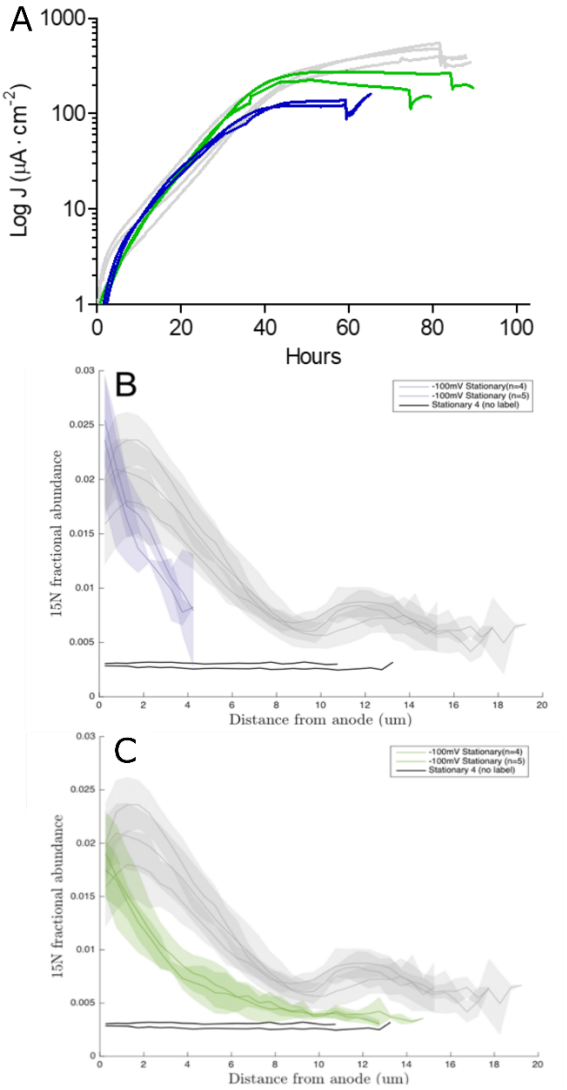

Figure 2.5 Lowering reduction potential of poised electrode changes small features but not overall anabolic activity pattern of *G. sulfurreducens* biofilms. (**A**) Current density production by *G. sulfurreducens* biofilms grown with graphite electrodes poised at -100 mV vs. SHE as sole terminal electron acceptor. Normal growth media was exchanged with stable isotope labeled media at two time points (see arrow) with duplicates represented in blue and green. (**B-C**) Anabolic activity patterns in replicate *G. sulfurreducens* biofilms. Blue and green lines represent the average ^{15}N fractional abundance for analyses of different locations within a single biofilm and match their respective sample color in **A**. Transparent envelopes surrounding lines represent standard deviation of fractional abundance at each distance. Black lines represent controls that were chemically fixed before incubating with isotopically labeled media. For comparison, data from **A-C** is overlayed on data in gray from **Fig. 2.1A** and **Fig. 2.2D**, respectively.

2.4.4 **Altering energetics at the electrode surface does not immediately change anabolic activity pattern.**

To determine whether the features lost during growth at -100 mV could be rapidly recovered by a sudden transition to +0.240 mV, we grew two additional biofilms at -100 mV to maximum current, added labeled growth media and changed the electrode potential to +240 mV. The resulting ^{15}N fractional abundance plots resembled those grown and labeled at -100 mV, including the immediate decrease in isotope incorporation and lack of significant peaks at the surface of the biofilm (Fig. 2.6). This indicated that these biofilms could not remodel within 6 h to alter this dominant stratification profile, and that increased driving force at the base of the biofilm could not be used by cells distant from the electrode during this 6 h labeling experiment.

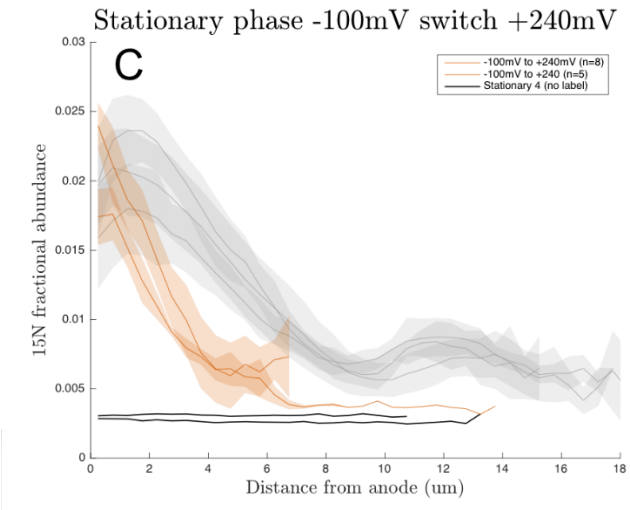

Figure 2.6 Anabolic activity pattern does not change once biofilms reach maximum current, even if reduction potential is more favorable. Duplicate *G. sulfurreducens* biofilms were grown with graphite electrodes poised at -100 mV vs. SHE as sole terminal electron acceptor. After maximum current was reached, normal growth media was exchanged with stable isotope labeled media and the reduction potential of the working electrode was raised to +240 mV vs. SHE. Orange lines represent the average ^{15}N fractional abundance for analyses of different locations within a single biofilm. Transparent envelopes surrounding lines represent standard deviation of fractional abundance at each distance. Black lines represent controls that were chemically fixed before incubating with isotopically labeled media. For comparison, data is overlayed on data in gray from **Fig. 2.2D**.

2.4.5 **Extended biofilm operation does not change location of metabolically active cells.**

The above results indicate that as the biofilm transitions from an exponential growth to a phase of maximum current, cells in the outer layers of the biofilm are at a great anabolic disadvantage compared to their counterparts at the biofilm-anode interface. However, most microbial electrochemical applications utilize biofilms maintained for weeks in this plateau phase, and many of the conflicting reports describing stratification of live cells to the top of the biofilm are derived from such long-term experiments.

To investigate metabolic activity in biofilms maintained for weeks without interruption, four replicate *G. sulfurreducens* biofilms were grown for two weeks with normal growth media. Medium was exchanged as needed to maintain current production above 500 $\mu A \cdot cm^{-2}$ for this entire period. After this extended operation biofilms were labeled and prepared as before. Electron

microscopy images revealed biofilms that were very thick, up to 80 µm. However, cells on the top surface of the biofilm had begun to lyse or consume their cellular material as all cells had very low density in all four replicates (Fig. 2.7). The frequency of intact cells increased with depth into the biofilm, until at the anode-biofilm interface where nearly all cells still appeared intact, as determined by cell morphology and electron density in the cytoplasm. Representative nanoSIMS images demonstrate that cells located at the anode were still metabolically active at levels similar to those during early stages of biofilm growth. Intact cells in the biofilm far from the anode were for the most part anabolically inactive, with only occasional weak enrichment.

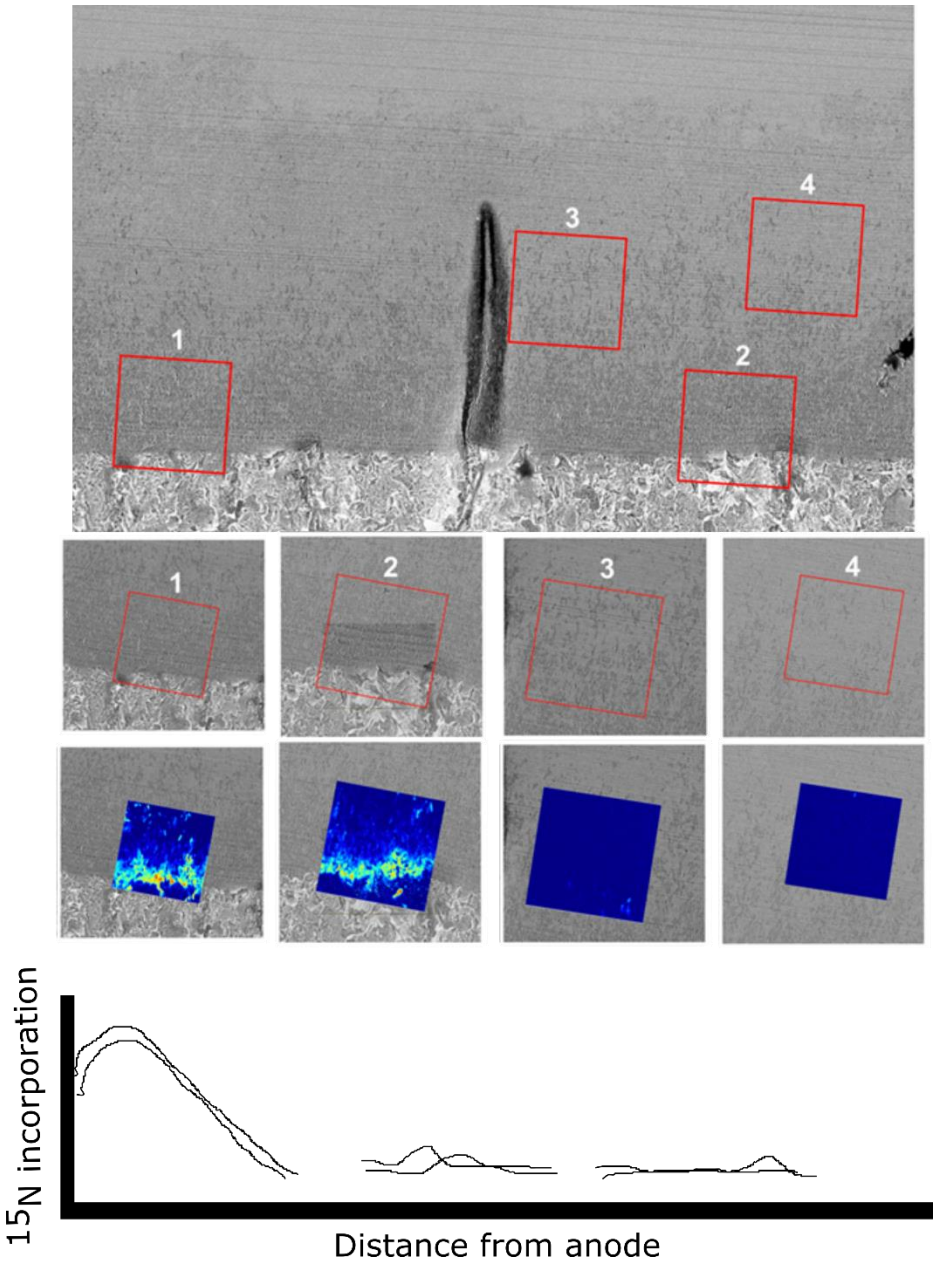

Figure 2.7 Anabolic activity pattern of *G. sulfurreducens* biofilms does not change after current plateau is maintained for two weeks. Electron microscopy and nanoSIMS analysis of representative two-week old biofilm. Large overview image of a two week old biofilm grown at +240 mV demonstrates the thickness of the biofilm and the presence of regions of cell lysis in the upper light layers. Representative nanoSIMS images were taken in regions 1-4. The $^{14}N^{12}C^-$ ion image is shown overlaid on the SEM image along with the ^{15}N fractional abundance images.

2.5 **Discussion**

The results presented here demonstrate that *G. sulfurreducens* biofilms experience a growth penalty with increasing distance from the anode surface. This result is robust to both the level of biofilm maturation and the reduction potential of the anode. Similar level of ^{15}N incorporation is observed by cells at the anode surface in thin biofilms during exponential phase and thick biofilms producing maximum current, indicating that cells in the upper layers of the biofilm do not inhibit the inner layers by consuming substrate or by the production of toxic byproducts. Additionally, the fastest cell growth rates in exponential and stationary phases are indistinguishable, so this does not appear to be the explanation for why current generation reaches a limit. The pattern of anabolic activity dominating in a relatively thin region at the anode surface was true even after two weeks of biofilm growth, indicating that the dominant synthesis of new biomass throughout all stages of biofilm development occurs at the anode, pushing old, anabolically inactive, biomass outward.

The transition between exponential growth phase and current generation plateau seems to correlate with two major changes in the biofilm. First, our results reveal that at 10 microns the anabolic activity is at a minimum, regardless of the reduction potential at which the electrode is poised. Second, the

orientation of the cells roughly perpendicular to the anode surface breaks down at approximately this same point. After this transition the high and low potential biofilms diverge in total current production and anabolic activity patterns. The biofilms grown at high potential increase their current at a slower but steady rate (Fig. 2.1A), and exhibit modest anabolic activity in their outermost layers (Fig. 2.2D). The low potential biofilms on the other hand exhibit a sharp end of current increase (Fig. 2.5A), as well as a lack of surface anabolic activity (Fig. 2.5B and C). We hypothesize that in the high potential experiments this outer layer of cells may be adapting to respiration at redox potentials well below the applied +240 mV. This notion is consistent with the redox potential and *c*-cytochrome oxidation state measurements made previously (44, 48, 119, 120, 130, 131). The low effective redox potential in these outer layers must still be high enough to allow acetate oxidation to proceed since the increase in biomass in this outer layer contributes positively to the current, but the energetics are not as favorable as those supporting the cells growing in the inner layers, leading to the decreased anabolic activity in these upper layers. The physiological shift to lower redox potentials could be due to the utilization of different extracellular electron transfer pathway, such as the low potential-specific quinol oxidase CbcL(129). The difference in cell yield between the high potential (ImcH) and low potential (CbcL) system has been

quantified, showing that higher cell yields are achieved when only the high potential system is available (8). A metabolic shift at distance from the anode surface is consistent with the recently proposed increase in importance of pili over cytochromes in *G. sulfurreducens* cells above 10 microns in current producing biofilms (132). It is possible that the spottiness of anabolic activity in these outer layers is the result of some cells being "disconnected" from whatever electrical conduits their active neighbors still maintain with the higher potential inner layers.

The biofilms grown with the anode poised at -100 mV vs. SHE will experience a decrease in redox potential from a starting point 340 mV more negative than the high potential biofilms. By the time these biofilms reach stationary phase the prevailing redox potentials at the surface of the biofilm maybe be too negative to support any metabolism, catabolic or anabolic. This would explain why increasing biofilm depth in phase does not lead to increased current generation, and why there is no second peak of anabolic activity in the outer layers. The biofilm will continue to grow in thickness due to the anabolic activity of the cells at the anode surface, but the cells at the top of the biofilm will be metabolically inactive and contribute nothing to the catabolic current. Even under high potential conditions it appears that the biofilm can grow too thick to support the growth of cells in the outer layers, leading to inactivity and ultimately cell lysis.

Here we have presented the first direct measurement of *G. sulfurreducens* anabolic activity at high spatial resolution within current-producing biofilms. Our results highlight the uniqueness of current-producing biofilms, which stratify in a different pattern than canonical biofilm models, with the most anabolically active cells in bottom layers instead of dead or persistor cells. Our results demonstrate that the combined effect of all the factors influencing cellular metabolism within electroactive biofilms favors growth at the anode surface. This dispels the notion that pH and substrate limitation may inhibit the growth of cells in the inner layers of the biofilm, and suggests that the major mode of biofilm growth is cell proliferation at the anode pushing biomass outward. These results support the widely held conclusion that *G. sulfurreducens* can respire the anode at distances exceeding 10 µm from the anode surface, but that this metabolism-at-a-distance comes with an energetic cost, which is eventually inhibitory to cell growth at large enough distances. While the exact pattern of activity will vary between reactor designs, substrate concentrations, buffering capacity of the media, etc. we hope that the data presented here can be used to improve models of *G. sulfurreducens* growth and performance of electroactive biofilms. Follow-up studies testing some of these models using mutants in important extracellular electron transfer pathways and additional growth condition variations will further help to understand the physiology of *G.*

sulfurreducens biofilms. Additionally, these findings help understand how the limitations of the extracellular electron transfer process may affect the structure of natural communities thought to be dependent on this process.

Chapter 3. Different gene clusters encoding putative outer membrane electron conduits are necessary or sufficient during metal and electrode respiration in *Geobacter sulfurreducens*.

Fernanda Jiménez Otero, Chi Ho Chan, and Daniel R. Bond

(Modified from Jiménez Otero *et al*., submitted 2018)

3.1 **Summary**

At least five gene clusters in the *Geobacter sulfurreducens* genome encode putative outer membrane 'electron conduits', or complexes containing a periplasmic multiheme *c*-cytochrome, integral outer membrane anchor, and outer membrane redox lipoprotein(s). Markerless single gene cluster deletions and all possible multiple deletion combinations were constructed and grown with soluble Fe(III) citrate, Fe(III)- and Mn(IV)-oxides, and graphite electrodes poised at +0.24 V and -0.1 V vs. SHE. Different gene clusters were necessary for reduction of each electron acceptor. During metal oxide reduction, deletion of the previously described *omcBC* cluster caused defects, but deletion of additional components in the Δ*omcBC* background, such as *extEFG,* was needed to produce defects greater than 50% compared to wild type. Deletion of all five gene clusters abolished all metal reduction. During electrode reduction, only the Δ*extABCD* mutant had a severe growth defect at both redox potentials, but this mutation did not affect Fe(III)-oxide, Mn(IV)-oxide, or Fe(III) citrate reduction, further suggesting substrate-specific pathways. Some mutants containing only one cluster were able to reduce particular terminal electron acceptors better than wild type, suggesting routes for improvement by targeting substrate-specific electron transfer pathways. Transcriptomic comparisons between wild type and the strain containing only *extABCD* detected no significant changes in the expression of known redox proteins

or pilin components suggesting this strain has a streamlined pathway for electron transfer across the outer membrane not resulting from off-target effects. Our results suggest *G. sulfurreducens* may utilize different outer membrane conduits depending on the available extracellular electron acceptor.

3.2 **Introduction**

Microorganisms capable of extracellular respiration can alter the redox state of particulate metal oxides in soils and sediments, controlling their solubility and bioavailability (92, 133–137). To respire extracellular metals, bacteria must transfer electrons from the cell interior to outer surface redox proteins, requiring unique mechanisms compared to growth with intracellularly-reduced electron acceptors. The use of surface-exposed electron transfer proteins also presents opportunities for transformation of heavy metals, biological nanoparticle synthesis, and a new generation of microbially-powered electrochemical devices using bacteria grown on electrodes (22, 24, 26, 33, 106, 138, 139).

An extracellular electron transfer strategy must overcome several biological and inorganic issues. In Gram-negative cells, a conductive pathway capable of crossing the inner membrane, periplasm, and outer membrane must first be constructed (78, 140). Such pathways are capable of delivering electrons to

soluble metals or redox-active molecules, but insoluble metal oxides present additional challenges. Fe(III)- and Mn(IV)-oxides vary widely in chemistry, surface charge, redox state, and surface area, thus an additional suite of proteins or appendages may be needed to link cell surfaces with different terminal minerals (3, 141, 142).

Many metal-reducing bacteria can also transfer electrons to electrodes (26, 47, 48, 143). Unlike metal oxide particles, electrodes represent an unlimited electron acceptor allowing cells directly in contact with the inorganic surface to remain in contact with and support growth of more distant cells, creating a conductive network of proteins that relay electrons to cells at the electrode. The physiological and chemical differences between soluble and insoluble metals, or between metal particles and electrodes, raises the possibility that different electron transfer proteins may be needed to access each kind of extracellular mineral, surface, or molecule.

A model organism widely studied for its ability to reduce a diversity of metals and electrodes is the δ-Proteobacterium *Geobacter sulfurreducens*, and recent work suggests this organism uses different membrane-bound electron transfer proteins depending on conditions. CbcL, a combination *c*- and *b*-type inner membrane cytochrome (63), is only required when extracellular metals and electrodes are below redox potentials of -0.1 V vs.

SHE, while the inner membrane *c*-type cytochrome ImcH (62), is essential when acceptors are at higher redox potentials (142). Beyond the outer surface, the secreted cytochrome OmcZ is needed only during electrode growth, while the secreted cytochrome PgcA only enhances reduction of Fe(III)-oxides (49, 87–89, 144–146). Between the initial CbcL/ImcH-dependent event of inner membrane proton motive force generation and extracellular OmcZ/PgcA interfacial interactions lies the outer membrane, a less well understood barrier that was recently found to contain electron transfer proteins of surprising complexity (69, 77, 81).

The only known mechanism for non-diffusive electron transfer across the outer membrane is through a '*c*-cytochrome electron conduit', consisting of an integral outer membrane protein proposed to anchor a periplasmic multiheme cytochrome to an outer surface lipoprotein cytochrome. By linking heme cofactors through a membrane spanning complex, electron flow is permitted (69, 70). The first electron conduit described was the ~210 kDa MtrCAB complex from *S. oneidensis*, which will catalyze electron transfer across membranes to extracellular substrates when purified and placed in lipid vesicles (79, 147, 148). The *mtrCAB* gene cluster is essential for reduction of all tested soluble metals, electron shuttles, metal oxides, and electrodes by *S. oneidensis* (72, 79, 149). Related *c*-cytochrome complexes capped with an extracellular DMSO reductase allow *Shewanella* to reduce DMSO on the cell exterior, while similar conduits support

electron uptake by Fe(II)-oxidizing *Rhodopseudomonas* TIE-1 cells (80, 150).

In *G. sulfurreducens*, a gene cluster encoding the periplasmic cytochrome OmbA, the outer membrane integral protein OmaB, and lipoprotein cytochrome OmcB also forms a conduit complex functionally similar to MtrCAB, though the two complexes lack sequence similarity (77). This '*ombB-omaB-omcB*' gene cluster is duplicated immediately downstream in the *G. sulfurreducens* genome as the near-identical '*ombC-omaC-omcC*', together forming the '*omcBC*' cluster. Antibiotic cassette insertions within *omcB*, as well as insertions replacing the entire '*ombB-omaB-omcB*' conduit decrease growth with Fe(III) as an electron acceptor, but the impact differs between reports and growth conditions (75, 76, 151). This variability between studies could be due to polar effects from inserted cassettes, partial complementation by duplicated components, or the presence of undiscovered alternative pathways able to catalyze electron transfer across the outer membrane. These conflicting results highlight the need for careful genetic analysis using genetic tools recently applied to *G. sulfurreducens*.

Further evidence for undiscovered outer membrane complexes was inferred from genomic data (81) and later detected in genome-wide transposon data, where insertions in *omcB* or *omcC* had no effect on *G. sulfurreducens* growth with electrodes poised at -0.1

vs. SHE, a low potential chosen to mimic the redox potential of Fe(III)-oxides (152). Transposon insertions within an unstudied four-gene cluster containing *c*-cytochrome conduit signatures caused significant defects during growth on -0.1 V electrodes (152). Deletion of this new cluster, named *extABCD*, severely affected growth on low-potential electrodes, while Δ*extABCD* mutants still grew similar to wild type with Fe(III)-oxides. In contrast, deletion of both conduits contained in the *omcBC* cluster had little impact on low-potential electrode growth (152). These data suggested that the outer membrane proteins essential for electron transfer could vary depending on environmental conditions, but also raised new questions; are different genes necessary at higher redox potentials, during growth with mineral forms such as Mn(VI), or when metals become soluble?

At least five outer membrane electron conduits may be encoded in the genome of *G. sulfurreducens*. Using new markerless deletion methods, this study constructed combinations of mutants lacking all possible combinations of these gene clusters, and compared growth using Fe(III)- and Mn(IV)-oxides, poised electrodes at two different redox potentials, and soluble Fe(III)-citrate as terminal electron acceptors. We found that, during metal reduction, the largest defects were in Δ*omcBC* strains, but deletion of the newly identified cluster *extEFG* in the Δ*omcBC* background was needed to severely inhibit Fe(III)-

reduction. Deletion of all five clusters was necessary to eliminate reduction of the soluble and insoluble metals tested. Strains containing only a single cluster showed preferences for reduction of different metals, such as the *extEFG*- and *extHIJKL*-only strains performing better with Mn(IV)-oxides than Fe(III)-oxides. During electrode reduction, only strains lacking *extABCD* showed a growth defect when electrodes were the electron acceptor, and this effect was similar at all redox potentials. A strain still containing *extABCD* but lacking all other conduit clusters grew faster and to a higher final density on electrodes. Whole genome sequencing and transcriptomic analysis found no unintended mutations in any strain or significant changes in expression in response to the deletions. These data provide evidence that different *G. sulfurreducens* conduit clusters are needed for extracellular electron transfer to different substrates.

3.3 **Materials and Methods**

Growth conditions. All experiments were performed with our laboratory strain of *Geobacter sulfurreducens* PCA as freshly streaked single colonies from freezer stocks. Anaerobic NB medium (0.38 g/L KCl, 0.2 g/L NH_4Cl, 0.069 g/L $NaH_2PO_4H_2O$, 0.04 g/L $CaCl_22H_2O$, 0.2 g/L $MgSO_47H_2O$, 1% v/v trace mineral mix, pH 6.8, buffered with 2 g/L $NaHCO_3$ and flushed with 20:80 N_2:CO_2 gas mix)

with 20 mM acetate as electron donor, 40 mM fumarate as electron acceptor was used to grow liquid cultures from colony picks. For metal reduction assays, 20 mM acetate was added with either 55 mM Fe(III) citrate, ~20 mM birnessite (Mn(IV)-oxide), or ~70 mM Fe(III)-oxide freshly precipitated from $FeCl_2$ by addition of NaOH and incubation at pH 7 for 1 h before washing in DI water. Fe(III)-oxide medium contained an increased concentration of 0.6 g/L $NaH_2PO_4H_2O$ to prevent further crystallization of the metal after autoclaving. All experiments were carried out at 30°C.

Deletion and complementation construction. Putative conduits were identified through a genomic search for gene clusters containing loci predicted to encode a β-barrel using PRED-TMBB (153), contiguous to periplasmic and extracellular multiheme *c*-cytochromes or other redox proteins. Localization was predicted by comparing PSORT (154) and the presence/absence of lipid attachment sites (155). Constructs to delete each gene cluster were designed to recombine to leave the site marker-free and also non-polar when located in larger transcriptional units, with most primers and plasmids for the single deletions described in Chan *et al.*, 2017. When genes were part of a larger transcriptional unit or contained an upstream promoter, it was left intact. For example, in the case of the *omcBC* cluster the transcriptional regulator *orfR* (GSU2741) was left intact, and in

extEFG the promoter and untranslated region was left intact so as to not disrupt the downstream loci.

For deletion mutant construction, the suicide vector pK18*mobsacB* (156) with ~750 bp flanking to the target region was used to induce homologous recombination as previously described (157). Briefly, two rounds of homologous recombination were selected for. The first selection used kanamycin resistance to select for mutants with the plasmid inserted into either up or downstream regions, and the second selection used sucrose sensitivity to select for mutants that recombine the plasmid out of the chromosome, resulting in either wild type or complete deletion mutants. Deletion mutants were identified using a kanamycin sensitivity test and verified by PCR amplification targeting the region. Multiple PCR amplifications with primers in different regions were used to confirm full deletion of each gene cluster (Chan *et al*., 2017 and Table S1).

During this work, we found that manipulations in the *omcBC* cluster, which contains large regions containing 100% identical sequences, frequently underwent recombination into unexpected hybrid mutants which could escape routine PCR verification. For example, when the *omaB* and *omaC* genes recombined, a large hybrid operon containing *omaB*-linked to *ombC*-*omc*C would result. Routine primer screening, especially targeting flanking regions, failed to detect the large product. Only via multiple internal primers (Chan *et al*., 2017 and Table S1), as well as longer-read or

single molecule sequencing, were we able to verify and isolate strains in which complete loss of the *omcBC* cluster occurred, and dispose of hybrid mutants. Whole-genome resequencing was also performed on strains containing only one cluster, such as the strain containing only *extABCD*, especially since this strain has an unexpected phenotype where it produced more current than wild type. Thorough verification by PCR and whole genome sequencing are recommended to confirm deletions of large and repetitive regions such as the *omcBC* cluster.

Mutants lacking a single gene region were used as parent strains to build additional mutations. In this manner, six double gene-cluster deletion mutants, four triple-cluster deletion mutants and one quintuple-cluster deletion mutant lacking up to nineteen genes were constructed (Fig. 1; Table 1). For complementation strains, putative conduits were amplified using primers listed in Table S1 and inserted into the *G. sulfurreducens* expression vector pRK2-Geo2 (157), which contains a constitutive promoter P_{acpP}. The putative conduit *extABCD* was

assembled into a single transcriptional unit to ensure expression.

Strains and Plasmids	Description or relevant genotype	Reference
Geobacter sulfurreducens strains		
DB1279	ΔGSU2731-39 (Δ*omcBC*)	Chan *et al.*, 2017
DB1280	ΔGSU2645-42 (Δ*extABCD*)	Chan *et al.*, 2017
DB1281	ΔGSU2940-36 (Δ*extHIJKL*)	Chan *et al.*, 2017
DB1282	ΔGSU2724-26 (Δ*extEFG*)	Chan *et al.*, 2017
DB1487	ΔGSU2731-39 ΔGSU2645-42 (Δ*omcBC* Δ*extABCD*)	This study
DB1488	ΔGSU2731-39 ΔGSU2724-26 (Δ*omcBC* Δ*extEFG*)	This study
DB1289	ΔGSU2731-39 ΔGSU2940-36 (Δ*omcBC* Δ*extHIJKL*)	This study
DB1489	ΔGSU2645-42 ΔGSU2724-26 (Δ*extABCD* Δ*extEFG*)	This study
DB1490	ΔGSU2645-42 ΔGSU2940-36 (Δ*extABCD* Δ*extHIJKL*)	This study
DB1290	ΔGSU2731-39 ΔGSU2940-36 ΔGSU2724-26 (*extABCD*$^{+}$)	This study
DB1291	ΔGSU2731-39 ΔGSU2645-42 ΔGSU2936-2940 (*extEFG*$^{+}$)	This study
DB1491	ΔGSU2731-39 ΔGSU2645-42 ΔGSU2726-24 (*extHIJKL*$^{+}$)	This study
DB1492	ΔGSU2645-42 ΔGSU2726-24 Δ2940-36 (*omcBC*$^{+}$)	This study
DB1493	ΔGSU2731-39 ΔGSU2645-42 ΔGSU2726-24 ΔGSU2940-36 (Δ5)	This study
Escherichia coli		
S17-1	*recA pro hsdR* RP4-2-Tc::Mu-Km::Tn7	Simon *et al.*, 1983
Plasmids		
pK18*mobsacB*		Simon *et al.*, 1983
pRK2-Geo2		Chan *et al.*, 2015
pD*omcBC*	Flanking regions of *omcBC* in pK18*mobsacB*	This study
pD*extABCD*	Flanking regions of *extABCD* in pK18*mobsacB*	This study
pD*extEFG*	Flanking regions of *extEFG* in pK18*mobsacB*	This study
pD*extHIJKL*	Flanking regions of *extHIJKL* in pK18*mobsacB*	This study
p*omcB*	*ombB-omaB-omcB* in pRK2-Geo2	This study
p*extABCD*	*extABCD* in pRK2-Geo2	This study

Table 3.1. Strains and plasmids used in this study.

Electrode reduction assays. Sterile three-electrode conical reactors containing 15 mL of NB with 40 mM acetate as electron donor and 50mM NaCl to equilibrate salt concentration were flushed with a mix of N_2-CO_2 gas (80:20, v/v) until the O_2 concentration reached less than 2 ppm. Liquid cultures were prepared by inoculating 1 ml liquid cultures from single colonies inside an anaerobic chamber. Once these cultures reached late exponential to stationary phase, they were used to inoculate 10 ml cultures with 10% v/v. Each reactor was then inoculated with 25% v/v from this liquid culture as it approached acceptor limitation, at an OD_{600} between 0.48 and 0.52. Working electrodes were set at either -0.1 V or +0.24 V vs SHE and average current density recorded every 12 seconds. Each liquid culture propagated from an individual colony pick served no more than two reactors, and at least three separate colonies were picked for all electrode reduction experiments for a final $n \geq 3$.

Metal reduction assays. NB medium with 20 mM acetate as electron donor and either 55 mM Fe(III)-citrate, ~70 mM Fe(III) oxide, or ~20 mM birnessite ($Mn(IV)O_2$) as electron acceptor was inoculated with a 0.1% inoculum of early stationary phase fumarate limited cultures. Time points were taken as necessary with anaerobic and sterile needles. These were diluted 1:10 into 0.5 N HCl for the Fe(III) samples and into 2 N HCl, 4mM $FeSO_4$ for Mn(IV) samples. Samples were diluted once more by 1:10 in the case of Fe(III) assays and by 1:5 in the case of Mn(IV) assays

into 0.5 N HCl. FerroZine^{R} reagent was then used to determine the Fe(II) concentration in each sample. Original Fe(II) concentrations were calculated for Fe(III) reduction assays by accounting for dilutions and original Mn(IV) concentrations were calculated by accounting for the concentration of Fe(II) oxidized by Mn(IV) based on the following: Mn(IV) + 2Fe(II) = Mn(II) + 2Fe(III). In other words, two molecules of Fe(II) are reduced by one molecule of Mn(IV). Therefore, the increase of Fe(II) concentration over time in our samples indicates a decrease of Mn(IV), or increase of Mn(II), in a 2:1 ratio.

RNAseq. For liquid-grown cultures, total RNA was extracted from 10 ml of *G. sulfurreducens* culture grown to mid-log (0.25 – 0.3 OD_{600}). For biofilm-grown cultures, total RNA was extracted from graphite electrodes of *G. sulfurreducens* biofilms grown to mid-log (300 µA/cm^2). Biofilms were rinsed to remove planktonic cells and removed from electrodes using a plastic spatula. Cell pellets from all samples were washed in RNAprotect (Qiagen) and frozen at -80°C before RNA extraction using RNeasy with on column DNase treatment (Qiagen). Ribosomal RNA was depleted using RiboZero (Illumina) by the University of Minnesota Genomics Center before stranded synthesis and sequenced on Illumina HiSeq 2500, 125 bp pair-ended mode. Residual ribosomal RNA sequences were removed before analysis using Rockhopper (158). Duplicate biological samples were analyzed for each strain. An in-house re-

sequenced *G. sulfurreducens* genome and annotation was used as reference (152, 157).

Homolog search and alignment. Homologs to each of the individual cytochrome conduit proteins were queried on 11-30-2016 in the Integrated Microbial Genomes database (159) with a cutoff on 75% sequence length and 40% identity based on amino acid sequence within the Desulfuromonadales. A higher percent identity was demanded in this search due to the high heme binding site density with the invariable CXXCH sequence. Only ExtJ and ExtL were excluded from the search and the OmcBC region was collapsed into a single cluster due to the high identity shared between the two copies. The gene neighborhood around each homolog hit was analyzed. With a few exceptions (see Table S2), all homologs were found to be conserved in gene clusters predicted to encode cytochrome conduits and containing several additional homologs to each corresponding *G. sulfurreducens* conduit. The proteins within each homologous cytochrome conduit that did not fall within the set cutoff were aligned to the amino acid sequence of the *G. sulfurreducens* component they replaced using ClustalΩ (160).

3.4 **Results**

3.4.1 **Description of putative outer membrane electron conduits.**

At least five gene clusters can be identified in the *G. sulfurreducens* genome encoding putative *c*-cytochrome electron conduits. This identification is based on three key elements; (1) a multiheme periplasmic *c*-type cytochrome, (2) an outer membrane integral protein with transmembrane ß-sheets, and (3) one or more outer membrane lipoproteins with redox cofactors (Fig. 3.1A). Two of these clusters correspond to the well-studied OmcB-based (*omb*B-*oma*B-*omc*B, GSU2739-2737) conduit and its near-identical duplicate OmcC-based cluster immediately downstream (*omb*C-*oma*C-*omc*C, GSU2733-2731). For clarity, and due to the fact that *omaBC* and *ombBC* are identical, these are together referred to as the "*omcBC*" cluster.

The *ext* genes comprise three new clusters, named for their putative roles in extracellular electron transfer (152). Relative protein orientations were predicted using a combination of protein localization prediction software (154), integral membrane prediction software (153), and lipid attachment site prediction software (155). The *extABCD* (GSU2645-2642) cluster encodes ExtA, a periplasmic dodecaheme *c*-cytochrome, ExtB, an outer membrane integral protein with 18 trans-membrane domains, and ExtCD, two outer membrane lipoprotein *c*-cytochromes with 5 and 12 heme binding sites, respectively. The second cluster, *extEFG* (GSU2726-

2724), encodes ExtE, an outer membrane integral protein with 21 trans-membrane domains, ExtF, an outer membrane lipoprotein pentaheme *c*-cytochrome, and ExtG, a periplasmic dodecaheme *c*-cytochrome. The final cluster, *extHIJKL* (GSU2940-2936) lacks an outer membrane *c*-cytochrome, but encodes ExtH, a rhodanese-family lipoprotein, ExtI, a 21 trans-membrane domain outer membrane integral protein, ExtK, a periplasmic pentaheme *c*-cytochrome, and ExtJL, two small outer membrane lipoproteins.

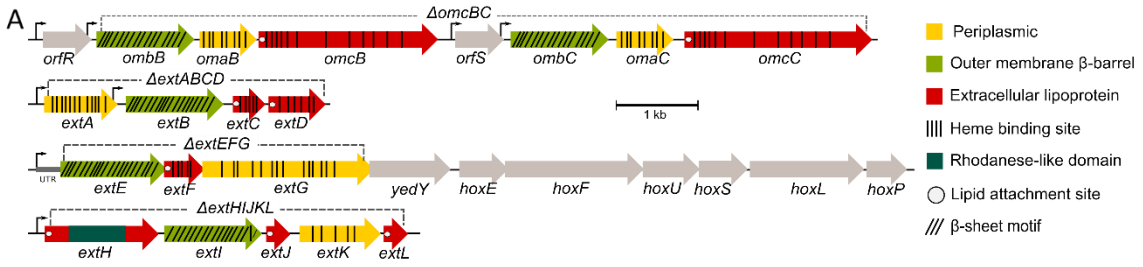

B

Percent Identity based on Amino Acid Sequence

Periplasmic cytochromes

	ExtA	ExtG	ExtK	OmaB	OmaC
ExtA	100	25.9	17.9	23.9	23.9
ExtG		100	20.9	23.2	23.2
ExtK			100	19.7	19.7
OmaB				100	100
OmaC					100

β-barrels

	ExtB	ExtE	ExtI	OmbB	OmbC
ExtB	100	30.2	21.1	22	22
ExtE		100	20.2	20.4	20.4
ExtI			100	17.1	17.1
OmbB				100	100
OmbC					100

Lipoprotein cytochromes

	ExtC	ExtD	ExtF	OmcB	OmcC
ExtC	100	16.3	41.5	21.2	24.2
ExtD		100	31.3	26.9	28.5
ExtF			100	22.9	23
OmcB				100	70.8
OmcC					100

Figure 3.1 The outer membrane electron conduit gene clusters of *G. sulfurreducens*. A) Genetic organization and predicted features of operons containing putative outer membrane conduits. Deletion constructs indicated by dashed line. B) Identity matrix from amino acid sequence alignment of each cytochrome or ß-barrel component using ClustalΩ.

A significant difference between *G. sulfurreducens* Ext clusters and the *S. oneidensis* Mtr conduits (70), is that the *c*-cytochrome conduits in *S. oneidensis* are paralogs. The periplasmic MtrA and MtrD cytochromes share over 50% identity,

are similar in size and heme content, and can cross complement (68). The lipoprotein outer surface cytochromes of *Shewanella* also demonstrate high sequence, functional, and structural conservation (68, 69, 161, 162). In contrast, no component of the Ext or OmcBC complexes share any homology. For example, the predicted periplasmic *c*-cytochromes ExtA, ExtG, ExtK, and OmaB vary in size from 25 to 72 kDa, contain 5 to 15 hemes, and share 18%-26% identity (Fig. 3.1B).

To test physiological roles of these loci, single cluster mutants were first constructed in an isogenic background, comprising Δ*extABCD*, Δ*extEFG*, Δ*extHIJKL*, and Δ*omb*B-*oma*B-*omc*B-*orfS*-*omb*C-*oma*C-*omc*C (abbreviated as the Δ*omcBC* cluster) mutants. As these mutant strains lack any antibiotic cassettes, they were used as backgrounds for further deletions. Multiple cluster deletion mutants leaving only one conduit cluster on the genome are referred to by their single remaining cluster, e.g. "*extABCD*$^{+}$" = Δ*extEFG* Δ*extHIJKL* Δ*omcB*C, while the mutant lacking the *extABCD*, *extEFG*, *extHIJKL*, *omcB*-based and *omcC*-based clusters is referred to as "Δ5". After resequencing terminal strains (such as *extABCD*$^{+}$ and Δ5) to verify no other off-target mutations accumulated during the many rounds of insertions and recombinations, these strains were tested under six different extracellular growth conditions varying in solubility, chemical composition, and redox potential.

3.4.2 **Cells lacking single gene clusters have partial reduction defects with Fe(III) citrate.**

No single cluster deletion eliminated the majority of soluble Fe(III) citrate reduction. The most severe defect was observed in the Δ*omcBC* cluster mutant, which reduced 60% of Fe(III) citrate compared to wild type (Fig. 3.2A). Minor defects were observed for Δ*extEFG* and Δ*extHIJKL*, while Δ*extACBD* reduced Fe(III) citrate at wild-type levels. These results suggest that more than one cluster can be sufficient for soluble Fe(III) reduction.

3.4.3 **Any one gene cluster is sufficient for partial Fe(III) citrate reduction, and deletion of all 5 clusters eliminates electron transfer to this substrate.**

Deletion of the full suite of clusters eliminated all residual electron transfer to Fe(III) citrate (Fig. 3.2B). When multiple-deletion strains containing only one cluster were tested for Fe(III) citrate reduction, results supported key roles for *omcBC* and *extABCD* in soluble metal reduction, and little involvement by *extEFG* or *extHIJKL*. For example, Fe(III) citrate reduction by *omcBC*$^{+}$ and *extABCD*$^{+}$ was comparable to that of wild type, while *extEFG*$^{+}$ and *extHIJKL*$^{+}$ strains reduced Fe(III) citrate to just 20% of wild type. Further delineation of the effect of tandem deletions was investigated.

3.4.4 **Only strains lacking both *omcBC* and *extABCD* had a significant defect in Fe(III) citrate reduction.**

Because Δ*omcBC* demonstrated the largest defect in Fe(III) citrate reduction, additional deletions in this background were tested for their ability to reduce this substrate (Fig. 3.2C). Out of these, only the double cluster deletion mutant Δ*omcBC* Δ*extABCD* reduced Fe(III) citrate at a significantly reduced rate compared to the Δ*omcBC* strain. Compared to growth of strains containing *extEFG*$^{+}$ or *extHIJKL*$^{+}$ alone (Fig. 3.2B), the Δ*omcBC* Δ*extABCD* mutant (containing both *extEFG* and *extHIJKL*) reduced Fe(III)-citrate to the same level as their single-cluster strains (Fig. 3.2C). These data suggest that when both *extEFG* and *extHIJKL* remained in the genome their contribution was not additive.

Not shown in Fig 3.2 is metal reduction data for intermediate deletion mutants such as Δ*extEFG* Δ*extHIJKL*. Screens performed after such double mutants were constructed revealed no changes that deviated from wild type or their parent single-cluster deletions. Only intermediate strains with phenotypes, such as Δ*omcBC* background strains, are shown in Fig 3.2.

3.4.5 **Expression of single conduit clusters is sufficient to recover Fe(III) citrate reduction.**

When compared to empty-vector controls, complementation of the Δ5 strain with single *omcB* (as *ombB-omaB-omcB*) or *extABCD*

clusters restored Fe(III) citrate reduction to levels within 90% of the respective *omcBC*$^{+}$ and *extABCD*$^{+}$ strains (Fig. 3.2D). These data sets are the first evidence that a putative outer membrane complex different from *omcBC* is sufficient for extracellular substrate reduction.

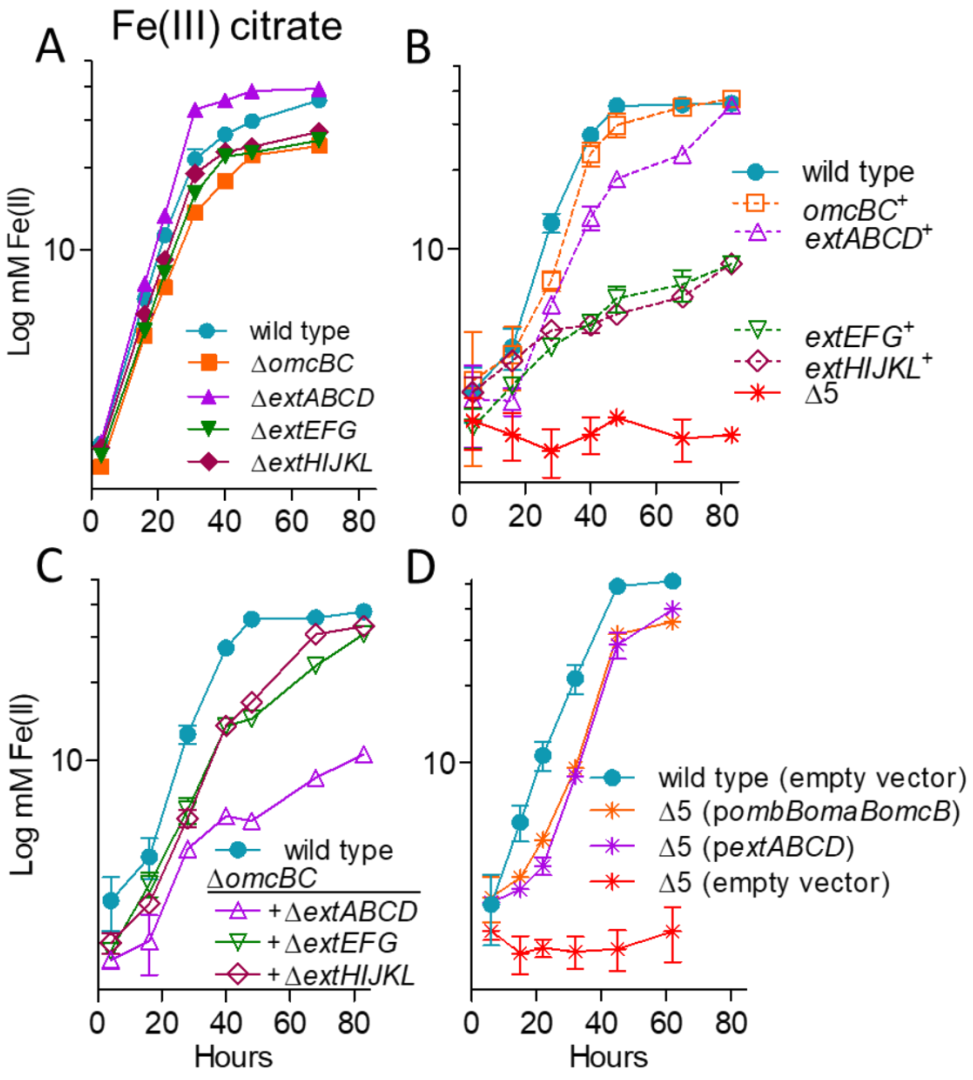

Figure 3.2 OmcBC or ExtABCD are sufficient during Fe(III)-citrate reduction, deletion of all clusters eliminates Fe(III)-citrate reduction. Growth using 55 mM Fe(III)-citrate as an electron acceptor by A) single conduit cluster deletion mutants, B) triple mutants

lacking all but one cytochrome conduit, as well as the Δ5 strain lacking all five cytochrome conduits, C) mutants in an Δ*omcBC* background strain, and D) Δ5 mutants expressing *omcB* or *extABCD* or carrying an empty expression vector as control. All experiments were conducted in triplicate and curves are average ± SD of n ≥ 3 replicates.

3.4.6 **Only strains lacking multiple gene clusters have significant defects in Fe(III)- and Mn(IV)-oxide reduction.**

As with Fe(III) citrate, deletion of single conduit clusters *in G. sulfurreducens* only had modest effects on metal oxide reduction (Fig. 3.3A and C) and additional conduit cluster deletions were needed to severely impact growth (Fig. 3.3B and D). The most severe defect was observed in the Δ*omcBC* cluster mutant, which reduced 68% of Fe(III)-oxide compared to wild type (Fig. 3.3A). Minor defects were observed for Δ*extEFG* and Δ*extHIJKL*, while Δ*extACBD* reduced Fe(III)-oxide near wild-type levels. None of the single mutants displayed defects with Mn(IV)-oxides (Fig. 3.3C).

As with soluble metal reduction, deletion of the full suite of clusters eliminated all residual electron transfer to Fe(III)- and Mn(IV)-oxides (Fig. 3.3B and D). Unlike soluble metal reduction, however, when multiple-deletion strains containing only one cluster were tested for Fe(III)-oxide reduction, results supported key roles for *omcBC* and *extEFG* in metal oxide reduction and little involvement by *extABCD*. For example, Fe(III)-oxide reduction by *omcBC*$^{+}$ was nearly 80% of wild type, *extEFG*$^{+}$ was over

60%, but the *extABCD*$^{+}$ strain reduced less than 30% of wild type. The *omcBC*$^{+}$, *extEFG*$^{+}$, and *extHIJKL*$^{+}$ strains achieved about 80% of wild type Mn(IV)-reduction at 80 hours, but the *extABCD*$^{+}$ strain again displayed poor Mn(IV)-oxide reduction.

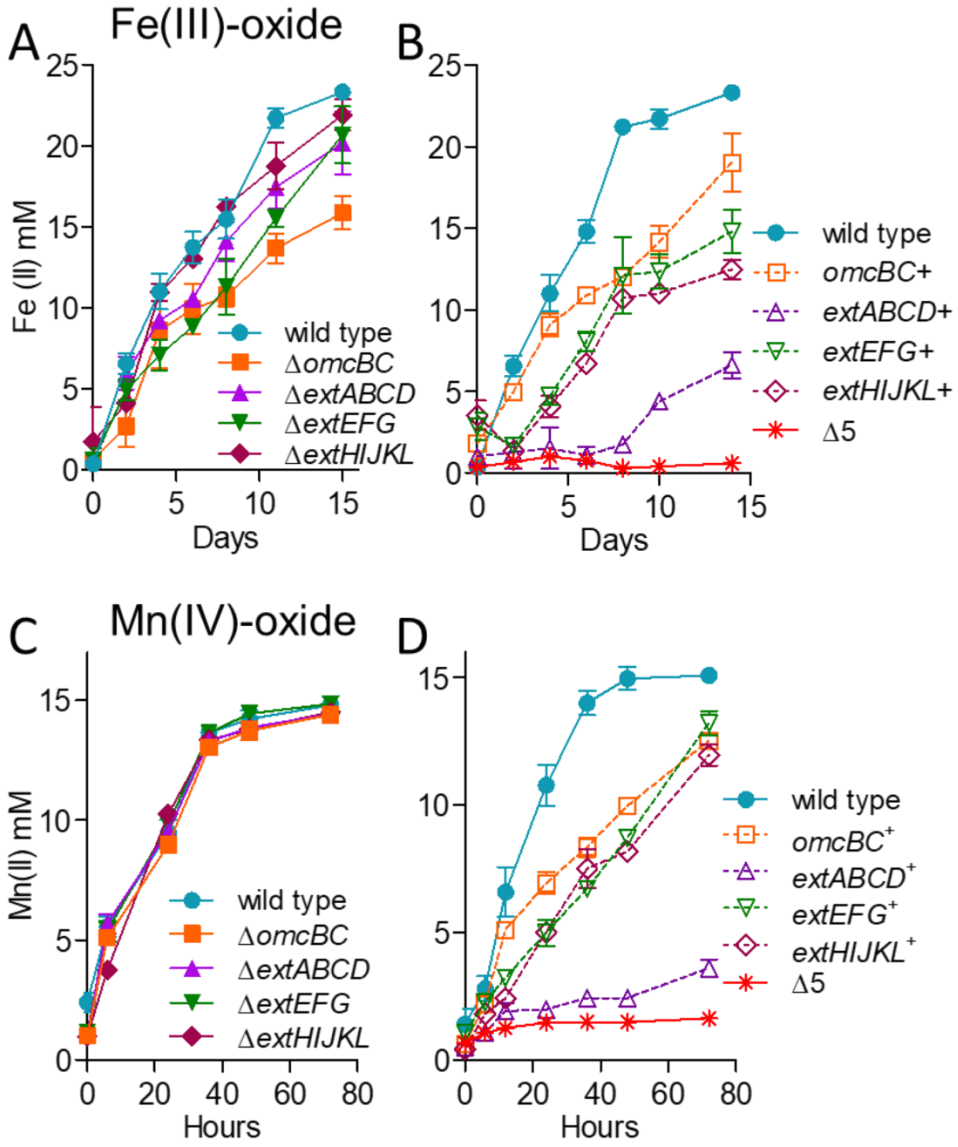

Figure 3.3 No single outer membrane cluster is essential but all are necessary for wild type levels of electron transfer to Fe(III)- and Mn(IV)-oxides. Growth of single cluster deletion mutants and triple mutants lacking all but one cytochrome conduit cluster, as well as the

Δ5 mutant lacking all clusters utilizing A) 70 mM Fe(III)-oxide or B) 20 mM Mn(IV)-oxide as terminal electron acceptor. All experiments were conducted in triplicate and curves are average ± SD of n ≥ 3 replicates.

3.4.7 **Only strains lacking both *omcBC* and *extEFG* had a significant defect in Fe(III)- and Mn(IV)-oxide reduction.**

Since Δ*omcBC* demonstrated the largest defect in Fe(III)-oxide reduction, additional deletions in this background were tested for Fe(III) and Mn(IV)-oxide reduction (Fig. 3.4). Fe(III)-oxide reduction by Δ*omcBC* Δ*extEFG* was less than 25% of wild type, while the Δ*omcBC* Δ*extACBD*, and Δ*omcBC* Δ*extHIJKL* strains still reduced Fe(III)-oxides similar to the Δ*omcBC* strain. The Δ*omcBC* Δ*extEFG* strain also had a severe Mn(IV)-oxide reduction defect. Unlike Fe(III)-oxide reduction, the Δ*omcBC* Δ*extABCD* and Δ*omcBC* Δ*extHIJKL* strains had a modest Mn(IV) reduction defect, suggesting higher contributions of the *extABCD* and *extHIJKL* clusters in the presence of Mn(IV) compared to Fe(III).

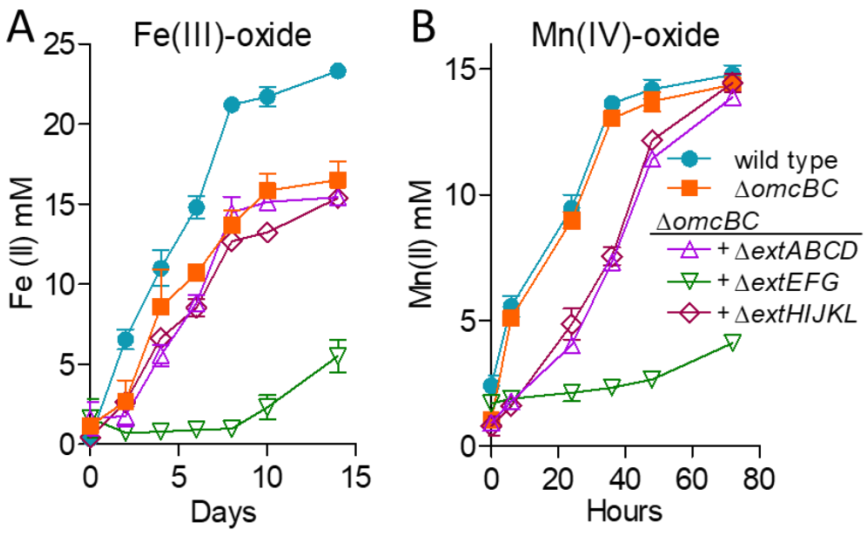

Figure 3.4 OmcBC and ExtEFG have additive roles in Fe(III)- and Mn(IV)-oxide reduction. Reduction of A) 70 mM Fe(III)-oxide or B) 20 mM Mn(IV)-oxide by the Δ*omcBC* strain and additional deletions in an Δ*omcBC* background. All experiments were conducted in triplicate and curves are average ± SD of n ≥ 3 replicates.

The poor growth of the Δ*omcBC* Δ*extEFG* mutant on insoluble metals was surprising since this strain still contained *extHIJKL*, and the *extHIJKL*$^{+}$ strain reduced 50% of Fe(III)-oxide and 75% of Mn(IV)-oxide compared to wild type (Fig. 3.3B and D; Table 3.2). This suggests *extHIJKL* expression or function of its product could be negatively affected by the level or activity of other clusters.

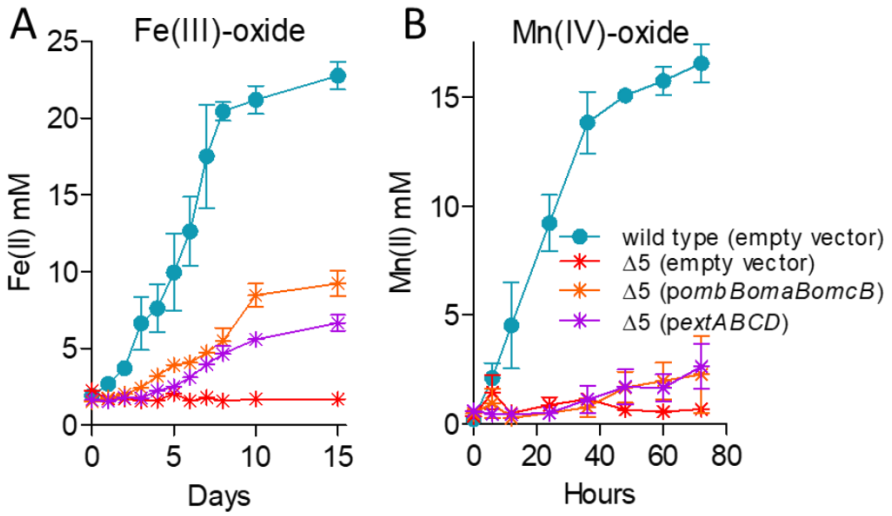

Figure 3.5 Partial complementation by single conduit clusters supports hypothesis that multiple conduit complexes are necessary for wild-type levels of metal oxide reduction. Reduction of A) 70 mM Fe(III)-oxide or B) 20 mM Mn(IV)-oxide by the Δ5 mutant expressing *extABCD* or the *omcB* cluster compared to the empty vector control. All experiments were conducted in triplicate and curves are average ± SD of n ≥ 3 replicates.

3.4.8 **Expression of single conduit clusters partially recovers Fe(III)- and Mn(IV)-oxide reduction.**

Plasmids containing either *ombB-omaB-omcB* or *extABCD* clusters resulted in partial recovery (Fig. 3.5), consistent with the intermediate phenotypes displayed by mutants retaining single clusters on the genome. Expression of the *omcB* cluster reestablished Fe(III)-oxide reduction, although to a level less than that seen in the *omcBC*$^{+}$ strain containing the full duplicated cluster in its original context (Fig. 3.4B). Expressing *extABCD* from a plasmid restored Fe(III)-oxide reduction in the Δ5 strain

near the low levels of the *extABCD*$^{+}$ strain. Reduction of Mn(IV)-oxides by *omcB* or *extABCD*-expressing strains was even lower.

3.4.9 **Mutants lacking *extABCD* are defective in electrode growth at all redox potentials, while mutants containing only *extABCD* outperform wild type.**

In contrast to metal reduction, when grown with electrodes poised at high (0.24 V vs. SHE) or low (-0.1 V, (152)) redox potentials, only Δ*extABCD* mutants showed a defect in rate and extent of growth. Mutants lacking the *omcBC* and *extEFG* clusters grew similar to wild type, while Δ*extHIJKL* demonstrated a lag before growing with a similar doubling time as wild type to nearly wild type final current density (Fig. 3.6A). In all experiments, Δ*extABCD* grew with a doubling time slower than 20 h, or over 3-fold slower than wild type, and could only achieve 20% of wild type final current density, or 116 ± 33 μA/cm^2 vs. 557 ± 44 μA/cm^2 ($n \geq 5$).

Mutants containing only one gene cluster (*extABCD*$^{+}$, *extEFG*$^{+}$, *extHIJKL*$^{+}$, *omcBC*$^{+}$) as well as a mutant lacking all gene clusters (Δ5) were then analyzed for growth on electrodes. The Δ5 mutant grew at the same low rate and extent of growth as the Δ*extABCD* single mutant at both redox potentials, suggesting than none of the additional clusters were responsible for residual growth originally seen in Δ*extABCD*. In contrast, *extABCD*$^{+}$ grew faster than wild type (4.5 ± 0.2 h vs. 6.5 ± 0.3 h doubling time, $n \geq 9$)

and reached a final current density 40% higher than wild type (768 ± 52 μA/cm^2 vs. 557 ± 44μA/cm^2, n≥9). All other multiple-deletion strains containing only one cluster grew as poorly as the Δ5 mutant, further indicating that under these conditions, *extEFG*, *extHIJKL*, and *omcBC* were not required for electron transfer to electrodes (Fig. 3.6B).

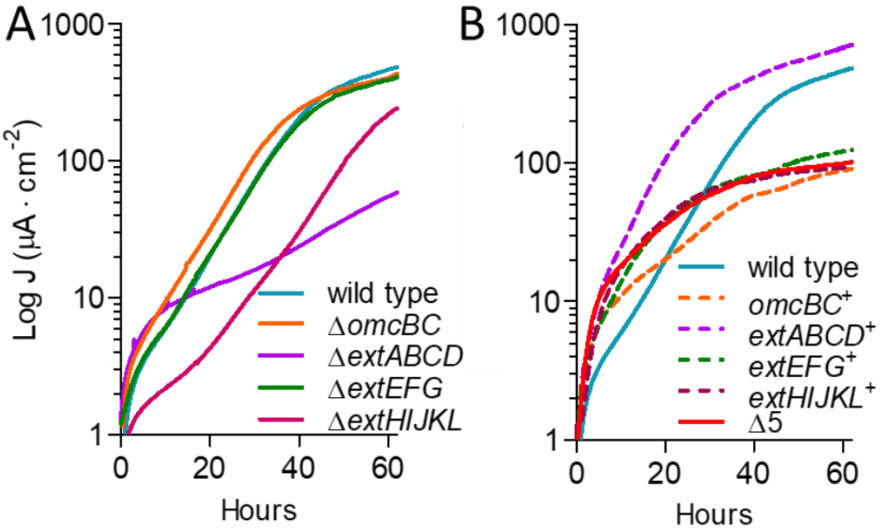

Figure 3.6 Only the ExtABCD conduit cluster is necessary for electrode reduction. Current density produced by A) single and B) multiple-cluster deletion mutants on graphite electrodes poised at +0.24 V vs. SHE. All mutants were grown in at least two separate experiments, and curves are representative of n ≥ 3 independent replicates per experiment. Similar results were obtained at lower (-0.1 V vs. SHE) redox potentials.

3.4.10 **A 5-conduit deletion mutant expressing *extABCD* has a faster growth rate on electrodes than wild type.**

To further investigate the specific effect of *extABCD* on electrode growth, *extABCD* was provided on a vector in the Δ5

strain. The 3-gene *omcB* conduit cluster (*omb*B-*oma*B-*omc*B) was also placed in the Δ5 strain using the same vector, and both were compared to wild type cells containing the empty vector. While the plasmid is stable for multiple generations, routine vector maintenance requires growth with kanamycin, and kanamycin carry-over into biofilm electrode experiments is reported to have deleterious effects on electrode growth (62, 157). Thus, we first re-examined growth of the empty vector strain. When selective levels of kanamycin (200 $\mu g \cdot ml^{-1}$) were present in electrode reactors, colonization was slowed and final current production decreased 74% even though cells carried a kanamycin resistance cassette. At levels resulting from carry-over during passage of cells into the electrode reactor (5 $\mu g \cdot ml^{-1}$) growth rate was not affected, but final current was decreased up to 30%, suggesting interference with biofilm thickness rather than respiration (Fig. 3.7A). All subsequent complementation was performed in the presence of 5 $\mu g \cdot ml^{-1}$ residual kanamycin and compared to these controls.

Expressing the *omcB* conduit cluster in the Δ5 strain failed to increase growth with electrodes as electron acceptors. These data further supported the hypothesis that the *omcB* conduit cluster was not involved in electrode reduction, consistent with the lack of an effect seen in Δ*omcBC* deletions, as well as the poor growth of *omcBC*$^{+}$ mutants still containing both the OmcB and OmcC clusters in their native genomic context (Fig. 3.7B).

However, when *extABCD* was expressed on the same vector in the Δ5 background, colonization was faster and cells reached a higher final current density compared to wild type carrying the empty vector (421 ± 89 μA/cm^2 vs. 297 ± 11 μA/cm^2, n=3) (Fig. 3.7B). This enhancement by plasmid-expressed *extABCD* (141% of wild type with empty vector) was similar to the positive effect observed in the *extABCD*$^+$ strain (137% of wild type) (Fig. 3.6B), and further supported the hypothesis that *extABCD* is both necessary and sufficient for at least 80% of wild type levels of electron transfer to electrodes.

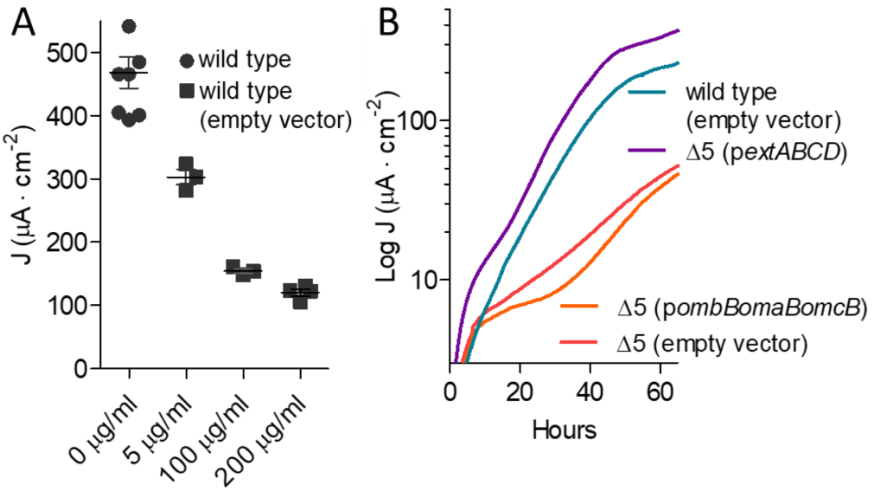

Figure 3.7 Effect of kanamycin on final current density, and comparison of ExtABCD and OmcBC complementation. A) Final current density of wild type *G. sulfurreducens* compared to wild type carrying an empty vector in the presence of increasing kanamycin concentrations. B) Current density produced by the Δ5 strain plus either *extABCD* or *omcB* cluster-containing vectors, in the presence of 5 μg/ml residual kanamycin. Wild type and Δ5 strains carrying the empty vector were used as controls. All experiments were conducted in duplicate and curves are representative of n ≥ 3 replicates per experiment.

Growth of any of the two-conduit deletion mutants was unchanged from single-cluster strains (Fig. S1). For example, just as the mutant lacking *extABCD* produced the same phenotype as the Δ5 strain (Fig. 3.6), deletion of a second cluster from the Δ*extABCD* strain produced similar results as Δ*extABCD* alone, and no two-cluster combination of *omcBC*, *extEFG* or *extHIJKL* showed defects to suggest they were required during these electrode growth conditions, or to indicate their presence controlled expression of *extABCD*. The Δ*extABCD* and Δ5 strains were also monitored during extended incubation times to determine if final current density increased after an extended incubation period, but current remained unchanged even after 150-200 h (Fig. S2).

3.4.11 **Transcriptomic analysis reveals no off-target effects in *extABCD*$^{+}$.**

It has been previously observed that replacement of a *c*-cytochrome with an antibiotic resistance cassette can influence expression of other genes (163), and that deletion of pili-related genes can depress *c*-cytochrome abundance due to expression changes (40, 164). While we have designed our genetic analysis to have numerous independent observations of each deletion (single, double, triple and quadruple deletions) in order to confirm all phenotypes, as well as complemented relevant strains, the observation that the *extABCD*$^{+}$ strain produces more current than wild type remains a significant hurdle to the

publication of this work. Therefore, in order to attempt to find the reason behind this phenotype, the transcriptome of the *extABCD*$^{+}$ strain was analyzed under fumarate- and electrode-respiring conditions and compared to wild type.

First, we determined the expression level of the gene clusters analyzed in this study under electrode-respiring conditions compared to liquid cultures in the wild type *G. sulfurreducens* strain (Fig. 3.8A). It is noteworthy that none of the putative conduits are up- or down-regulated regardless of their importance or irrelevance during electrode respiration. Similarly, known inner membrane electron transfer pathways did not change in expression, regardless of their role in electron transfer to electrodes poised at +240 mV (62, 63, 142). The genes for respiratory pathways that showed the highest change in expression during electrode growth were *cbcAB* , encoding for inner membrane *c*- and *b*-tye cytochromes, which are also upregulated during Fe(III)-oxide reduction (165) but have not been assigned an electrode-reduction phenotype in previous random mutagenesis studies (152). As has been shown before (49), *omcZ* was upregulated during electrode-reduction (Fig. 3.8A-B). The transcriptional profile of liquid grown cells and electrode respiring cells were then compared between *extABCD*$^{+}$ and wild type strains. Surprisingly, no significant changes in the expression of known electron transfer pathways were found in either

condition between the two strains (Fig. 3.8C-D). Full data sets plotted on Figure 3.8 can be found in Table S3.

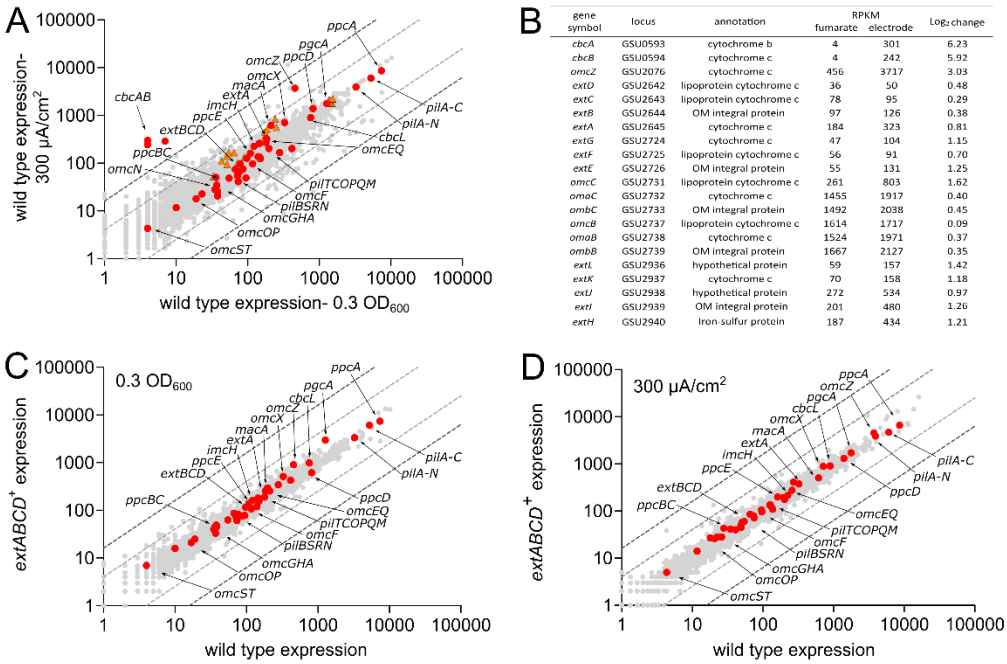

gene symbol	locus	annotation	RPKM fumarate	RPKM electrode	Log_2 change
cbcA	GSU0593	cytochrome b	4	301	6.23
cbcB	GSU0594	cytochrome c	4	242	5.92
omcZ	GSU2076	cytochrome c	456	3717	3.03
extD	GSU2642	lipoprotein cytochrome c	36	50	0.48
extC	GSU2643	lipoprotein cytochrome c	78	95	0.29
extB	GSU2644	OM integral protein	97	126	0.38
extA	GSU2645	cytochrome c	184	323	0.81
extG	GSU2724	cytochrome c	47	104	1.15
extF	GSU2725	lipoprotein cytochrome c	56	91	0.70
extE	GSU2726	OM integral protein	55	131	1.25
omcC	GSU2731	lipoprotein cytochrome c	261	803	1.62
omaC	GSU2732	cytochrome c	1455	1917	0.40
ombC	GSU2733	OM integral protein	1492	2038	0.45
omcB	GSU2737	lipoprotein cytochrome c	1614	1717	0.09
omaB	GSU2738	cytochrome c	1524	1971	0.37
ombB	GSU2739	OM integral protein	1667	2127	0.35
extL	GSU2936	hypothetical protein	59	157	1.42
extK	GSU2937	cytochrome c	70	158	1.18
extJ	GSU2938	hypothetical protein	272	534	0.97
extI	GSU2939	OM integral protein	201	480	1.26
extH	GSU2940	Iron-sulfur protein	187	434	1.21

Figure 3.8. Transcriptomic analysis shows no significant differences in expression between *extABCD*⁺ and wild type strains. A) Comparison of expression levels of wild type exponentially growing cells under fumarate- and electrode-respiring conditions. Gene clusters studied in this work are represented as orange triangles and all other known electron transfer pathways are shown in red circles and labeled. Dark and light gray dotted lines represent a change of 4 and 2 Log_2, respectively. B) RPKM and Log_2 change of ORFs with largest expression changes as well as genes studied in this work (for additional data, see Table S2). Comparison of the transcriptome of wild type and *extABCD*⁺ cells exponentially growing using C) fumarate or D) graphite electrode poised at +240 mV as terminal electron acceptor. Average shown of duplicate samples.

3.4.12 **Proposed role(s) for the Omc and Ext electron conduit gene clusters.** Table 3.2 summarizes all extracellular reduction phenotypes of single cluster deletions and deletions leaving only one conduit on the genome, adjusted to wild type performance. In

all cases, each gene cluster was necessary under different conditions. Many of the recently described *ext* gene clusters are necessary for wild-type metal reduction, yet few are sufficient. For example, *extEFG* and *extHIJKL* were necessary for Fe(III) citrate reduction, as strains lacking these clusters only reduced ~65% of wild type levels. But when only *extEFG* or only *extHIJKL* was present, they were not sufficient to reduce Fe(III) citrate to more than 25% of wild type levels. In contrast, the *omcBC* cluster or the *extABCD* cluster alone was sufficient for Fe(III) citrate reduction, and the *extABCD* cluster alone was sufficient for electrode growth. Deletion of all five conduit clusters resulted in complete elimination of metal reduction abilities, while some residual activity remained when the same Δ5 strain was grown using electrodes as terminal electron acceptor. These comparisons show each gene cluster is necessary under at least one of the conditions studied, and provides evidence for additional undiscovered mechanisms enabling transmembrane electron transfer.

	% of wild type								
Substrate	Δ*omcBC*	Δ*extABCD*	Δ*extEFG*	Δ*extHIJKL*	*omcBC*$^{+}$	*extABCD*$^{+}$	*extEFG*$^{+}$	*extHIJKL*$^{+}$	Δ5
Fe(III) citrate	61.2 ± 10.5	105 ± 6.6	62.5 ± 4.9	66.3 ± 2.5	101.1 ± 8.4	99.2 ± 11.3	22.5 ± 2.4	23.8 ± 6.4	0.1 ± 0.6
FeIII)-oxide	68.9 ± 8.4	83.3 ± 12.1	87.5 ± 14.9	95.8 ± 24.9	78.8 ± 3.9	29.2 ± 2.6	60.4 ± 9.5	52.1 ± 3.7	0.1 ± 0.3
Mn(IV)-oxide	94.5 ± 6.4	95.1 ± 2.8	99.6 ± 3.4	97.9 ± 6.1	83.3 ± 14.1	26.7 ± 5.9	86.8 ± 6.5	75.6 ± 7.3	1.7 ± 0.9
Electrode	76.5 ± 16.5	20.9 ± 6.0	104.8 ± 2.1	86.3 ± 15.3	28.3 ± 5.2	137.9 ± 9.5	21.2 ± 6.5	25.9 ± 4.2	21.9 ± 4.4

Table 3.2. Comparative performance of *G. sulfurreducens* strains lacking one cluster, or containing only one cluster. Growth of single cytochrome conduit deletion mutants and mutants lacking all clusters except one, averaged from eight biological replicates or more and represented as the percent of wild type growth. Averages and standard deviation represented.

3.5 Discussion

Sequencing of the *G. sulfurreducens* genome revealed an unprecedented number of electron transfer proteins, with twice as many genes dedicated to respiratory and redox reactions as organisms with similarly-sized genomes (166). Out of 111 *c*-type cytochromes, 43 had no known homolog, and many were predicted to reside in the outer membrane. The large complement of outer membrane redox proteins in *G. sulfurreducens* became even more of an anomaly as the electron transfer strategy of metal-reducing *S. oneidensis* emerged, where only a single outer membrane conduit was used to reduce a multitude of substrates (68, 72, 147, 149).

Evidence that more than one *G. sulfurreducens* outer membrane pathway exists for reduction of extracellular substrates has accumulated since the discovery of OmcB (75–77). Deletion of *omcB* impacted Fe(III)-reduction, but had little effect on U(IV) or Mn(IV)-oxide reduction (165, 167). A Δ*omcB* suppressor strain evolved for improved Fe(III)-citrate growth still reduced Fe(III)-oxides poorly (151). Strains lacking *omcB* grew similar to wild type with electrodes in four different studies, (49, 50, 89, 168), and OmcB abundance was lowest on cells near the electrode (169). An insertional mutant lacking six secreted and outer

membrane-associated cytochromes in addition to *omcB* still demonstrated some Fe(III)-oxide reduction (170). After replacing the entire *omcBC* region with an antibiotic cassette and also finding residual Fe(III)-reducing ability, Liu *et al.* (2015) speculated that other *c*-cytochrome-like clusters in the genome might be active. Most recently, Tn-seq analysis of electrode-grown cells found little effect of *omcB* cluster mutations, yet noted significant defects from insertions in cytochromes with *c*-cytochrome features (152). This evidence led us to study if alternative *ext*-family conduit gene clusters could explain growth by *omcB* mutants.

The genetic analysis presented here supports a role for these unstudied conduit gene clusters during extracellular respiration. All mutants still containing at least one cluster retained partial activity towards metals, while deletion of the *omcBC* region, plus all three *ext* clusters, finally was able to eliminate metal reduction. This need to delete more than one conduit cluster helps explain prior variability and rapid evolution of suppressors in Δ*omcB* mutants.

In the case of electrodes at both high and low potential, only deletion of *extABCD* affected growth. Additionally, the strain with only *extABCD* remaining on the genome outperformed wild type in terms of growth rate and final current density when grown on electrodes. Whether this effect is due to expression

differences in the absence of other conduits, more efficient interactions between ExtABCD and key partners, or upregulation of unidentified components is yet to be determined. Since residual electron transfer to electrodes was still detected after deletion of all studied clusters, additional mechanisms remain to be discovered.

Overall, these data show that for all tested metal and electrode acceptors, the presence of more than one conduit cluster is required for wild type levels of reduction, and the presence of only one cluster is sufficient for partial reduction. Whether the products of these *ext* gene clusters indeed function as conduits to transfer electrons across the outer membrane will require further biochemical and biophysical analysis. Why certain conduit clusters are linked to growth with specific substrates remains a subject of speculation. Perhaps some clusters simply are not expressed in the presence of certain acceptors. The fact that driving expression of the *omcB* cluster from a plasmid could not complement electrode growth, while *extABCD* could, along with published evidence that the *omcB* cluster is highly expressed under most studied conditions (165), argues against such an explanation for electrode phenotypes. Similar complementation data under metal-reducing conditions suggests lack of expression does not explain why the *extABCD* cluster is not sufficient to support Fe(III)- or Mn(IV)-oxide reduction.

It is plausible, in the case of particles or surfaces, that each complex preferentially interacts with other secreted extracellular proteins responsible for carrying electrons to the final destination. If activity from a complex is masked by the absence of its partner protein, forced expression of a single conduit might not be enough to support respiration. In this case, the apparent specificity during reduction of insoluble minerals or electrodes could arise from expression patterns of extracellular components. Many extracellular proteins are known to be involved in electron transfer, such as OmcS, OmcE, OmcZ, PgcA, and pili. A lack of genes for secreted proteins encoded within *omcBC* or *ext* gene clusters argues against co-evolution of highly dedicated partners, but given the long distances separating the outer membrane and metals or electrodes, extracellular protein partners should be considered in some of these cases.

Finally, it is important to consider lessons from previous insertional deletions in *G. sulfurreducens*, such as the diheme peroxidase MacA. Initially hypothesized to be an inner membrane quinone oxioreductase, based on the defective phenotype of Δ*macA* mutants during Fe(III)-citrate reduction (171), this defect was discovered to be due to Δ*macA* mutants not expressing *omcB*, as the Δ*macA* phenotype can be rescued by expressing *omcB* (172, 173). As MacA is a peroxidase, oxidative stress in Δ*macA* could have resulted in global downregulation of cytochromes. In our work,

the availability of every combination of gene cluster deletion and acceptor condition allows some types of general downregulation hypotheses to be eliminated. For example, if deletion of *extABCD* somehow suppressed production of pili or cytochromes such as OmcS, Δ*extABCD* mutants would show an electrode defect as observed. However, strains would also be predicted to show a defect with metal oxides, which we did not observe. A thorough transcriptomic analysis was still performed to address this concern. While interesting results were obtained by comparing wild type transcriptomes from liquid- and electrode-grown cells, we failed to detect *macA*–like downregulation of key electron transfer pathways between the *extABCD*$^{+}$ and wild type strains, regardless of electron acceptor conditions. As noted above, it is still possible that off-target post-translational regulation is affected by the presence/absence of conduit clusters, such as the polymerization of PilA monomers into pili filaments. Such effects will have to be addressed in future studies.

The genetic context of *ext* genes may reveal other clues to their intended function, and aid identification of similar clusters in genomes of other organisms. None of the *ext* regions fits the *mtr* 3-gene 'cytochrome conduit' operon of one small (~40 kDa) periplasmic cytochrome, an integral outer membrane protein, and one large (>90 kDa) lipoprotein cytochrome. For example, *extABCD* includes two small lipoprotein cytochromes, *extEFG* is

part of a hydrogenase-family transcriptional unit, and *extHIJKL* contains a rhodanese-like lipoprotein instead of an extracellular cytochrome (Fig. 3.1). The transcriptional unit beginning with *extEFG* includes a homolog of YedY-family periplasmic protein repair systems described in *E. coli* (174), followed by a NiFe hydrogenase similar to bidirectional Hox hydrogenases used to recycle reducing equivalents in Cyanobacteria (175–177). Rhodanase-like proteins related to ExtH typically are involved in sulfur metabolism (178–180) and an outer surface rhodanese-like protein is linked to extracellular oxidation of metal sulfides by *Acidithiobacillus ferrooxidans* (181). Future searches for electron conduit clusters should consider the possibility of non-cytochrome components, such as FeS clusters, and be aware that conduits might be part of larger complexes that could draw electrons from pools other than periplasmic cytochromes, such as hydrogenase complexes.

Including genes from *ext* operons in searches of other genomes reveals an interesting pattern in putative conduit regions throughout Desulfuromonadales strains isolated from freshwater, saline, subsurface, and fuel cell environments (Fig. 3.9). In about 1/3 of cases, the entire cluster is conserved intact, such as *extABCD* in *G. anodireducens*, *G. soli*, and *G. pickeringii* (Fig. 3.9B). However, when differences exist, they are typically non-orthologous replacements of the outer surface lipoprotein, such as where *extABC* is followed by a new cytochrome

in *G. metallireducens, Geoalkalibacter ferrihydriticus,* and *Desulfuromonas soudanensis.* Conservation of the periplasmic cytochrome coupled with replacement of the outer surface redox protein also occurs in the *omcB* and *extHIJKL* clusters (Fig 3.9A and D). For example, of 18 *extHIJKL* regions, 10 contain a different extracellular rhodanese-like protein upstream of *extIJKL*, each with less than 40% identity to *extH*. This remarkable variability in extracellular components, compared to conservation of periplasmic redox proteins, suggests constant lateral gene transfer and selection of domains that are exposed to electron acceptors and the external environment.

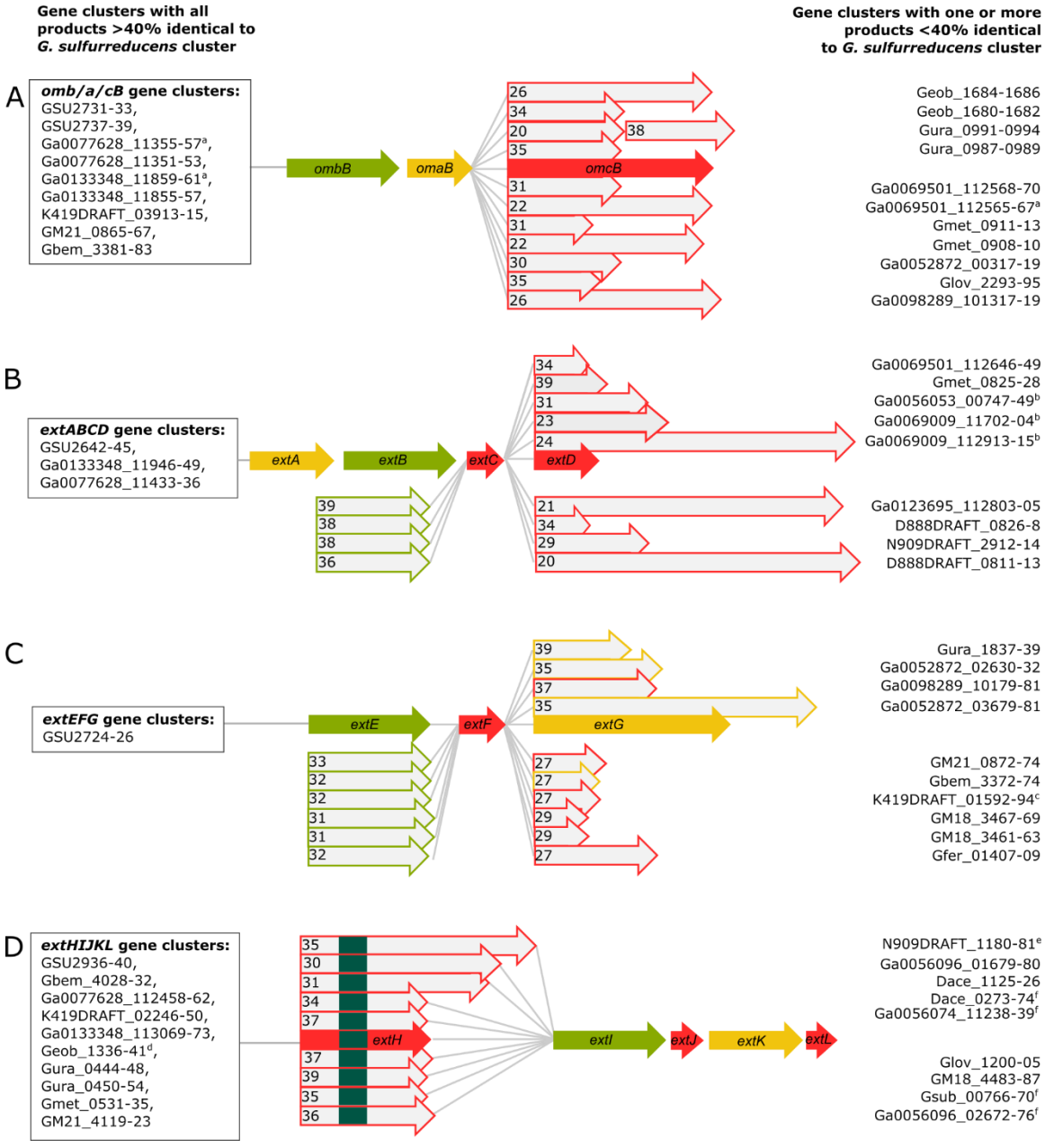

Figure 3.9. Cytochrome conduit conservation across the Order Desulfuromonodales. Representation of cytochrome conduit clusters from the Desulfuromonodales with homologs to either A) OmcBC, B) ExtABCD, C) ExtEFG, or D) ExtHIJKL. Red arrows = putative outer membrane products with a predicted lipid attachment site, yellow arrows = predicted periplasmic components, green arrows = predicted outer membrane anchor components. Complete clusters with all components sharing >40% identity to the corresponding *G. sulfurreducens* cytochrome conduit are indicated in boxes to the left of each gene cluster. Clusters in which one or more proteins are replaced by a new element with <40% identity are

listed on the right side of each gene cluster. Proteins with numbers indicate the % identity to the *G. sulfurreducens* version. [a]OmcBC homologs in these gene clusters also encode Hox hydrogenase complexes. [b]Gene clusters have contiguous *extBCD* loci but *extA* is not in vicinity, as *extA* was found in separate parts of the genome for some of those organisms (see Supplemental Table S2). [c]Gene cluster has additional lipoprotein decaheme *c*-cytochrome upstream of *extE*. [d]Lipid attachment sites corresponding to ExtJL could not be found but there is an additional small lipoprotein encoded within the gene cluster. For ExtHIJKL clusters, homologs depicted above *extH* are found in gene clusters containing only *extI*, whereas homologs depicted below *extH* are found in gene clusters containing full *extHIJKL* loci. Upstream and on the opposite strand to all gene clusters homologous to *extHIJKL* there is a transcription regulator of the LysR family, except [e], where there is no transcriptional regulator in that region, and [f], where there are transcriptional regulators of the TetR family instead.

The data presented here significantly expands the number of genes encoding outer membrane redox proteins necessary during electron transfer in *G. sulfurreducens* and highlights a key difference in the *Geobacter* electron transfer strategy compared to other model organisms. In general, the pattern of multiple genes encoding seemingly overlapping or redundant roles is less like solitary respiratory reductases, and more reminiscent of systems in cellulolytic bacteria that produce numerous similar β-glucosidases to attack a constantly changing polysaccharide substrate (72, 147, 182). A need for multiple outer membrane strategies could be a response to the complexity of metal oxides during reduction; minerals rapidly diversify to become multiphase assemblages of more crystalline phases, the cell:metal interface can become enriched in Fe(II), and organic materials can bind to alter the surface (9, 183, 184). Expressing an array of electron transfer pathways could make cells competitive at all stages with

all electron acceptors, allowing *Geobacter* to outgrow more specialized organisms during perturbations in the environment.

Chapter 4. Enhancing current production through genetic manipulation of *Geobacter sulfurreducens*.

Fernanda Jiménez Otero

4.1 **Summary**

Recently constructed mutant strains of *Geobacter sulfurreducens* altered in key electron transfer or regulatory proteins produce 140% greater current density compared to wild type. Increased current density could be due to a range of factors including per-cell changes in respiration rate, to whole-biofilm modifications such as thickness or long distance conductivity. Respiration and maximum growth rates, maximum current densities, and conductivity via double potential step chronoamperomentry were measured for wild type and mutant biofilms using electrodes poised at +0.24 V vs SHE. Biofilms were also sectioned and imaged using electron microscopy to determine changes in biofilm thickness and cell density. Biofilms incubated in the presence of nitrogen and carbon stable isotopes were analyzed using NanoSIMS to localize metabolically active zones. Finally, differences in protein abundance of exponentially growing biofilms were analyzed using iTRAQ. Our results reveal that *G. sulfurreducens* mutants reached higher current densities through higher per-cell respiration rates, which support faster growth rates, and a denser packing of cells close to the electrode. NanoSIMS analysis confirmed higher per-cell growth rates, and revealed that the zone of cells growing within biofilms remained within 10 microns from the electrode surface, similar to wild-type biofilms. Proteomic comparisons did not detect any significant changes in the abundance of electron

transfer proteins such as multi-heme *c*-cytochromes or pili in exponentially-growing cultures. The combination of imaging, physiological and proteomic tools determined that current-producing bacteria are capable of producing more current per cell and, in combination with higher biofilm density within the active zone near the electrode, can produce a final current density almost twofold greater than wild type. However, there still remain cells in these biofilms that are not contributing to current production. Overcoming the limitation that creates the stratification of metabolically active zones remains a major challenge.

4.2 **Introduction**

Microbial electrochemical technologies consisting of microbes using an anode as electron acceptor, have the potential to solve many problems of modern civilization. The electrochemical processes from these systems can be used for water desalination (20, 21), oxidation of organic matter during waste water treatment (24), electro-fermentation of profitable products (22, 23), and bio-production of electricity. All of these applications still require higher efficiency, primarily in terms of the current density produced at the anode, in order to be profitable in real-world scenarios (28).

Much research has focused on the design of the abiotic components of electrochemical systems, such as varied anode materials, reactor designs, and electrochemical components (28). Another less explored but promising alternative is to engineer the biotic components of these systems. Recent studies of extracellular electron transfer pathways in *Geobacter sulfurreducens* demonstrated that streamlining extracellular electron transfer pathways to only those found to be necessary to reduce electrodes resulted in higher current production (185). Understanding how engineered strains are able to produce more current is essential to be able to design improved biological systems for real-world applications.

Several pathways exist for electron transfer across the outer membrane of *G. sulfurreducens* but out of those studied in Chapter 3, only the deletion of *extABCD* predicted to encode a conductive cytochrome-based conduit across the outer membrane, results in a significant deficiency in electrode reduction (Fig. 4.1A). Deleting three outer membrane electron transfer pathway gene clusters found to be unnecessary, while leaving *extABCD* intact (referred to as strain *extABCD*$^{+}$), results in a 30% faster increase in current density during exponential phase and a 40% higher final current density (Fig. 4.1B-C). Here, we present an analysis of the *extABCD*$^{+}$ strain to delineate the characteristics of this strain that enable higher current production.

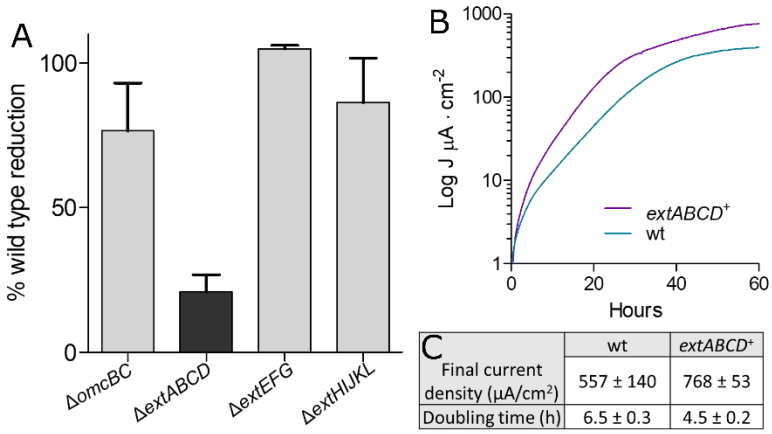

Figure 4.1. Only *extABCD* is necessary for wild-type levels of current production and the *extABCD*⁺ strain reaches a higher current density in a shorter time than wild type. A) Final current densities of outer membrane electron transfer pathway deletion mutants normalized to percent of wild type activity. B) Representative chronoamperometry of wild type and *extABCD*⁺ strains and C)average values of final current density and doubling times for n>8 replicates. (Modified from (185))

4.3 Materials and Methods

Cell growth and electrode reduction assays. All protocols were followed as described in Section 3.3

Strains used in this study

Strains	Description or relevant genotype	Reference
Geobacter sulfurreducens strains		
DB	ΔGSU2645 (Δ*extA*)	This study
DB	ΔGSU2644 (Δ*extB*)	This study
DB	ΔGSU2643 (Δ*extC*)	This study
DB	ΔGSU2642 (Δ*extD*)	This study
DB1280	ΔGSU2645-42 (Δ*extABCD*)	Chan *et al.*, 2017
DB1290	ΔGSU2731-39 ΔGSU2940-36 ΔGSU2724-26 (*extABCD*⁺)	Jiménez Otero et al., 2018
DB1493	ΔGSU2731-39 ΔGSU2645-42 ΔGSU2726-24 ΔGSU2940-36 (Δ5)	Jiménez Otero et al., 2018

Table 4.1 Strains used in this study

Biofilm staining and embedding. All protocols were followed as described in Section 2.3

Protein concentration measurements. *G. sulfurreducens* biofilms were grown to desired current density, rinsed to remove planktonic cells, and incubated (still attached to graphite flag) in 1 mL of 0.2 N NaOH for 1 hour at room temperature. Samples were then stored at 4 °C for at least 24 hours. Protein concentration was measured using Pierce® BCA Protein Assy Kit (Thermo Scientific). Bovine albumin (BSA) dissolved in 0.2 N NaOH was used to prepare standard protein concentration curve. All samples, including standards, were incubated for 10 minutes at 100 °C to ensure sample homogeneity and cooled to room temperature before measuring protein concentration.

Proteomic analysis. Single colonies of each strain from freshly streaked plates were used to inoculate 1 ml liquid cultures of NB media with 20 mM acetate and 40 mM fumarate. Once full grown, these were used to inoculate 10 ml cultures of the same media. Cells were harvested by centrifugation when cultures reached an OD_{600} between 0.4 – 0.45. Two biological replicates of each strain were obtained by repeating this process from a separate plate. Washed cell pellets were lysed with 7M urea, and digested with trypsin at a protein:trypsin ratio of 40 before labeling each sample with iTRAQ reagent. Scaffold Q+ (version Scaffold_4.8.4, Proteome Software Inc., Portland, OR) was used to

quantitate Label Based Quantitation (iTRAQ, TMT, SILAC, etc.) peptide and protein identifications. Peptide identifications were accepted if they could be established at greater than 85.0% probability to achieve an FDR less than 1.0% by the Scaffold Local FDR algorithm. Protein identifications were accepted if they could be established at greater than 54.0% probability to achieve an FDR less than 1.0% and contained at least 2 identified peptides. Protein probabilities were assigned by the Protein Prophet algorithm (186). Proteins that contained similar peptides and could not be differentiated based on MS/MS analysis alone were grouped to satisfy the principles of parsimony. Proteins sharing significant peptide evidence were grouped into clusters. Channels were corrected by the matrix
[0.000,0.000,0.929,0.0689,0.00220];
[0.000,0.00940,0.930,0.0590,0.00160];
[0.000,0.0188,0.931,0.0490,0.001000];
[0.000,0.0282,0.932,0.0390,0.000700];
[0.000600,0.0377,0.933,0.0288,0.000];
[0.000900,0.0471,0.933,0.0188,0.000];
[0.00140,0.0566,0.933,0.00870,0.000];
[0.000,0.000,0.000,0.000,0.000];
[0.00270,0.0744,0.921,0.00180,0.000] in all samples according to the algorithm described in i-Tracker (187). Normalization was performed iteratively (across samples and spectra) on intensities, as described in Statistical Analysis of Relative

Labeled Mass Spectrometry Data from Complex Samples Using ANOVA (188). Medians were used for averaging. Spectra data were log-transformed, pruned of those matched to multiple proteins, and weighted by an adaptive intensity weighting algorithm. Of 25866 spectra in the experiment at the given thresholds, 24785 (96%) were included in quantitation. Differentially expressed proteins were determined by applying Permutation Test with unadjusted significance level $p < 0.05$ corrected by Benjamini-Hochberg. Due to inherent noise of iTRAQ experiments, few conduit components were detected at low levels in strains in which they were deleted.

4.4 **Results**

4.4.1 **Single-gene deletions of *extB*, *extC*, or *extD* produce stronger defects in electrode reduction than the deletion of *extA*.**

In order to determine if only one component of the *extABCD* cluster is responsible for the phenotype of the Δ*extABCD* strain, single deletions of each gene were constructed and analyzed for their ability to reduce graphite electrodes poised at +240 mV vs. SHE. Deletions of *extB*, *extC*, or *extD* were as detrimental to final current density as the deletion of the full *extABCD* gene cluster, with final current density never surpassing 100 $\mu A \cdot cm^2$ (Fig. 4.2), n=4. Surprisingly, deletion of *extA* resulted in a

less pronounced defect, with doubling time extended to ~8 hours and final current density reaching ~490 μA·cm^2 after 100 hours (Fig 4.2), n=4. From section 3.4.11, we know that *extA* is expressed 2.5 - 6.5 fold higher than *extBCD* during electrode reduction, yet all the less-expressed genes in *extBCD*, encoding for the putative outer membrane integral protein and extracellular cytochromes, are responsible for the phenotype of Δ*extABCD*.

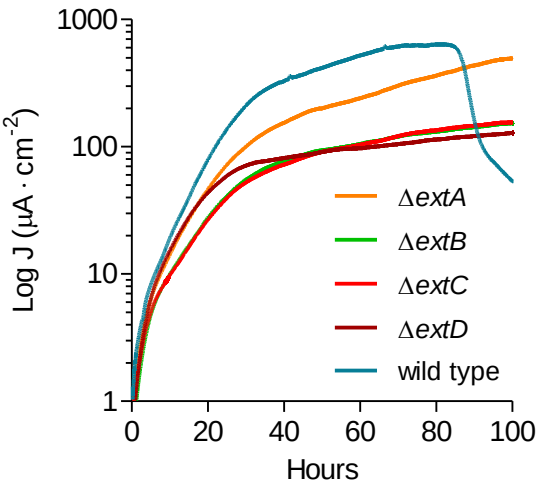

Figure 4.2 Deletion of *extBCD* results in severe deficiency in electrode reduction, while deletion of *extA* only affects doubling time. Single gene deletion mutants of extABCD were grown using graphite electrodes poised at +240 mV vs. SHE as sole terminal electron acceptor. Representative curves of current production over time shown from n=4.

4.4.2 **Overexpression of *extABCD* is detrimental during electrode reduction.**

One hypothesis about the increased performance of *extABCD*$^{+}$ was that in this strain, more ExtABCD was produced in the absence of other electron conduits. In order to test if higher expression levels of *extABCD* could increase current density, these genes were inserted into the expression vector pGeo2 under the expression of p*acpP,* a strong and constitutive *G. sulfurreducens* promoter (pGeo2::p*acpP-extABCD*). The electrode reduction ability of a Δ5 strain containing this plasmid was compared to the one used as a complement in section 3.4, where *extABCD* is expressed under the *extA* promoter as a single transcriptional unit (pGeo2::p*extA-extABCD*). Additionally, a wild type (pGeo2::p*acpP-extABCD*) strain was also analyzed. It was found that only pGeo2::p*extA-extABCD* rescued the Δ5 strain phenotype. Expressing extABCD with a much stronger promoter (~9x stronger according to RNAseq data from section 3.4) resulted in no change in electrode reduction in a Δ5 strain, regardless of the presence of *extABCD*, and it resulted in a long lag and lower final current density in wild type (Fig. 4.3).

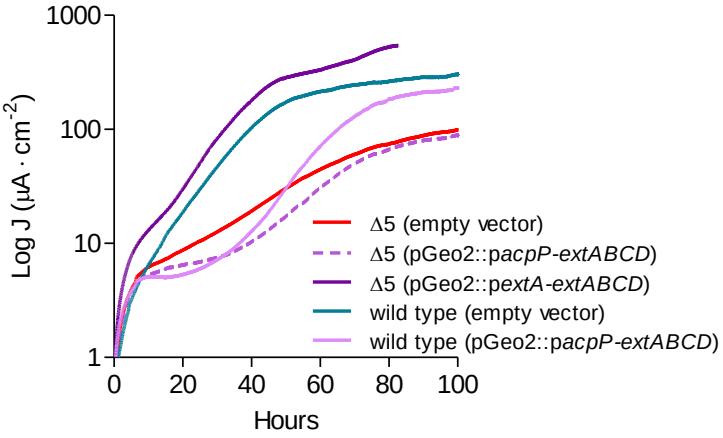

Figure 4.3. High expression levels of *extABCD* do not rescue Δ5 electrode reduction activity and cause defect in wild type. Current production of wild type and Δ5 strains carrying either empty pGeo2 plasmids, pGeo2::p*acpP-extABCD*, or pGeo2::p*extA-extABCD* plasmids grown using poised electrodes as sole terminal electron acceptor. Curves representative of n=4.

Attempts at using an inducible system resulted in high expression even in the un-induced samples. The inducible system pGeo3 has a p*acpP* promoter inhibited by a vanillate repressor, but is leaky. Therefore, even without inducing all strains tested were defective during electrode reduction (data not shown). Future attempts of tuning the expression levels of *extABCD* would be wise to use genomic insertions instead of plasmids and carefully chosen promoters that only increase expression slightly.

4.4.3 **Biofilms of strain *extABCD*$^+$ producing maximum current density have higher cell density in the 5 µm closest to electrode than wild type biofilms.**

In order to determine the structure of *extABCD*$^+$ biofilms, both wild type and *extABCD*$^+$ biofilms were grown until maximum current density was reached, and visualized using electron microscopy. Both strains formed biofilms of the same thickness, but *extABCD*$^+$ biofilms were denser at the electrode:biofilm interface (Fig. 4.4).

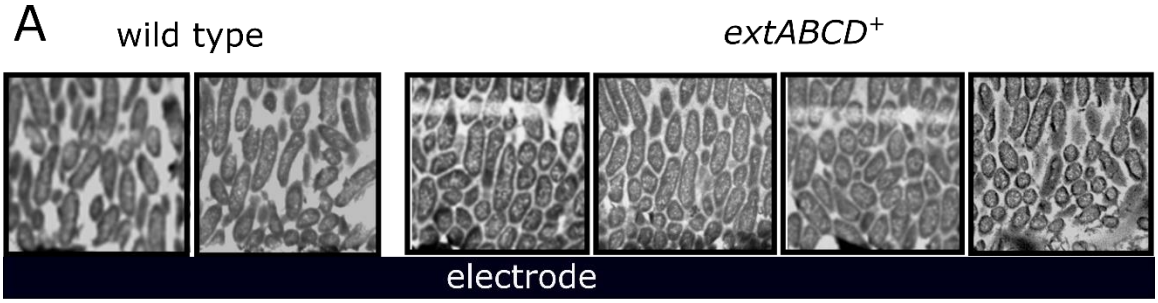

B	Cells in 5 µm^2
wild type	*extABCD*$^+$
42.7 ± 2.1	54.6 ± 4.3

Figure 4.4. Biofilms of *extABCD*$^+$ cells are denser in the area closest to the electrode. A) Electron microscopy images of representative 5 µm^2 areas closest to the electrode of wild type and *extABCD*$^+$ biofilms. B) Average cell counts and standard deviation of 5 µm^2 squares of four biofilms of each strain, with three squares counted for each biofilm.

4.4.4 **Current to protein ratios remain constant during biofilm development of *extABCD*$^+$ biofilms and decrease in wild type biofilms.**

In order to determine if the respiration rate per cell increased in *extABCD*$^+$ biofilms and wild type biofilms, total protein content was measured for biofilms of both strains at different time points during development. The ratio of current produced per unit protein, a measure of electron transfer rate averaged over all cells within the biofilm, was similar for both strains producing ~250 μA·cm^2 (Fig. 4.5). Once current production increased past that level, wild type biofilms accumulated more protein without a proportional increase in current, resulting in a decrease in current:protein ratio. In contrast, biofilms of *extABCD*$^+$ continued to increase in both protein and current production rate, maintaining the current:protein ratio of ~2.7 μA·μg for current densities measured up to 600 μA·cm^2 (Fig. 4.5). This suggested that as *extABCD*$^+$ biofilms grow, new cells are added in a manner that they remain able to transfer electrons to the electrode, compared to new cells of wild type.

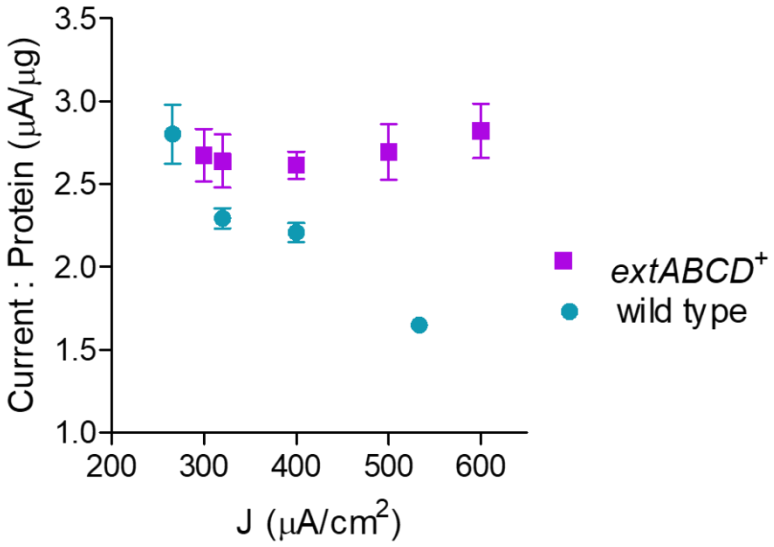

Figure 4.5. Protein accumulates faster in wild type biofilms than current density increases, while protein accumulation and current density increases at constant rate in *extABCD*⁺ biofilms. Total protein content of *extABCD*⁺ and wild type biofilms harvested at increasing current densities. Duplicate samples plotted with error bars representing standard deviation.

4.4.5 Whole genome protein abundance analysis confirms deletion constructs did not alter abundance of additional electron transfer pathways.

In section 3.4.11, transcriptomic analyses confirmed that the genetic deletions made to construct the *extABCD*⁺ strain did not alter the expression of any other known electron transfer pathways. In order to confirm that this was still true after post-transcriptional regulation, whole genome protein abundance of selected strains was compared. The Δ5 strain, with *omcBC-extABCD-EFG-HIJKL* conduit clusters deleted, was used to determine if any of the deletions caused off-target effects. Additionally,

the Δ*extABCD* strain was analyzed due to the relevance of this gene cluster during electrode reduction. Similarly, the *extABCD*$^{+}$ strain was analyzed because of its significant phenotype during electrode reduction, even though the genome of this strain was also sequenced with no off-target mutations found.

Whole genome protein abundance of these three strains while exponentially growing in media containing fumarate and acetate was compared to that of wild type in duplicate. This condition was chosen as all assays in this study were inoculated with cells under these conditions and only growth using fumarate as substrate (as determined through OD_{600} measurements) is comparable among all these strains. Out of ~1490 proteins detected in this analysis, in some cases a few as two proteins were found with significantly altered abundance between the two strains. Proteins with abundances significantly different from wild type are shown in Figure 4.6. Within these, GSU0777, the major subunit of the periplasmically-oriented formate dehydrogenase, was more abundant in all strains where *extABCD* was deleted. This subunit was the one that increased most sharply in abundance between wild type and the Δ5 and Δ*extABCD* strains, but GSU0779 and GSU0778 the *b*-cytochrome and iron sulfur subunits of formate dehydrogenase, respectively, were also more abundant in these mutant strains. The abundance of GSU0777-79 remained unchanged in the *extABCD*$^{+}$ strain.

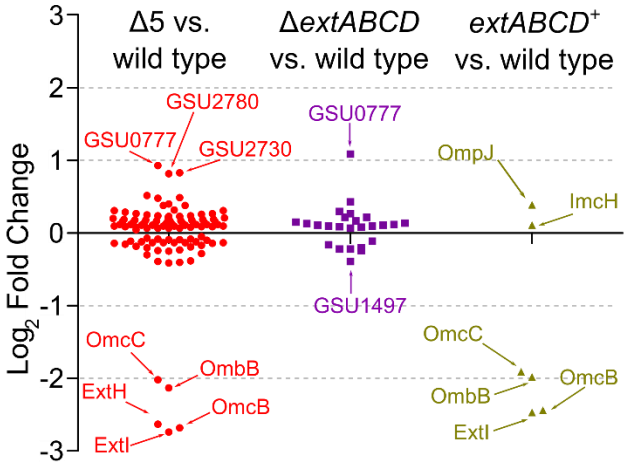

Figure 4.6. Abundance of electron transfer pathways does not change after deletion of putative electron conduits. Comparison of the abundance of proteins significantly different ($p < 0.05$) between wild type and deletion strains Δ5, Δ*extABCD*, and *extABCD*$^{+}$ as determined from duplicate samples. Proteins with a ratios >2 or <0.5 are labeled.

4.4.6 **Anabolic activity is higher in *extABCD*$^{+}$ biofilms than in wild type biofilms.**

Since in Chapter 2 the anabolically active layer in biofilms was determined to be only the 5-10 microns closest to the electrode, biofilm physiology showed denser areas in *extABCD*$^{+}$ biofilms than wild type in that same area in section 4.4.3, and current:protein ratios were higher for *extABCD*$^{+}$ than wild type biofilms producing maximum current in section 4.4.4, one hypothesis was that the anabolic activity of *extABCD+* biofilms was higher in this active zone near the electrode. Alternatively, the tighter packing of the biofilm could have increased conductivity to support cells farther from the electrode. To investigate these possibilities, we measured anabolic activity

within mutant biofilms using nanoSIMS to determine how it compared to wild type biofilms.

Following the same procedure as in chapter 2, the media in reactors containing fully developed *extABCD*$^{+}$ biofilms was exchanged for media containing isotopically labeled ^{15}N, ^{13}C, and deuterated water probes. After 6 hours of incubation, biofilms were fixed, stained, and embedded in resin. Sliced samples were then analyzed using nanoSIMS to measure the incorporation of isotope probe.

The anabolically active layer in *extABCD*$^{+}$ biofilms was found to be within the 5-10 µm closest to the electrode surface, as in wild type biofilms. However, the peak isotope incorporation within this active zone was 38% higher in *extABCD*$^{+}$ biofilms than in wild type biofilms (Fig. 4.7). The fractional abundance of ^{15}N added to growth media was 6%, therefore, previously unlabeled cells doubling in 6 hours would be expected to reach a ^{15}N fractional abundance value of approximately 3%. Peak value of fractional abundance was 2.9% ± 0.3 for *extABCD*$^{+}$ while it was only 2.1% ± 0.3 for wild type cells near the anode surface (Fig. 4.7). from this, we can infer that during the six hours of the stable isotope probing experiment, 48% of the biomass near electrodes was new biomass in *extABCD*$^{+}$ biofilms, compared to 35% in wild type biofilms.

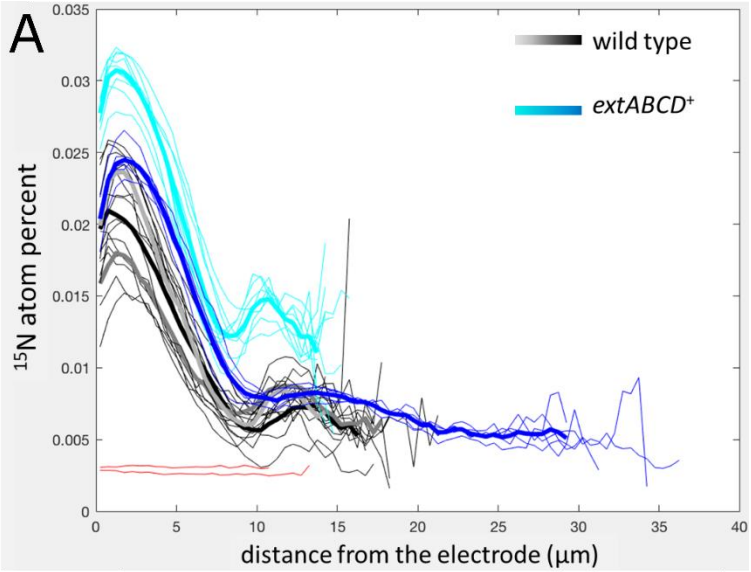

B	wild type	*extABCD*⁺
Percent ^{15}N enriched	2.1 ± 0.3	2.9 ± 0.3
New biomass	35%	48%

Figure 4.7. ^{15}N incorporation in *extABCD*⁺ biofilms compared to wild type biofilms. A) *extABCD*⁺ biofilms producing maximum current were analyzed using nanoSIMS to measure the abundance of ^{15}N probe incorporated by cells during a 6 hour incubation. Data from duplicate *extABCD*⁺ biofilms is superimposed on data from chapter 2, section 2.4. B) Calculation of new biomass formed during isotope probe experiment for wild type and *extABCD*⁺ biofilms.

4.5 **Discussion**

Construction of a strain with three electron conduit gene clusters deleted and *extABCD* intact (*extABCD*⁺) was previously found to produce more current (185). In order to determine what individual cell or biofilm changes were present in this strain, *extABCD*⁺ was analyzed in depth using a combination of proteomics, cell yield measurements, electron microscopy, nanoSIMS, and

electrochemical analysis of single gene deletion mutants. Our results show that the main difference between wild type and *extABCD*$^{+}$ biofilms is that the latter are densely packed at the electrode:biofilm interface, where they are also more metabolically active. This effect is not seen in wild type biofilms, suggesting both higher metabolic activity and denser packing result in higher current density.

From the four components of this gene cluster, deletion of the gene encoding the putative periplasmic cytochrome, ExtA, was not found to be as detrimental as the deletion of *extB*, *extC*, or *extD*, encoding the outer membrane integral protein and two extracellular cytochromes, respectively. These results suggest that ExtBCD may be able to interact with additional periplasmic cytochromes in the absence of ExtA, but the activity of this putative electron conduit complex is disrupted by the absence of either ExtB, ExtC, or ExtD. These results also highlight the disconnect between expression level and essentiality of a gene under electrode reduction conditions, since *extA* is expressed at levels as high as 6.5 times higher than *extBCD*, yet Δ*extA* is still able to reach 490 μA·cm^{2} after 100 hours and Δ*extB-D* never surpass 100 μA·cm^{2} (Fig. 4.2). A similar effect is observed for the *omcBC* gene cluster, which is not needed during electrode reduction, and yet it is highly expressed under this condition (185). Homologs of *extA* can be found both accompanied by *extBCD*

homologs or on their own (185), suggesting ExtA might be able to function without ExtBCD, or with other partners.

One hypothesis for the increase in current production by *extABCD*$^{+}$ was that biofilms of this engineered strain would be thicker. While this was not found to be true, the density of *extABCD*$^{+}$ biofilms in the area closest to the surface of the electrodes was 30% higher than the same region in wild type biofilms. This correlates well with the fact that current:protein ratios remained constant as current density increases in *extABCD*$^{+}$ biofilms and the fact that the cell layers closest to the surface of the electrode in *extABCD*$^{+}$ biofilms were more anabolically active than the same layers of wild type biofilms. As *extABCD*$^{+}$ cells double in the early stages of biofilm growth, and those cells remain close to the electrode, then this new biomass is still able to contribute to current production. In contrast, in wild type biofilms fewer cells are present in that area and are 38% less metabolically active, so accumulation of biomass does not translate into increased current production. One hypotheis for this increased packing could be the lack of the extraneous electron conduits on the cell exterior, such as the highly expressed *ombB/omaB/omcB* cluster.

Another possible reason for the increase in current production of *extABCD*$^{+}$ is that other electron transfer pathways were affected by the genetic deletions done to construct this

strain. Comparing the protein abundance of *extABCD*$^{+}$ and wild type strains supported the findings in section 3.4.11, where expression levels of other electron transfer components were not significantly different between these strains. While no significant differences in transcriptional and translational regulation have been detected, it always remains a possibility that post-translational regulation is somehow an off-target effect of the genetic manipulation of outer membrane complexes.

While current density was increased significantly through the engineering of the *extABCD*$^{+}$ strain, a solution to extending the anabolically active layers within current-producing biofilms is yet to be identified. Weeks-old biofilms can reach 50 µm in thickness, yet only the bottom 5-10 µm contain cells contributing to current production. Considerable increases in current density could be reached by eliminating distance from the electrode as a limitation to further increase of current production. Future studies will be needed to determine if additional factors influence the effect in current production seen in the *extABCD*$^{+}$ strain, such as iron supply or outer membrane space availability. Anodes being an artificial substrate, we believe there are undoubtedly more ways in which *G. sulfurreducens* can be engineered to produce more current.

Chapter 5. Future directions

Fernanda Jimenez Otero

Within the time frame of this thesis, many aspects of the extracellular electron transfer pathway of *G. sulfurreducens* have been elucidated. While more extracellular electron transfer pathways remain to be described, just from those we now know, there are many remaining questions.

Specifically, from the work done in Chapter 2, two main mysteries remain: what is the source of the second peak of activity about 12-15 µm away from the electrode surface, and how can the limit of distance from the electrode be overcome? As is stated in the text, since the second peak is only present when biofilms are grown with electrode poised at +240 mV and not when biofilms are grown with electrodes poised at -100 mV, it is possible that the second peak is a redox-dependent phenomenon. A good experiment to analyze that would be to use this same technique to visualize anabolically active zones within biofilms of Δ*cbcL* and Δ*imcH* strains, which can only respire electrodes at +240 mV and -100 mV, respectively. If the second peak is hypothesized to be a low redox potential zone where CbcL is active, then the ^{15}N incorporation curve should not have that second peak in Δ*cbcL* biofilms.

An attempt at targeting the question of extending the area of metabolic activity was to visualize *extABCD*$^{+}$ biofilms after isotopic label incorporation using nanoSIMS. However, we found that in this mutant the peak of ^{15}N incorporation increased in

intensity, rather than amplitude. Further analysis of the physiology of *G. sulfurreducens* during electrode reduction might elucidate additional pathways to target for metabolic engineering, such as the periplasmic components of the extracellular electron transfer pathway.

A remaining mystery from Chapter 3 was whether additional electron conduit gene clusters were present in the genome of *G. sulfurreducens* since 20% of wild type electrode reduction activity is still present in a Δ5 strain. Two more gene clusters (GSU3222-3226 and GSU2494-2495) were deleted, creating a Δ7 strain, but this strain was found to reduce electrodes in a similar fashion to Δ5 (Fig. 5.1) and single mutants of each gene cluster (ΔGSU3222-226 and ΔGSU2494-2495) showed phenotypes comparable to wild type. There are additional genes encoding periplasmic, lipoprotein cytochromes, and integral outer membrane proteins that are not organized in gene clusters. It is possible that some of these may be responsible for the residual activity of the Δ5 strain, but only with a genome-scale strategy, such as Tn-seq, finding such targets would be possible.

An interesting characteristic about strains lacking *extABCD*, including Δ*extABCD*, Δ5, and Δ7, is that they are all able to produce ~100 $\mu A \cdot cm^{-2}$. Similar current densities (~50 $\mu A \cdot cm^{-2}$ in different reactor setup) have been attributed before to single-layer *G. sulfurreducens* biofilms (39). It is possible that

ExtABCD is needed for electron transfer across multi-cell-layer biofilms, but not for direct electron transfer to electrodes. Additional electron transfer pathways may be responsible for direct electron transfer to electrodes, such as pili or additional cytochromes. Further imaging of the biofilms formed by Δ*extABCD* and Δ5 strains is needed to test this hypothesis.

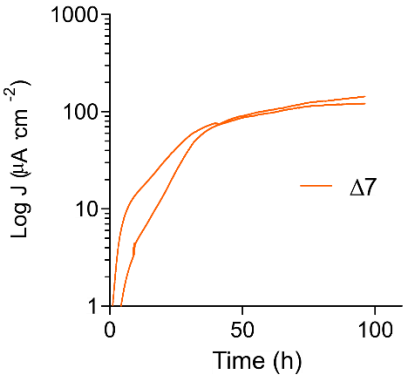

Figure 5.1 Residual current production by Δ7 strain. Current production by the Δ7 strain reaches ~150 μA·cm^2, similarly to a Δ5 strain. Both replicates shown.

One of the areas of this field with high potential to answer many hypothesis is structural biochemistry. The structure of many proteins and complexes from *S. oneidensis* have been solved through X-ray crystallography, resulting in very detailed descriptions of Mtr complexes (161, 189) and outer membrane proteins (162). Such structures of *G. sulfurreducens* outer membrane or extracellular cytochromes would be very informative. One of the hypothesis about the poor sequence similarity between multiheme cytochromes is that heme arrangement and environment

might be structurally similar between cytochromes with similar functions, but the rest of the protein is under low pressure to maintain sequence similarity. Answers to such questions can only be answered through solving the structure of several multiheme cytochromes, which are not simple to overexpress and purify.

With the complexity of extracellular electron transfer pathways in *G. sulfurreducens*, it will be necessary to use the information from fundamental studies as this one to create libraries of individual parts assembled into new pathways through synthetic biology to determine which combinations produce the most efficient pathways. Further work is necessary in the periplasmic components of the extracellular electron pathway, but this kind of high-throughput assay is closer to being possible with the information we have gained about outer membrane components.

Bibliography

1. Hayes JM, Waldbauer JR. 2006. The carbon cycle and associated redox processes through time. Philos Trans R Soc B Biol Sci 361:931–950.

2. Cornell RM, Schwertmann U. 1996. The iron oxides : structure, properties, reactions, occurrences and uses /. VCH, Weinheim ;

3. Majzlan J. 2013. Minerals and aqueous species of iron and manganese as reactants and products of microbial metal respiration, p. 1–28. *In* Gescher, J, Kappler, A (eds.), Microbial Metal Respiration. Springer Berlin Heidelberg.

4. Essington ME. 2015. Soil and water chemistry: An integrative approach, 2nd ed. CRC Press, Boca Raton, FL.

5. Kappler A, Emerson D, Gralnick JA, Roden EE, Muehe EM. 2016. Geomicrobiology of Iron, p. 343–399. *In* Ehrlich's Geomicrobiology, 6th ed. CRC Press, Boca Raton, FL.

6. Yang H, Lu R, Downs RT, Costin G. 2006. Goethite, α-FeO(OH), from single-crystal data. Acta Crystallogr Sect E Struct Rep Online 62:i250–i252.

7. Orsetti S, Laskov C, Haderlein SB. 2013. Electron transfer between iron minerals and quinones: Estimating the reduction potential of the Fe(II)-goethite surface from AQDS speciation. Environ Sci Technol 47:14161–14168.

8. Levar CE, Hoffman CL, Dunshee AJ, Toner BM, Bond DR. 2017. Redox potential as a master variable controlling pathways of metal reduction by *Geobacter sulfurreducens*. ISME J 11:741.

9. Cutting RS, Coker VS, Fellowes JW, Lloyd JR, Vaughan DJ. 2009. Mineralogical and morphological constraints on the reduction of Fe(III) minerals by *Geobacter sulfurreducens*. Geochim Cosmochim Acta 73:4004–4022.

10. Blake RL, Hessevick RE, Zoltai T, Finger LW. 1966. Refinement of the hematite structure. Am Mineral 51:123–129.

11. Johnston CP, Chrysochoou M. 2014. Mechanisms of chromate adsorption on hematite. Geochim Cosmochim Acta 138:146–157.

12. Li Y-L, Vali H, Yang J, Phelps TJ, Zhang CL. 2006. Reduction of iron oxides enhanced by a sulfate-reducing bacterium and biogenic H2S. Geomicrobiol J 23:103–117.

13. Hill RJ, Craig JR, Gibbs GV. 1979. Systematics of the spinel structure type. Phys Chem Miner 4:317–339.

14. Schwertmann U, Murad E. 1990. The influence of aluminum on iron oxides: XIV. Al-Substituted magnetite synthesized at ambient temperatures. Clays Clay Miner 38:196–202.

15. Manceau A, Drits VA. 1993. Local structure of ferrihydrite and feroxyhite by EXAFS spectroscopy. Clay Miner 28:165–184.

16. Michel FM, Ehm L, Antao SM, Lee PL, Chupas PJ, Liu G, Strongin DR, Schoonen MAA, Phillips BL, Parise JB. 2007. The structure of ferrihydrite, a nanocrystalline material. Science 316:1726–1729.

17. Thamdrup B. 2000. Bacterial manganese and iron reduction in aquatic sediments, p. 41–84. *In* Advances in Microbial Ecology. Springer, Boston, MA.

18. Schwertmann U, Fischer WR. 1973. Natural "amorphous" ferric hydroxide. Geoderma 10:237–247.

19. Eggleston CM, Hochella MFJ. 1992. The structure of hematite [001] surfaces by scanning tunneling microscopy: Image interpretation, surface relaxation, and step structure. Am Mineral 77:911–922.

20. Cao X, Huang X, Liang P, Xiao K, Zhou Y, Zhang X, Logan BE. 2009. A new method for water desalination using microbial desalination cells. Environ Sci Technol 43:7148–7152.

21. Brastad KS, He Z. 2013. Water softening using microbial desalination cell technology. Desalination 309:32–37.

22. Schievano A, Pepé Sciarria T, Vanbroekhoven K, De Wever H, Puig S, Andersen SJ, Rabaey K, Pant D. 2016. Electro-fermentation – Merging electrochemistry with fermentation in industrial applications. Trends Biotechnol 34:866–878.

23. Moscoviz R, Toledo-Alarcón J, Trably E, Bernet N. 2016. Electro-fermentation: How to drive fermentation using electrochemical systems. Trends Biotechnol 34:856–865.

24. Logan BE, Rabaey K. 2012. Conversion of wastes into bioelectricity and chemicals by using microbial electrochemical technologies. Science 337:686–690.

25. Tender LM, Reimers CE, Stecher HA, Holmes DE, Bond DR, Lowy DA, Pilobello K, Fertig SJ, Lovley DR. 2002. Harnessing

microbially generated power on the seafloor. Nat Biotechnol 20:821–825.

26. Bond DR, Lovley DR. 2003. Electricity production by *Geobacter sulfurreducens* attached to electrodes. Appl Environ Microbiol 69:1548–1555.

27. Potter MC, D S, A M. 1911. Electrical effects accompanying the decomposition of organic compounds. Proc R Soc Lond B 84:260–276.

28. Santoro C, Arbizzani C, Erable B, Ieropoulos I. 2017. Microbial fuel cells: From fundamentals to applications. A review. J Power Sources 356:225–244.

29. Zhang L, Zhang B, Zhu X, Chang H, Ou S, Wang H. 2018. Role of bioreactors in microbial biomass and energy conversion, p. 39–78. *In* Bioreactors for Microbial Biomass and Energy Conversion. Springer, Singapore.

30. Ishii S 'ichi, Watanabe K, Yabuki S, Logan BE, Sekiguchi Y. 2008. Comparison of electrode reduction activities of *Geobacter sulfurreducens* and an enriched consortium in an air-cathode microbial fuel cell. Appl Environ Microbiol 74:7348–7355.

31. Massazza D, Busalmen JP, Parra R, Romeo HE. 2018. Layer-to-layer distance determines the performance of 3D bio-electrochemical lamellar anodes in microbial energy transduction processes. J Mater Chem A.

32. Oh S, Min B, Logan BE. 2004. Cathode performance as a factor in electricity generation in microbial fuel cells. Environ Sci Technol 38:4900–4904.

33. Bond DR, Holmes DE, Tender LM, Lovley DR. 2002. Electrode-reducing microorganisms that harvest energy from marine sediments. Science 295:483–485.

34. Boulos L, Prévost M, Barbeau B, Coallier J, Desjardins R. 1999. LIVE/DEAD BacLight : application of a new rapid staining method for direct enumeration of viable and total bacteria in drinking water. J Microbiol Methods 37:77–86.

35. Nevin KP, Richter H, Covalla SF, Johnson JP, Woodard TL, Orloff AL, Jia H, Zhang M, Lovley DR. 2008. Power output and columbic efficiencies from biofilms of *Geobacter sulfurreducens* comparable to mixed community microbial fuel cells. Environ Microbiol 10:2505–2514.

36. Schrott GD, Ordoñez MV, Robuschi L, Busalmen JP. 2014. Physiological Stratification in Electricity-Producing Biofilms of *Geobacter sulfurreducens*. ChemSusChem 7:598–603.

37. Sun D, Cheng S, Wang A, Li F, Logan BE, Cen K. 2015. Temporal-spatial changes in viabilities and electrochemical properties of anode biofilms. Environ Sci Technol 49:5227–5235.

38. Sun D, Chen J, Huang H, Liu W, Ye Y, Cheng S. 2016. The effect of biofilm thickness on electrochemical activity of *Geobacter sulfurreducens*. Int J Hydrog Energy 41:16523–16528.

39. Reguera G, Nevin KP, Nicoll JS, Covalla SF, Woodard TL, Lovley DR. 2006. Biofilm and nanowire production leads to increased current in *Geobacter sulfurreducens* fuel cells. Appl Environ Microbiol 72:7345–7348.

40. Steidl RJ, Lampa-Pastirk S, Reguera G. 2016. Mechanistic stratification in electroactive biofilms of *Geobacter sulfurreducens* mediated by pilus nanowires. Nat Commun 7:12217.

41. Franks AE, Glaven RH, Lovley DR. 2012. Real-time spatial gene expression analysis within current-producing biofilms. ChemSusChem 5:1092–1098.

42. Kirchhoff C, Cypionka H. 2017. Propidium ion enters viable cells with high membrane potential during live-dead staining. J Microbiol Methods 142:79–82.

43. Flemming H-C, Wingender J. 2010. The biofilm matrix. Nat Rev Microbiol 8:623–633.

44. Babauta JT, Nguyen HD, Harrington TD, Renslow R, Beyenal H. 2012. pH, redox potential and local biofilm potential microenvironments within *Geobacter sulfurreducens* biofilms and their roles in electron transfer. Biotechnol Bioeng 109:2651–2662.

45. Torres CI, Kato Marcus A, Rittmann BE. 2008. Proton transport inside the biofilm limits electrical current generation by anode-respiring bacteria. Biotechnol Bioeng 100:872–881.

46. Renslow R, Babauta J, Majors P, Beyenal H. 2013. Diffusion in biofilms respiring on electrodes. Energy Environ Sci 6:595–607.

47. Snider RM, Strycharz-Glaven SM, Tsoi SD, Erickson JS, Tender LM. 2012. Long-range electron transport in *Geobacter sulfurreducens* biofilms is redox gradient-driven. Proc Natl Acad Sci 109:15467–15472.

48. Robuschi L, Tomba JP, Schrott GD, Bonanni PS, Desimone PM, Busalmen JP. 2013. Spectroscopic slicing to reveal internal redox gradients in electricity-producing biofilms. Angew Chem Int Ed 52:925–928.

49. Nevin KP, Kim B-C, Glaven RH, Johnson JP, Woodard TL, Methé BA, Jr RJD, Covalla SF, Franks AE, Liu A, Lovley DR. 2009. Anode biofilm transcriptomics reveals outer surface components essential for high density current production in *Geobacter sulfurreducens* fuel cells. PLOS ONE 4:e5628.

50. Richter H, P. Nevin K, Jia H, A. Lowy D, R. Lovley D, M. Tender L. 2009. Cyclic voltammetry of biofilms of wild type and mutant *Geobacter sulfurreducens* on fuel cell anodes indicates possible roles of OmcB, OmcZ, type IV pili, and protons in extracellular electron transfer. Energy Environ Sci 2:506–516.

51. Inoue K, Leang C, Franks AE, Woodard TL, Nevin KP, Lovley DR. 2011. Specific localization of the *c*-type cytochrome OmcZ at the anode surface in current-producing biofilms of *Geobacter sulfurreducens*. Environ Microbiol Rep 3:211–217.

52. Walker DJ, Adhikari RY, Holmes DE, Ward JE, Woodard TL, Nevin KP, Lovley DR. 2018. Electrically conductive pili from pilin genes of phylogenetically diverse microorganisms. ISME J 12:48–58.

53. Vargas M, Malvankar NS, Tremblay P-L, Leang C, Smith JA, Patel P, Synoeyenbos-West O, Nevin KP, Lovley DR. 2013. Aromatic amino acids required for pili conductivity and long-range extracellular electron transport in *Geobacter sulfurreducens*. mBio 4:e00105-13.

54. Cosert KM, Steidl RJ, Castro-Forero A, Worden RM, Reguera G. 2017. Electronic characterization of *Geobacter sulfurreducens* pilins in self-assembled monolayers unmasks tunnelling and hopping conduction pathways. Phys Chem Chem Phys 19:11163–11172.

55. Reguera G, Pollina RB, Nicoll JS, Lovley DR. 2007. Possible nonconductive role of *Geobacter sulfurreducens* pilus nanowires in biofilm formation. J Bacteriol 189:2125–2127.

56. Richter LV, Franks AE, Weis RM, Sandler SJ. 2017. Significance of a posttranslational modification of the PilA protein of *Geobacter sulfurreducens* for surface attachment, biofilm formation, and growth on insoluble extracellular electron acceptors. J Bacteriol 199:e00716-16.

57. Myers JM, Myers CR. 2000. Role of the tetraheme cytochrome CymA in anaerobic electron transport in cells of *Shewanella putrefaciens* MR-1 with normal levels of menaquinone. J Bacteriol 182:67–75.

58. Myers CR, Myers JM. 1997. Cloning and sequence of *cymA*, a gene encoding a tetraheme cytochrome *c* required for reduction of iron(III), fumarate, and nitrate by *Shewanella putrefaciens* MR-1. J Bacteriol 179:1143–1152.

59. Schwalb C, Chapman SK, Reid GA. 2003. The tetraheme cytochrome CymA is required for anaerobic respiration with dimethyl sulfoxide and nitrite in *Shewanella oneidensis*. Biochemistry (Mosc) 42:9491–9497.

60. Myers JM, Antholine WE, Myers CR. 2004. Vanadium(V) reduction by *Shewanella oneidensis* MR-1 requires menaquinone and cytochromes from the cytoplasmic and outer membranes. Appl Environ Microbiol 70:1405–1412.

61. Li D-B, Cheng Y-Y, Wu C, Li W-W, Li N, Yang Z-C, Tong Z-H, Yu H-Q. 2014. Selenite reduction by *Shewanella oneidensis* MR-1 is mediated by fumarate reductase in periplasm. Sci Rep 4.

62. Levar CE, Chan CH, Mehta-Kolte MG, Bond DR. 2014. An inner membrane cytochrome required only for reduction of high redox potential extracellular electron acceptors. mBio 5:e02034-14.

63. Zacharoff L, Chan CH, Bond DR. 2016. Reduction of low potential electron acceptors requires the CbcL inner membrane cytochrome of *Geobacter sulfurreducens*. Bioelectrochemistry 107:7–13.

64. Ding Y-HR, Hixson KK, Giometti CS, Stanley A, Esteve-Núñez A, Khare T, Tollaksen SL, Zhu W, Adkins JN, Lipton MS, Smith RD, Mester T, Lovley DR. 2006. The proteome of dissimilatory metal-reducing microorganism *Geobacter sulfurreducens* under various growth conditions. Biochim Biophys Acta BBA - Proteins Proteomics 1764:1198–1206.

65. Lloyd JR, Leang C, Hodges Myerson AL, Coppi MV, Cuifo S, Methe B, Sandler SJ, Lovley DR. 2003. Biochemical and genetic characterization of PpcA, a periplasmic *c*-type cytochrome in *Geobacter sulfurreducens*. Biochem J 369:153–161.

66. Alves MN, Neto SE, Alves AS, Fonseca BM, Carrêlo A, Pacheco I, Paquete CM, Soares CM, Louro RO. 2015. Characterization of the periplasmic redox network that sustains the versatile anaerobic metabolism of *Shewanella oneidensis* MR-1. Front Microbiol 6.

67. Schuetz B, Schicklberger M, Kuermann J, Spormann AM, Gescher J. 2009. Periplasmic Electron Transfer via the c-Type Cytochromes MtrA and FccA of Shewanella oneidensis MR-1. Appl Environ Microbiol 75:7789–7796.

68. Coursolle D, Gralnick JA. 2010. Modularity of the Mtr respiratory pathway of *Shewanella oneidensis* strain MR-1. Mol Microbiol 77:995–1008.

69. Richardson DJ, Butt JN, Fredrickson JK, Zachara JM, Shi L, Edwards MJ, White G, Baiden N, Gates AJ, Marritt SJ, Clarke TA. 2012. The "porin–cytochrome" model for microbe-to-mineral electron transfer. Mol Microbiol 85:201–212.

70. Hartshorne RS, Reardon CL, Ross D, Nuester J, Clarke TA, Gates AJ, Mills PC, Fredrickson JK, Zachara JM, Shi L, Beliaev AS, Marshall MJ, Tien M, Brantley S, Butt JN, Richardson DJ. 2009. Characterization of an electron conduit between bacteria and the extracellular environment. Proc Natl Acad Sci 106:22169–22174.

71. Nakano CM, Byun HS, Ma H, Wei T, El-Naggar MY. 2015. A framework for stochastic simulations and visualization of biological electron-transfer dynamics. Comput Phys Commun 193:1–9.

72. Coursolle D, Baron DB, Bond DR, Gralnick JA. 2010. The Mtr respiratory pathway is essential for reducing flavins and electrodes in *Shewanella oneidensis*. J Bacteriol 192:467–474.

73. Hau HH, Gilbert A, Coursolle D, Gralnick JA. 2008. Mechanism and consequences of anaerobic respiration of cobalt by *Shewanella oneidensis* strain MR-1. Appl Environ Microbiol 74:6880–6886.

74. Jensen HM, Albers AE, Malley KR, Londer YY, Cohen BE, Helms BA, Weigele P, Groves JT, Ajo-Franklin CM. 2010. Engineering of a synthetic electron conduit in living cells. Proc Natl Acad Sci 107:19213–19218.

75. Leang C, Coppi MV, Lovley DR. 2003. OmcB, a *c*-type polyheme cytochrome, involved in Fe(III) reduction in *Geobacter sulfurreducens*. J Bacteriol 185:2096–2103.

76. Liu Y, Fredrickson JK, Zachara JM, Shi L. 2015. Direct involvement of *ombB*, *omaB*, and *omcB* genes in extracellular reduction of Fe(III) by *Geobacter sulfurreducens* PCA. Front Microbiol 1075.

77. Liu Y, Wang Z, Liu J, Levar C, Edwards MJ, Babauta JT, Kennedy DW, Shi Z, Beyenal H, Bond DR, Clarke TA, Butt JN, Richardson DJ, Rosso KM, Zachara JM, Fredrickson JK, Shi L. 2014. A trans-outer membrane porin-cytochrome protein complex for extracellular electron transfer by *Geobacter sulfurreducens* PCA. Environ Microbiol Rep 6:776–785.

78. Shi L, Dong H, Reguera G, Beyenal H, Lu A, Liu J, Yu H-Q, Fredrickson JK. 2016. Extracellular electron transfer mechanisms between microorganisms and minerals. Nat Rev Microbiol 14:651–662.

79. Coursolle D, Gralnick JA. 2012. Reconstruction of extracellular respiratory pathways for iron(III) reduction in *Shewanella oneidensis* strain MR-1. Front Microbiol 3.

80. Gralnick JA, Vali H, Lies DP, Newman DK. 2006. Extracellular respiration of dimethyl sulfoxide by *Shewanella oneidensis* strain MR-1. Proc Natl Acad Sci U S A 103:4669–4674.

81. Shi L, Fredrickson JK, Zachara JM. 2014. Genomic analyses of bacterial porin-cytochrome gene clusters. Front Microbiol 5:657.

82. Marsili E, Baron DB, Shikhare ID, Coursolle D, Gralnick JA, Bond DR. 2008. *Shewanella* secretes flavins that mediate extracellular electron transfer. Proc Natl Acad Sci 105:3968–3973.

83. von Canstein H, Ogawa J, Shimizu S, Lloyd JR. 2008. Secretion of flavins by *Shewanella* species and their role in extracellular electron transfer. Appl Environ Microbiol 74:615–623.

84. Kotloski NJ, Gralnick JA. 2013. Flavin Electron Shuttles Dominate Extracellular Electron Transfer by *Shewanella oneidensis*. mBio 4:e00553-12.

85. Xu S, Jangir Y, El-Naggar MY. 2016. Disentangling the roles of free and cytochrome-bound flavins in extracellular electron transport from *Shewanella oneidensis* MR-1. Electrochimica Acta 198:49–55.

86. Rollefson JB, Stephen CS, Tien M, Bond DR. 2011. Identification of an Extracellular Polysaccharide Network Essential for Cytochrome Anchoring and Biofilm Formation in Geobacter sulfurreducens. J Bacteriol 193:1023–1033.

87. Leang C, Qian X, Mester T, Lovley DR. 2010. Alignment of the *c*-type cytochrome OmcS along pili of *Geobacter sulfurreducens*. Appl Environ Microbiol 76:4080–4084.

88. Zacharoff LA, Morrone D, Bond DR. 2017. *Geobacter sulfurreducens* extracellular multiheme cytochrome PgcA facilitates respiration to Fe(III) oxides but not electrodes. Front Microbiol 8:2481.

89. Peng L, Zhang Y. 2017. Cytochrome OmcZ is essential for the current generation by *Geobacter sulfurreducens* under low electrode potential. Electrochimica Acta 228:447–452.

90. Stoodley P, Sauer K, Davies DG, Costerton JW. 2002. Biofilms as complex differentiated communities. Annu Rev Microbiol 56:187–209.

91. Flemming H-C, Wingender J, Szewzyk U, Steinberg P, Rice SA, Kjelleberg S. 2016. Biofilms: an emergent form of bacterial life. Nat Rev Microbiol 14:563–575.

92. Tadanier CJ, Schreiber ME, Roller JW. 2005. Arsenic mobilization through microbially mediated deflocculation of ferrihydrite. Environ Sci Technol 39:3061–3068.

93. Ehrlich HL. 2016. Uppermost lithosphere as a microbial habitat, p. 55–68. *In* Ehrlich's Geomicrobiology, 6th ed. CRC Press, Boca Raton, FL.

94. Battin TJ, Kaplan LA, Denis Newbold J, Hansen CME. 2003. Contributions of microbial biofilms to ecosystem processes in stream mesocosms. Nature 426:439–442.

95. Islam FS, Gault AG, Boothman C, Polya DA, Charnock JM, Chatterjee D, Lloyd JR. 2004. Role of metal-reducing bacteria in arsenic release from Bengal delta sediments. Nature 430:68–71.

96. Gantzer CJ, Rittmann BE, Herricks EE. 1988. Mass transport to streambed biofilms. Water Res 22:709–722.

97. Domozych DS, Domozych CR. 2008. Desmids and biofilms of freshwater wetlands: development and microarchitecture. Microb Ecol 55:81–93.

98. Ramsing NB, Kühl M, Jørgensen BB. 1993. Distribution of sulfate-reducing bacteria, O2, and H2S in photosynthetic biofilms determined by oligonucleotide probes and microelectrodes. Appl Environ Microbiol 59:3840–3849.

99. Stoodley P, Dodds I, Boyle JD, Lappin-Scott HM. 1998. Influence of hydrodynamics and nutrients on biofilm structure. J Appl Microbiol 85 Suppl 1:19S–28S.

100. de Beer D, Stoodley P, Roe F, Lewandowski Z. 1994. Effects of biofilm structures on oxygen distribution and mass transport. Biotechnol Bioeng 43:1131–1138.

101. Sauer K, Camper AK, Ehrlich GD, Costerton JW, Davies DG. 2002. Pseudomonas aeruginosa displays multiple phenotypes during development as a biofilm. J Bacteriol 184:1140–1154.

102. Wilmes P, Remis JP, Hwang M, Auer M, Thelen MP, Banfield JF. 2009. Natural acidophilic biofilm communities reflect distinct organismal and functional organization. ISME J 3:266–270.

103. Lemaire R, Webb RI, Yuan Z. 2008. Micro-scale observations of the structure of aerobic microbial granules used for the treatment of nutrient-rich industrial wastewater. ISME J 2:528–541.

104. Sleutels THJA, Ter Heijne A, Buisman CJN, Hamelers HVM. 2012. Bioelectrochemical Systems: An Outlook for Practical Applications. ChemSusChem 5:1012–1019.

105. Bond DR, Holmes DE, Tender LM, Lovley DR. 2002. Electrode-Reducing Microorganisms That Harvest Energy from Marine Sediments. Science 295:483–485.

106. Holmes DE, Bond DR, O'Neil RA, Reimers CE, Tender LR, Lovley DR. 2004. Microbial communities associated with electrodes harvesting electricity from a variety of aquatic sediments. Microb Ecol 48:178–190.

107. Jung S, Regan JM. 2007. Comparison of anode bacterial communities and performance in microbial fuel cells with different electron donors. Appl Microbiol Biotechnol 77:393–402.

108. Lee H-S, Parameswaran P, Kato-Marcus A, Torres CI, Rittmann BE. 2008. Evaluation of energy-conversion efficiencies in microbial fuel cells (MFCs) utilizing fermentable and non-fermentable substrates. Water Res 42:1501–1510.

109. Tejedor Sanz S, Fernández Labrador P, Hart S, Torres CI, Esteve-Núñez A. 2018. *Geobacter* dominates the inner layers of a stratified biofilm on a fluidized anode during brewery wastewater treatment. Front Microbiol 9:387.

110. Summers ZM, Fogarty HE, Leang C, Franks AE, Malvankar NS, Lovley DR. 2010. Direct Exchange of Electrons Within Aggregates of an Evolved Syntrophic Coculture of Anaerobic Bacteria. Science 330:1413–1415.

111. Sun D, Cheng S, Wang A, Li F, Logan BE, Cen K. 2015. Temporal-Spatial Changes in Viabilities and Electrochemical Properties of Anode Biofilms. Environ Sci Technol 49:5227–5235.

112. Stephen CS, LaBelle EV, Brantley SL, Bond DR. 2014. Abundance of the Multiheme c-Type Cytochrome OmcB Increases in Outer Biofilm Layers of Electrode-Grown Geobacter sulfurreducens. PLoS ONE 9:e104336.

113. Marsili E, Rollefson JB, Baron DB, Hozalski RM, Bond DR. 2008. Microbial biofilm voltammetry: direct electrochemical characterization of catalytic electrode-attached biofilms. Appl Environ Microbiol 74:7329–7337.

114. Reguera G, Nevin KP, Nicoll JS, Covalla SF, Woodard TL, Lovley DR. 2006. Biofilm and Nanowire Production Leads to Increased Current in Geobacter sulfurreducens Fuel Cells. Appl Environ Microbiol 72:7345–7348.

115. Franks AE, Nevin KP, Glaven RH, Lovley DR. 2010. Microtoming coupled to microarray analysis to evaluate the spatial metabolic status of *Geobacter sulfurreducens* biofilms. ISME J 4:509.

116. Franks AE, Glaven RH, Lovley DR. 2012. Real-Time Spatial Gene Expression Analysis within Current-Producing Biofilms. ChemSusChem 5:1092–1098.

117. Jain A, Gazzola G, Panzera A, Zanoni M, Marsili E. 2011. Visible spectroelectrochemical characterization of Geobacter sulfurreducens biofilms on optically transparent indium tin oxide electrode. Electrochimica Acta 56:10776–10785.

118. Liu Y, Kim H, Franklin RR, Bond DR. 2011. Linking Spectral and Electrochemical Analysis to Monitor c-type Cytochrome Redox Status in Living Geobacter sulfurreducens Biofilms. ChemPhysChem 12:2235–2241.

119. Lebedev N, Strycharz-Glaven SM, Tender LM. 2014. Spatially resolved confocal resonant Raman microscopic analysis of anode-grown *Geobacter sulfurreducens* biofilms. ChemPhysChem 15:320–327.

120. Robuschi L, Tomba JP, Busalmen JP. 2017. Proving *Geobacter* biofilm connectivity with confocal Raman microscopy. J Electroanal Chem 793:99–103.

121. Babauta JT, Nguyen HD, Harrington TD, Renslow R, Beyenal H. 2012. pH, redox potential and local biofilm potential microenvironments within Geobacter sulfurreducens biofilms and their roles in electron transfer. Biotechnol Bioeng 109:2651–2662.

122. E. Franks A, P. Nevin K, Jia H, Izallalen M, L. Woodard T, R. Lovley D. 2009. Novel strategy for three-dimensional real-time imaging of microbial fuel cell communities: monitoring the inhibitory effects of proton accumulation within the anode biofilm. Energy Environ Sci 2:113–119.

123. Renslow RS, Babauta JT, Dohnalkova AC, Boyanov MI, Kemner KM, Majors PD, Fredrickson JK, Beyenal H. 2013. Metabolic spatial variability in electrode-respiring Geobacter sulfurreducens biofilms. Energy Environ Sci 6:1827–1836.

124. Kato Marcus A, Torres CI, Rittmann BE. 2007. Conduction-based modeling of the biofilm anode of a microbial fuel cell. Biotechnol Bioeng 98:1171–1182.

125. Torres CI, Kato Marcus A, Rittmann BE. 2008. Proton transport inside the biofilm limits electrical current generation by anode-respiring bacteria. Biotechnol Bioeng 100:872–881.

126. Marsili E, Rollefson JB, Baron DB, Hozalski RM, Bond DR. 2008. Microbial Biofilm Voltammetry: Direct Electrochemical Characterization of Catalytic Electrode-Attached Biofilms. Appl Environ Microbiol 74:7329–7337.

127. Marsili E, Sun J, Bond DR. 2010. Voltammetry and Growth Physiology of Geobacter sulfurreducens Biofilms as a Function of Growth Stage and Imposed Electrode Potential. Electroanalysis 22:865–874.

128. Kopf SH, McGlynn SE, Green-Saxena A, Guan Y, Newman DK, Orphan VJ. 2015. Heavy water and 15N labelling with NanoSIMS analysis reveals growth rate-dependent metabolic heterogeneity in chemostats. Environ Microbiol 17:2542–2556.

129. Zacharoff L, Chan CH, Bond DR. 2016. Reduction of low potential electron acceptors requires the CbcL inner membrane cytochrome of Geobacter sulfurreducens. Bioelectrochemistry 107:7–13.

130. Jain A, Gazzola G, Panzera A, Zanoni M, Marsili E. 2011. Visible spectroelectrochemical characterization of *Geobacter sulfurreducens* biofilms on optically transparent indium tin oxide electrode. Electrochimica Acta 56:10776–10785.

131. Liu Y, Kim H, Franklin RR, Bond DR. 2011. Linking spectral and electrochemical analysis to monitor *c*-type cytochrome redox status in living *Geobacter sulfurreducens* biofilms. Chemphyschem Eur J Chem Phys Phys Chem 12:2235–2241.

132. Steidl RJ, Lampa-Pastirk S, Reguera G. 2016. Mechanistic stratification in electroactive biofilms of *Geobacter sulfurreducens* mediated by pilus nanowires. Nat Commun 7:12217.

133. N'Guessan AL, Vrionis HA, Resch CT, Long PE, Lovley DR. 2008. Sustained removal of uranium from contaminated groundwater following stimulation of dissimilatory metal reduction. Environ Sci Technol 42:2999–3004.

134. Toner BM, Fakra SC, Manganini SJ, Santelli CM, Marcus MA, Moffett JW, Rouxel O, German CR, Edwards KJ. 2009. Preservation of iron(II) by carbon-rich matrices in a hydrothermal plume. Nat Geosci 2:197–201.

135. Williams KH, Long PE, Davis JA, Wilkins MJ, N'Guessan AL, Steefel CI, Yang L, Newcomer D, Spane FA, Kerkhof LJ, McGuinness L, Dayvault R, Lovley DR. 2011. Acetate availability and its influence on sustainable bioremediation of uranium-contaminated groundwater. Geomicrobiol J 28:519–539.

136. Yelton AP, Williams KH, Fournelle J, Wrighton KC, Handley KM, Banfield JF. 2013. Vanadate and acetate biostimulation of contaminated sediments decreases diversity, selects for specific taxa, and decreases aqueous V5+ soncentration. Environ Sci Technol 47:6500–6509.

137. Couture R-M, Charlet L, Markelova E, Madé B, Parsons CT. 2015. On–off mobilization of contaminants in soils during redox oscillations. Environ Sci Technol 49:3015–3023.

138. Ren Z, Steinberg LM, Regan JM. 2008. Electricity production and microbial biofilm characterization in cellulose-fed microbial fuel cells. Water Sci Technol 58:617–622.

139. Schrader PS, Reimers CE, Girguis P, Delaney J, Doolan C, Wolf M, Green D. 2016. Independent benthic microbial fuel cells powering sensors and acoustic communications with the MARS underwater observatory. J Atmospheric Ocean Technol 33:607–617.

140. Gralnick JA, Newman DK. 2007. Extracellular respiration. Mol Microbiol 65:1–11.

141. Navrotsky A, Mazeina L, Majzlan J. 2008. Size-driven structural and thermodynamic complexity in iron oxides. Science 319:1635–1638.

142. Levar CE, Hoffman CL, Dunshee AJ, Toner BM, Bond DR. 2017. Redox potential as a master variable controlling pathways of metal reduction by *Geobacter sulfurreducens*. ISME J 11:741–752.

143. Marsili E, Sun J, Bond DR. 2010. Voltammetry and growth physiology of *Geobacter sulfurreducens* biofilms as a function of growth stage and imposed electrode potential. Electroanalysis 22:865–874.

144. Tremblay P-L, Summers ZM, Glaven RH, Nevin KP, Zengler K, Barrett CL, Qiu Y, Palsson BO, Lovley DR. 2011. A *c*-type cytochrome and a transcriptional regulator responsible for enhanced extracellular electron transfer in *Geobacter sulfurreducens* revealed by adaptive evolution. Environ Microbiol 13:13–23.

145. Qian X, Mester T, Morgado L, Arakawa T, Sharma ML, Inoue K, Joseph C, Salgueiro CA, Maroney MJ, Lovley DR. 2011. Biochemical characterization of purified OmcS, a *c*-type cytochrome required for insoluble Fe(III) reduction in *Geobacter sulfurreducens*. Biochim Biophys Acta BBA - Bioenerg 1807:404–412.

146. Smith JA, Tremblay P-L, Shrestha PM, Snoeyenbos-West OL, Franks AE, Nevin KP, Lovley DR. 2014. Going wireless: Fe(III) oxide reduction without pili by *Geobacter sulfurreducens* strain JS-1. Appl Environ Microbiol 80:4331–4340.

147. Wang Z, Liu C, Wang X, Marshall MJ, Zachara JM, Rosso KM, Dupuis M, Fredrickson JK, Heald S, Shi L. 2008. Kinetics of reduction of Fe(III) complexes by outer membrane cytochromes MtrC and OmcA of *Shewanella oneidensis* MR-1. Appl Environ Microbiol 74:6746–6755.

148. White GF, Shi Z, Shi L, Wang Z, Dohnalkova AC, Marshall MJ, Fredrickson JK, Zachara JM, Butt JN, Richardson DJ, Clarke

TA. 2013. Rapid electron exchange between surface-exposed bacterial cytochromes and Fe(III) minerals. Proc Natl Acad Sci 110:6346–6351.

149. Baron D, LaBelle E, Coursolle D, Gralnick JA, Bond DR. 2009. Electrochemical measurement of electron transfer kinetics by *Shewanella oneidensis* MR-1. J Biol Chem 284:28865–28873.

150. Jiao Y, Newman DK. 2007. The *pio* operon is essential for phototrophic Fe(II) oxidation in *Rhodopseudomonas palustris* TIE-1. J Bacteriol 189:1765–1773.

151. Leang C, Lovley DR. 2005. Regulation of two highly similar genes, *omcB* and *omcC*, in a 10 kb chromosomal duplication in *Geobacter sulfurreducens*. Microbiology 151:1761–1767.

152. Chan CH, Levar CE, Jiménez Otero F, Bond DR. 2017. Genome scale mutational analysis of *Geobacter sulfurreducens* reveals distinct molecular mechanisms for respiration and sensing of poised electrodes vs. Fe(III) oxides. J Bacteriol 119:e00340-17.

153. Bagos PG, Liakopoulos TD, Spyropoulos IC, Hamodrakas SJ. 2004. PRED-TMBB: a web server for predicting the topology of β-barrel outer membrane proteins. Nucleic Acids Res 32:W400–W404.

154. Yu NY, Wagner JR, Laird MR, Melli G, Rey S, Lo R, Dao P, Sahinalp SC, Ester M, Foster LJ, Brinkman FSL. 2010. PSORTb 3.0: improved protein subcellular localization prediction with refined localization subcategories and predictive capabilities for all prokaryotes. Bioinformatics 26:1608–1615.

155. Juncker AS, Willenbrock H, von Heijne G, Brunak S, Nielsen H, Krogh A. 2003. Prediction of lipoprotein signal peptides in Gram-negative bacteria. Protein Sci Publ Protein Soc 12:1652–1662.

156. Simon R, Priefer U, Pühler A. 1983. A broad host range mobilization system for in vivo genetic engineering: Transposon mutagenesis in Gram negative bacteria. Nat Biotechnol 1:784–791.

157. Chan CH, Levar CE, Zacharoff L, Badalamenti JP, Bond DR. 2015. Scarless genome editing and stable inducible expression vectors for *Geobacter sulfurreducens*. Appl Environ Microbiol 81:7178–7186.

158. McClure R, Balasubramanian D, Sun Y, Bobrovskyy M, Sumby P, Genco CA, Vanderpool CK, Tjaden B. 2013. Computational analysis of bacterial RNA-Seq data. Nucleic Acids Res 41:e140–e140.

159. Markowitz VM, Chen I-MA, Palaniappan K, Chu K, Szeto E, Grechkin Y, Ratner A, Jacob B, Huang J, Williams P, Huntemann M, Anderson I, Mavromatis K, Ivanova NN, Kyrpides NC. 2012. IMG: the integrated microbial genomes database and comparative analysis system. Nucleic Acids Res 40:D115–D122.

160. Sievers F, Wilm A, Dineen D, Gibson TJ, Karplus K, Li W, Lopez R, McWilliam H, Remmert M, Söding J, Thompson JD, Higgins DG. 2011. Fast, scalable generation of high-quality protein multiple sequence alignments using Clustal Omega. Mol Syst Biol 7:539.

161. Clarke TA, Edwards MJ, Gates AJ, Hall A, White GF, Bradley J, Reardon CL, Shi L, Beliaev AS, Marshall MJ, Wang Z, Watmough NJ, Fredrickson JK, Zachara JM, Butt JN, Richardson DJ. 2011. Structure of a bacterial cell surface decaheme electron conduit. Proc Natl Acad Sci 108:9384–9389.

162. Edwards MJ, Hall A, Shi L, Fredrickson JK, Zachara JM, Butt JN, Richardson DJ, Clarke TA. 2012. The crystal structure of the extracellular 11-heme cytochrome UndA reveals a conserved 10-heme motif and defined binding site for soluble iron chelates. Structure 20:1275–1284.

163. Kim B-C, Leang C, Ding Y-HR, Glaven RH, Coppi MV, Lovley DR. 2005. OmcF, a putative *c*-type monoheme outer membrane cytochrome required for the expression of other outer membrane cytochromes in *Geobacter sulfurreducens*. J Bacteriol 187:4505–4513.

164. Juárez K, Kim B-C, Nevin K, Olvera L, Reguera G, Lovley DR, Methé BA. 2009. PilR, a transcriptional regulator for pilin and other genes required for Fe(III) reduction in *Geobacter sulfurreducens*. J Mol Microbiol Biotechnol 16:146–158.

165. Aklujkar M, Coppi MV, Leang C, Kim BC, Chavan MA, Perpetua LA, Giloteaux L, Liu A, Holmes DE. 2013. Proteins involved in electron transfer to Fe(III) and Mn(IV) oxides by *Geobacter sulfurreducens* and *Geobacter uraniireducens*. Microbiology 159:515–535.

166. Methé BA, Nelson KE, Eisen JA, Paulsen IT, Nelson W, Heidelberg JF, Wu D, Wu M, Ward N, Beanan MJ, Dodson RJ, Madupu R, Brinkac LM, Daugherty SC, DeBoy RT, Durkin AS, Gwinn M, Kolonay JF, Sullivan SA, Haft DH, Selengut J,

Davidsen TM, Zafar N, White O, Tran B, Romero C, Forberger HA, Weidman J, Khouri H, Feldblyum TV, Utterback TR, Aken SEV, Lovley DR, Fraser CM. 2003. Genome of Geobacter sulfurreducens: Metal Reduction in Subsurface Environments. Science 302:1967–1969.

167. Shelobolina ES, Coppi MV, Korenevsky AA, DiDonato LN, Sullivan SA, Konishi H, Xu H, Leang C, Butler JE, Kim B-C, Lovley DR. 2007. Importance of *c*-type cytochromes for U(VI) reduction by *Geobacter sulfurreducens*. BMC Microbiol 7:16.

168. Holmes DE, Chaudhuri SK, Nevin KP, Mehta T, Methé BA, Liu A, Ward JE, Woodard TL, Webster J, Lovley DR. 2006. Microarray and genetic analysis of electron transfer to electrodes in *Geobacter sulfurreducens*. Environ Microbiol 8:1805–1815.

169. Stephen CS, LaBelle EV, Brantley SL, Bond DR. 2014. Abundance of the multiheme *c*-type cytochrome OmcB increases in outer biofilm layers of electrode-grown *Geobacter sulfurreducens*. PLOS ONE 9:e104336.

170. Ueki T, DiDonato LN, Lovley DR. 2017. Toward establishing minimum requirements for extracellular electron transfer in *Geobacter sulfurreducens*. FEMS Microbiol Lett 364.

171. Butler JE, Kaufmann F, Coppi MV, Núñez C, Lovley DR. 2004. MacA, a diheme *c*-type cytochrome involved in Fe(III) reduction by *Geobacter sulfurreducens*. J Bacteriol 186:4042–4045.

172. Kim B-C, Lovley DR. 2008. Investigation of direct vs. indirect involvement of the *c*-type cytochrome MacA in Fe(III) reduction by *Geobacter sulfurreducens*. FEMS Microbiol Lett 286:39–44.

173. Seidel J, Hoffmann M, Ellis KE, Seidel A, Spatzal T, Gerhardt S, Elliott SJ, Einsle O. 2012. MacA is a second cytochrome *c* peroxidase of *Geobacter sulfurreducens*. Biochemistry (Mosc) 51:2747–2756.

174. Gennaris A, Ezraty B, Henry C, Agrebi R, Vergnes A, Oheix E, Bos J, Leverrier P, Espinosa L, Szewczyk J, Vertommen D, Iranzo O, Collet J-F, Barras F. 2015. Repairing oxidized proteins in the bacterial envelope using respiratory chain electrons. Nature 528:409–412.

175. Appel J, Phunpruch S, Steinmüller K, Schulz R. 2000. The bidirectional hydrogenase of *Synechocystis sp.* PCC 6803 works

as an electron valve during photosynthesis. Arch Microbiol 173:333–338.

176. Coppi MV. 2005. The hydrogenases of *Geobacter sulfurreducens*: a comparative genomic perspective. Microbiology 151:1239–1254.

177. Qiu Y, Cho B-K, Park YS, Lovley D, Palsson BØ, Zengler K. 2010. Structural and operational complexity of the *Geobacter sulfurreducens* genome. Genome Res 20:1304–1311.

178. Aussignargues C, Giuliani M-C, Infossi P, Lojou E, Guiral M, Giudici-Orticoni M-T, Ilbert M. 2012. Rhodanese functions as sulfur supplier for key enzymes in sulfur energy metabolism. J Biol Chem 287:19936–19948.

179. Prat L, Maillard J, Rohrbach-Brandt E, Holliger C. 2012. An unusual tandem-domain rhodanese harbouring two active sites identified in *Desulfitobacterium hafniense*. FEBS J 279:2754–2767.

180. Ravot G, Casalot L, Ollivier B, Loison G, Magot M. 2005. *rdlA*, a new gene encoding a rhodanese-like protein in *Halanaerobium congolense* and other thiosulfate-reducing anaerobes. Res Microbiol 156:1031–1038.

181. Ramírez P, Toledo H, Guiliani N, Jerez CA. 2002. An exported rhodanese-like protein is induced during growth of *Acidithiobacillus ferrooxidans* in metal sulfides and different sulfur compounds. Appl Environ Microbiol 68:1837–1845.

182. Nelson CE, Rogowski A, Morland C, Wilhide JA, Gilbert HJ, Gardner JG. 2017. Systems analysis in *Cellvibrio japonicus* resolves predicted redundancy of β-glucosidases and determines essential physiological functions. Mol Microbiol 104:294–305.

183. Coker VS, Byrne JM, Telling ND, Van Der Laan G, Lloyd JR, Hitchcock AP, Wang J, Pattrick R a. D. 2012. Characterisation of the dissimilatory reduction of Fe(III)-oxyhydroxide at the microbe – mineral interface: the application of STXM–XMCD. Geobiology 10:347–354.

184. Eusterhues K, Hädrich A, Neidhardt J, Küsel K, Keller TF, Jandt KD, Totsche KU. 2014. Reduction of ferrihydrite with adsorbed and coprecipitated organic matter: microbial reduction by *Geobacter bremensis* vs. abiotic reduction by Na-dithionite. Biogeosciences 11:4953–4966.

185. Jiménez Otero F, Bond DR. 2017. Gene clusters encoding putative outer membrane electron conduits have specific roles during metal and electrode respiration in *Geobacter sulfurreducens*. bioRxiv 169086.

186. Nesvizhskii AI, Keller A, Kolker E, Aebersold R. 2003. A statistical model for identifying proteins by tandem mass spectrometry. Anal Chem 75:4646–4658.

187. Shadforth IP, Dunkley TP, Lilley KS, Bessant C. 2005. i-Tracker: For quantitative proteomics using iTRAQ™. BMC Genomics 6:145.

188. Oberg AL, Mahoney DW, Eckel-Passow JE, Malone CJ, Wolfinger RD, Hill EG, Cooper LT, Onuma OK, Spiro C, Therneau TM, Bergen HR. 2008. Statistical analysis of relative labeled mass spectrometry data from complex samples using ANOVA. J Proteome Res 7:225–233.

189. Edwards MJ, Fredrickson JK, Zachara JM, Richardson DJ, Clarke TA. 2012. Analysis of structural MtrC models based on homology with the crystal structure of MtrF. Biochem Soc Trans 40:1181–1185.